

Utah State University

DigitalCommons@USU

All Graduate Theses and Dissertations

Graduate Studies

5-1991

Origins of Low-Angle Normal Faults Along the West Side of the Bear River Range in Northern Utah

Jon E. Brummer
Utah State University

Follow this and additional works at: <https://digitalcommons.usu.edu/etd>



Part of the [Geology Commons](#)

Recommended Citation

Brummer, Jon E., "Origins of Low-Angle Normal Faults Along the West Side of the Bear River Range in Northern Utah" (1991). *All Graduate Theses and Dissertations*. 6784.

<https://digitalcommons.usu.edu/etd/6784>

This Thesis is brought to you for free and open access by the Graduate Studies at DigitalCommons@USU. It has been accepted for inclusion in All Graduate Theses and Dissertations by an authorized administrator of DigitalCommons@USU. For more information, please contact digitalcommons@usu.edu.



ORIGINS OF LOW-ANGLE NORMAL FAULTS
ALONG THE WEST SIDE OF THE
BEAR RIVER RANGE IN
NORTHERN UTAH

by

Jon E. Brummer

A thesis submitted in partial fulfillment
of the requirements for the degree

of

MASTER OF SCIENCE

in

Geology

Approved:

UTAH STATE UNIVERSITY
Logan, Utah

1991

ACKNOWLEDGMENTS

For his advice, counsel, patience, and encouragement throughout my graduate education, Dr. James P. Evans deserves much praise. To Dr. James P. McCalpin, Dr. Robert Q. Oaks, Jr., Dr. Donald W. Fiesinger, Dr. Peter T. Kolesar, and Susan K. Morgan, I extend my appreciation for their assistance in the laboratory and field during the course of my thesis work. Dr. Evans, Dr. McCalpin, and Dr. Oaks deserve much thanks for reviewing this work and providing helpful suggestions and new ideas.

Great appreciation is imparted to the staff of the Utah Geological and Mineral Survey: Mark Jensen, Hellmut Doelling, and Grant C. Willis of the Geologic Mapping Section and Carolyn Olsen, Cynthia Brandt, and Robert W. Gloyn of the Economic Geology Section. Aerial photographs, base maps, orthophotos, well logs, and well cuttings supplied by the Utah Geological and Mineral Survey aided in the preparation of this report.

This project was funded in part by the Utah Geological and Mineral Survey under contract #88-3011, stipends from the J. Stewart Williams Graduate Fellowship, and a graduate teaching assistantship provided by the Department of Geology.

Dean Smith and Wyndon Ward of Richmond, Utah, and Dale Nilson of Smithfield, Utah, kindly allowed me access to their land.

My achievements and accomplishments would mean little without family and friends with which to share them. My parents deserve much credit, for they have provided me with the desire to learn and achieve.

Jon Brummer

TABLE OF CONTENTS

	Page
ACKNOWLEDGMENTS	ii
LIST OF FIGURES	v
LIST OF PLATES	vii
ABSTRACT	viii
INTRODUCTION	1
PROBLEM STATEMENT	1
OBJECTIVES	3
PREVIOUS WORK	3
GEOGRAPHIC AND GEOLOGIC SETTINGS	6
METHODS	11
FIELD MAPPING	11
COMPUTER ANALYSES	12
GEOPHYSICAL SURVEYS	14
WELL-LOG DATA	16
DESCRIPTIVE ANALYSIS	18
BEDROCK STRATIGRAPHY	18
Mutual Formation	18
Geertsen Canyon Quartzite	20
St. Charles Formation	20
Garden City Formation	21
Salt Lake Formation	22
GEOLOGIC STRUCTURES	27
Logan Peak Syncline	28
Normal Faults	28
High-Angle Normal Faults	28
Low-Angle Normal Faults	36
Thrust Faults	42
GEOPHYSICAL SURVEYS	42
INTERPRETATIONS	47

KINEMATIC ANALYSIS	47
HYPOTHESES	51
Folded Thrust Fault	52
Rotated High-Angle Normal Fault	55
Subhypothesis 1	55
Subhypothesis 2	59
Gravity Slide	60
Subhypothesis 1	61
Subhypothesis 2	74
Listric Normal Fault	75
Low-Angle Normal Fault	77
Subhypothesis 1	78
Subhypothesis 2	78
Subhypothesis 3	79
STRUCTURAL EVOLUTION	82
CONCLUSIONS	85
ORIGINS	85
REGIONAL APPLICABILITY	86
REFERENCES CITED	87
APPENDIX	94

LIST OF FIGURES

Figure		Page
1	Index map of northern Utah.....	2
2	Block diagrams illustrating the differences in amount of throw due to the angle of a fault	7
3	Generalized stratigraphic section of bedrock exposed in the study area	9
4	Lower-hemisphere stereograms showing great circles of bedding in the western limb of the Logan Peak syncline	13
5	Three-dimensional plots of southern and northern low-angle-normal-fault traces	15
6	Locations of wells logged for this study	17
7	Contact between the tuff (Tslt) and conglomerate (Tslc) units of the Salt Lake Formation	26
8	Oblique aerial photograph of the range front near Logan, Utah	30
9	Oblique aerial photograph of the range front near Hyde Park, Utah	31
10	Small graben in gravel pit south of High Creek near Richmond, Utah	32
11	Field sketch of a small graben exposed in a gravel pit north of High Creek	33
12	Gouge zone in conglomerate of the Salt Lake Formation along the trace of the southern low-angle normal fault	38
13	Fault contact on southern ridge of the northern low-angle normal fault	40
14	Bouguer gravity map of Cache Valley, Utah-Idaho	43
15	Gravity profiles from Figure 14	45
16	Amount of dip slip on the northern low-angle normal fault	48
17	Geologic map of northern Utah	50
18	Stereograms of present and restored bedding	54

19	Reduction of fault-plane dip due to tilting by a later fault in the footwall block of an older fault	56
20	Restoration of low-angle normal faults to hypothesized high-angle normal faults	58
21	Reorientation of principal stress axes during the transition from compressional to extensional tectonism	62
22	Shear and normal stresses acting on a sliding block on a cohesionless plane	65
23	Variance of the stress ratio for reactivation (R) with reactivation angle (θ)	67
24	Variance of the coefficient of friction (μ) with reactivation angle (θ)	68
25	Schematic Mohr diagrams showing stress states for fault reactivation	70
26	Dip of listric normal faults at surface	76

LIST OF PLATES

Plate

- 1 Geologic map of faults along the west side of the
Bear River Range in northern Utah pocket
- 2 Structure cross sections of faults along the west side of the
Bear River Range in northern Utah pocket
- 3 Schematic diagrams of the structural evolution of faults along
the west side of the Bear River Range in northern Utah pocket

ABSTRACT

Origins of Low-Angle Normal Faults
Along the West Side of the
Bear River Range in
Northern Utah

by

Jon E. Brummer, Master of Science
Utah State University, 1991

Major Professor: Dr. James P. Evans
Department: Geology

This paper presents new interpretations of two normal-slip, low-angle faults near Smithfield and Richmond, Utah. The faults have previously been interpreted as landslides, gravity slides, slide blocks, and depositional contacts. Recent work in the Basin and Range province allows new interpretations concerning the origins of the low-angle faults.

Working hypotheses used to interpret origins of the faults are classified as folded thrust fault, rotated high-angle normal fault, gravity slide, listric normal fault, and low-angle normal fault. Among these general categories are several subhypotheses. The evaluation of each hypothesis includes a description of the geologic requirements of the hypothesis, a comparison of field data to the requirements, and a conclusion regarding the hypothesis. Field maps, computer analyses of fault orientations, geophysical surveys, well logs, and published discussions of low-angle-fault origins provide the data base from which to derive conclusions.

The data best fit a low-angle-normal-fault hypothesis which states that low-angle normal faults in the study area represent a pre-Basin and Range style of extensional tectonism in which principal stress axes were in a transitional state between compressional tectonism and modern Basin and Range extensional tectonism. The northern low-angle normal fault formed as early as the late Eocene, followed by the southern low-angle normal fault in the early to middle Miocene (?). Episodes of high-angle normal faulting followed formation of the southern low-angle normal fault. The faulting history indicates that two distinct stress states existed resulting in two different styles of normal faults.

Schematic cross-sectional reconstructions based on two other low-angle-normal-fault subhypotheses and the gravity-slide subhypothesis 2 indicated that these subhypotheses could be valid. However, the two low-angle-normal-fault subhypotheses cannot account for transitional stress states, and the gravity-slide subhypothesis explains only the southern low-angle normal fault. On the basis of geologic simplicity, the best hypothesis should explain both low-angle faults because of their similarities in deformation, orientation, and age.

The applicability of the low-angle-normal-fault model to the rest of the Basin and Range province is somewhat limited. Too many local variables are involved to allow one model to be regionally applied.

(112 pages)

INTRODUCTION

PROBLEM STATEMENT

Faulting in the Basin and Range province has traditionally been characterized as slip along steeply dipping normal faults. However, evidence from recent mapping shows that low-angle faults with apparent normal-slip displacement are also prevalent in diverse settings throughout the Basin and Range region (Anderson, 1971; Armstrong, 1972; Wernicke, 1981; Dickinson and others, 1987). Previous geologists who studied Basin and Range geology (e.g., Curry, 1954; Baker, 1964) considered many of these faults, with younger rocks in the hanging wall over older rocks in the footwall, to be faults produced during compressional tectonism. In contrast to earlier work, many geologists now believe that many of these low-angle faults are related to Tertiary extension (Armstrong, 1972).

Even though many of the low-angle faults are believed to be extensional tectonic features, the detailed kinematics involved in their origin are still debated. Several geologists have proposed models to explain the origins of the low-angle normal faults (see Previous Work section). Structures in Nevada and central to southern Utah are examples on which most of the models were based. This study is based on examples along the western margin of the Bear River Range near Richmond and Smithfield, Utah (Fig. 1). This study is important because of 1) a different geologic setting from areas with previously reported examples of low-angle normal faults, 2) a scarcity of published literature concerning the origin of low-angle faults in northern Utah, 3) the possibility of forming new models or hypotheses to explain the origins of low-angle faults in northern Utah, and 4) well-exposed structures that will aid in the unravelling of the extensional history of eastern Basin and Range faulting in northern Utah. Results from this study

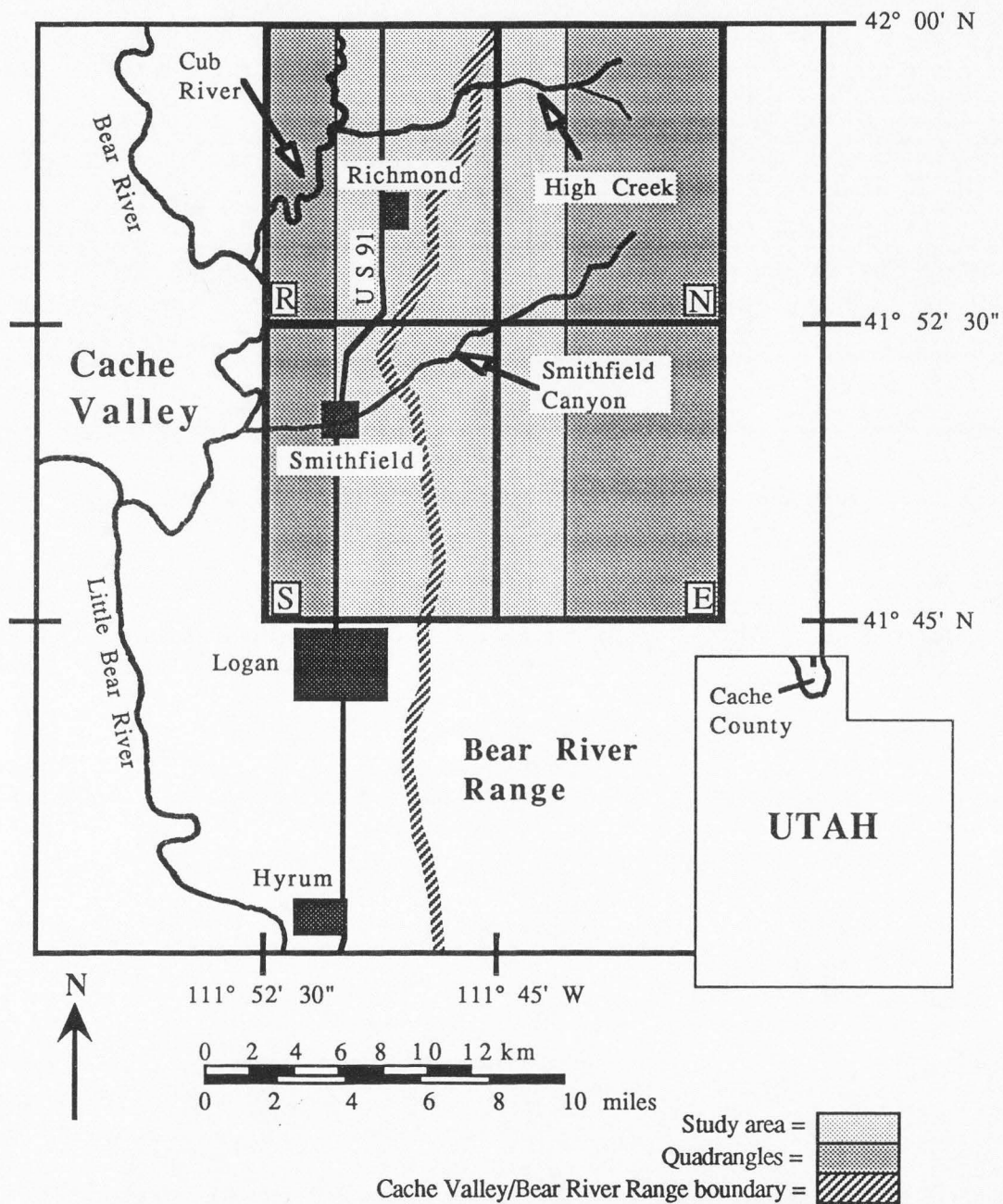


Figure 1. Index map of northern Utah. Location of the study area outlined in parts of the Mt. Elmer (E), Naomi Peak (N), Richmond (R), and Smithfield (S) quadrangles.

will also provide future geologists with a basis from which to solve other problems related to northern Utah geology.

Previously proposed origins of low-angle faults in the study area are landslides (Mendenhall, 1975; Dover, 1987), slide blocks (Galloway, 1970), and gravity slides on preexisting thrust-fault surfaces (Galloway, 1970; Sprinkel, 1979). Williams (1948) and Galloway (1970) described one of the low-angle faults as a depositional contact and not a fault as is concluded in this study. Bailey (1927) implied that low-angle faults were part of the normal-fault system that down faulted Cache Valley because the 30° to 35° dips of observed fault planes were similar to unmodified faceted spurs on the face of the range front. However, field data acquired during the present study allow new interpretations to be made concerning the evolution of the structures.

OBJECTIVES

The objectives of this study are to 1) provide descriptive and kinematic analyses of the faults located in the study area, 2) explain the origins of the low-angle faults in the project area by using published models or by formulating new models on the basis of descriptive and kinematic analyses, and 3) evaluate the regional applicability of the model that explains the origins of the faults in the study area.

PREVIOUS WORK

Geologic investigations in the project area include works by Bailey (1927), Williams (1948, 1958), Galloway (1970), Mendenhall (1975), Dover (1985, 1987), McCalpin (1989), and Brummer and McCalpin (1990). These investigations contain descriptions of stratigraphy, general structural geology, and surficial geology.

Many geologists have studied low-angle faulting in the Basin and Range province. Curry (1938, 1954), Drewes (1959), and Hunt and Mabey (1966) investigated low-angle faults known as turtleback faults at Death Valley, California, but

debated the origin of the structures. Varying explanations have been proposed for low-angle faults in Nevada and western Utah. Longwell (1945) provided one of the earliest discussions on the formation of low-angle normal faults with surface dips of 25° or less. He stated that low-angle normal faults in the Desert Range and Virgin Mountains in southern Nevada dipped inward toward the axis of a large anticline and that the faults formed concurrently with the growth of the anticline. Longwell also demonstrated that some of the normal faults exhibit a listric geometry. Anderson (1971) examined three possible causes for low-angle normal faults in southeastern Nevada near Longwell's study area. Anderson's hypotheses for the origin of the faults were 1) gravity sliding from an arch, 2) directed compression, which was suggested by Longwell (1945), and 3) crustal distension due to rising and spreading magma. Anderson (1971) concluded that the faults formed by crustal distension due to rising magma in the Tertiary Period. Young (1960) interpreted low-angle normal faults in the Schell Creek Range of eastern Nevada to be gravity slides that formed between episodes of high-angle normal faulting. Armstrong (1972) showed through geometric and chronologic analyses that, in the Sevier orogenic belt, many low-angle faults once thought to be compressional features were actually Tertiary extensional features. Armstrong (1972) used six models to explain many younger-on-older faults in the hinterland of the Sevier orogenic belt. Hose and Danes (1973) suggested that low-angle faults with normal-slip displacement form by differential uplift and gravity sliding. Wernicke (1981) suggested that low-angle normal faults root into a single, nearly horizontal fault zone. Dickinson and others (1987) described a set of range-bounding, low-angle normal faults located in southeast Arizona and suggested that the faults were listric faults or rotated normal faults. Beutner (1972), Burton (1973), Gray (1975), McDonald (1976), Sprinkel (1979), Mitchell and McDonald (1986), and Mattox and Weiss (1987) described Tertiary reactivation of Mesozoic thrust faults and hypothesized that thrust faults provided a plane of weakness

on which the hanging-wall block slid down the gradient under the influence of gravity. Burton (1973) and Gray (1975) examined several low-angle normal faults in the Malad Range near Clarkston Mountain on the west side of Cache Valley. Wise (1963) and Moores (1968) presented gravity-sliding models in different settings in Wyoming and Nevada, respectively.

For the low-angle faults in the study area, geologists have proposed varying origins. Galloway (1970) and Sprinkel (1979) believed that some of the low-angle normal faults formed by reverse gravitative movement on preexisting thrust faults. Galloway (1970) described a "west-dipping surface" formed on quartzite by a thrust fault. Her interpretation was that a preexisting, west-dipping thrust fault with an average surface dip of 22° accommodated later westward gravitative sliding. After westward sliding, the Salt Lake Formation was deposited on the exposed fault surface and hanging-wall block. Galloway (1970) included the fault planes of the two low-angle normal faults under investigation in this report as part of that west-dipping surface. Sprinkel (1979) supported Galloway's interpretation of reverse gravitative movement. The west-dipping surface described by Galloway is the same feature that Bailey (1927) described as a normal fault between Tertiary conglomerate and older quartzite. Bailey (1927) connected the low-angle normal fault with what is now known as the eastern splay of the East Cache fault (fault E, Plate 1). He attributed the presence of Tertiary conglomerate at the surface in the hanging wall to diminishing displacement northward along the fault. He explained that no Tertiary rocks were at the surface at the range front near Logan because displacement along faults was great enough that the hanging-wall block was placed far enough down relative to the present surface so that the Tertiary rocks were completely buried by later sediments. Bailey's explanation appears to be correct, although he did not explain the reasons for decreased displacement. Throw on low-angle normal faults is not so great as throw on high-angle

normal faults with the same heave (Fig. 2). Low-angle normal faults north of Green Canyon did not displace the Tertiary conglomerates far enough to allow complete burial by later sediments, whereas the high-angle normal faults south of Green Canyon did displace the conglomerates far enough. Mendenhall (1975) ascribed a landslide origin to one of the low-angle normal faults in the study area.

Peterson and Oriel (1970), Stanley (1972), Smith and Bruhn (1984), Zoback (1983), Mabey (1985, 1987), Evans (1990), and Evans and Oaks (1990) have used a variety of geophysical data to construct cross sections depicting the subsurface structure of the Cache Valley area. Their interpretations aid in determining the origins of the low-angle faults investigated in this study by providing depths to faults, subsurface geometry, the form of sediments above faults, and the amount of displacement along fault zones.

GEOGRAPHIC AND GEOLOGIC SETTINGS

The study area is in northern Cache County, near the towns of Richmond and Smithfield, Utah (Fig. 1). The area encompasses the western margin of the Bear River Range and the eastern edge of Cache Valley between west longitudes $111^{\circ} 42' 30''$ and $111^{\circ} 50'$ and between north latitudes $41^{\circ} 45'$ and $42^{\circ} 00'$. Low foothills near Richmond mark the transition from the rather flat valley floor in the west to the steep range front in the east. The foothills narrow southward in the field area and end between Smithfield and Logan, Utah. These foothills have important structural implications that will be discussed later in the report. Most of the land is privately owned and is used for growing crops and grazing cattle. The eastern margin of the study area is within the Cache National Forest in the Bear River Range. Access to much of the area is by paved, gravel, or dirt roads that connect to U.S. Highway 91 at the west edge of the study area. Horse trails and foot trails in the larger canyons and hollows furnish access to the higher

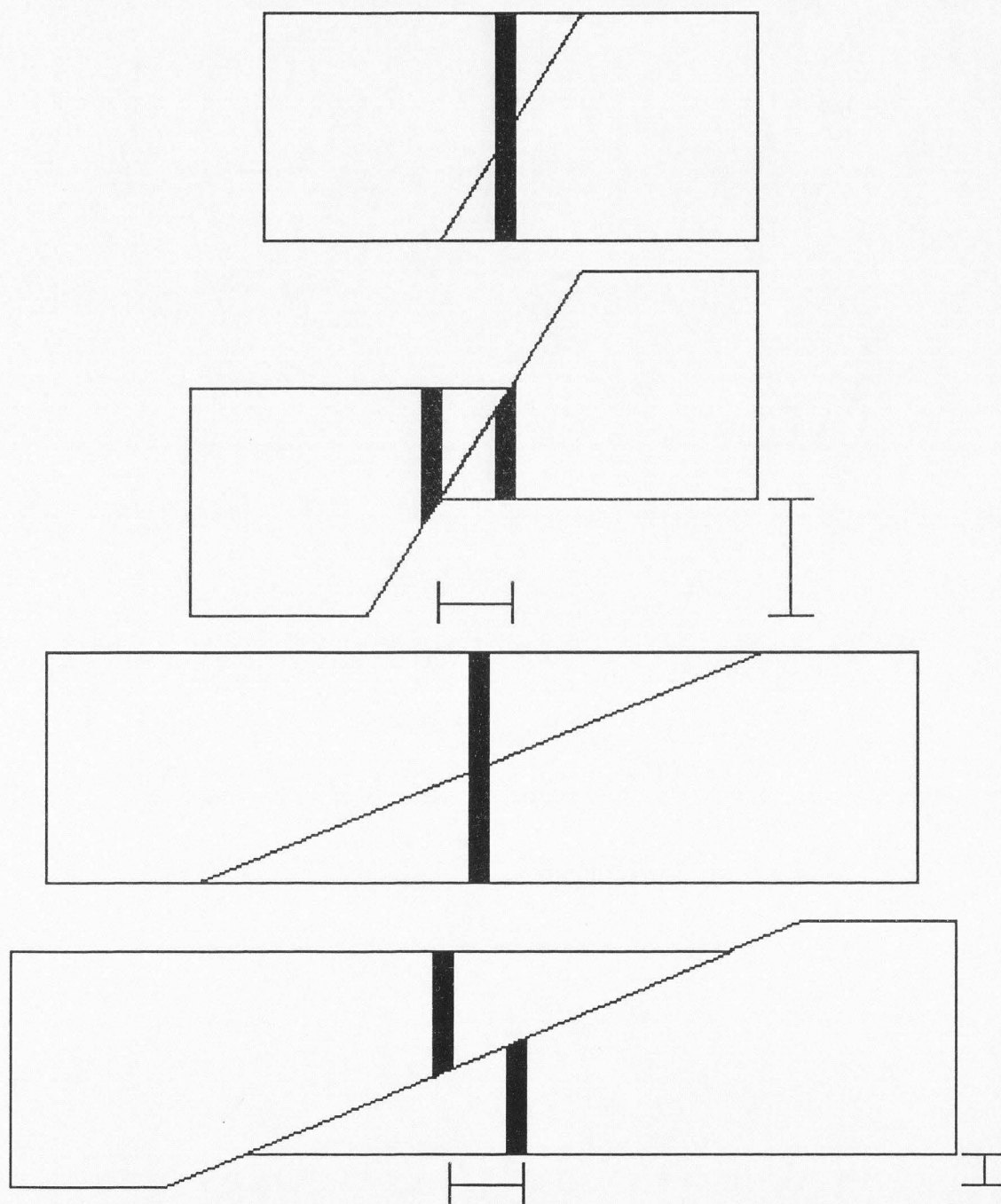


Figure 2. Block diagrams illustrating the differences in amount of throw due to the angle of a fault. Heave is equal in both cases, but throw varies greatly.

reaches of the Bear River Range. Altitudes range from 1356 m to 2865 m. The four 7.5-minute topographic quadrangles involved in the study are Smithfield and Mt. Elmer, Utah, and Naomi Peak and Richmond, Utah-Idaho (Fig. 1).

The study area is in the eastern Basin and Range physiographic province, near the boundary with the Middle Rocky Mountain province. Best and Hamblin (1978) suggested that the physiographic boundary set by Fenneman (1931, 1946) does not correlate with the geological and geophysical boundary. Best and Hamblin (1978) explained that a boundary determined by structural and geophysical properties would be at least 50 km farther east. Structures in the study area are related to two regional events: compression, folding, and thrust faulting associated with the Jurassic to early Tertiary Sevier Orogeny (Armstrong, 1968) and normal faulting which may have started as long as 30 million years ago in the province (Zoback and others, 1981). Basin and Range extensional tectonism continues today in northern Utah (Westaway and Smith, 1989).

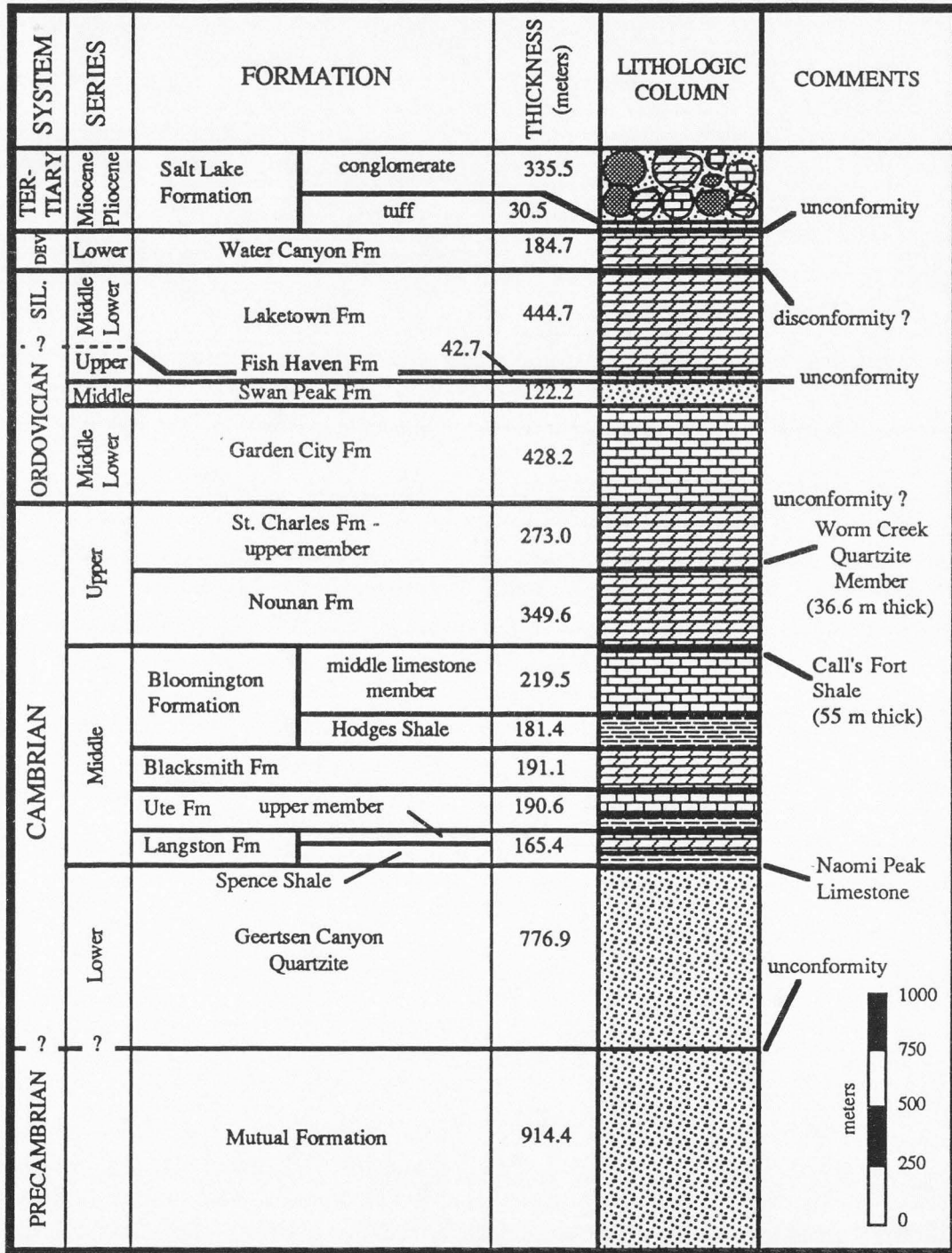
The stratigraphic sequence of bedrock along the western margin of the Bear River Range in the study area consists of Precambrian quartzites and argillites; Cambrian limestones, dolostones, shales, and quartzites; Ordovician limestones, dolostones, shales, and quartzites; Devonian dolostones and sandstones; Silurian dolostones; and Tertiary conglomerates and tuffs (Fig. 3). Surficial deposits of Quaternary age cover the valley floor and mantle many of the bedrock units at the range front. Precambrian and Paleozoic rocks make up the western limb of the Logan Peak syncline in the Bear River Range, whereas the Tertiary Salt Lake Formation forms low foothills at the range front.

Precambrian and Paleozoic rocks were thrust eastward approximately 104 km from their original site of deposition (Levy and Christie-Blick, 1989) and were folded into the broad, gently south-plunging Logan Peak syncline (Williams, 1948). Normal faulting ensued in the Tertiary and eventually produced the present-day Basin and Range

Figure 3. Generalized stratigraphic section of bedrock exposed in the study area.

Stratigraphy adapted from previous reports:

1. Salt Lake Formation - Mendenhall (1975)
2. Water Canyon Formation - Logan Canyon, Taylor (1963)
3. Laketown Formation - Logan Canyon, Budge (1966)
4. Fish Haven Formation to
Garden City Formation - Green Canyon, Williams (1948) and
Galloway (1970)
5. St. Charles Formation - High Creek, Maxey (1941, 1958)
6. Nounan Formation - High Creek, Gardiner (1974)
7. Bloomington Formation - High Creek, Maxey (1941, 1958)
8. Blacksmith Formation - High Creek, Hay (1982)
9. Ute Formation - High Creek, Deputy (1984)
10. Langston Formation - High Creek, Buterbaugh (1982)
11. Geertsen Canyon Quartzite - Birch Canyon, Galloway (1970)
Previously Brigham Formation
12. Mutual Formation - Mendenhall (1975)



topography of the area. During the Quaternary, Lake Bonneville occupied the valley and formed shoreline and deltaic deposits at several levels along the range front.

Since the recession of the lake, alluvial erosion and deposition have been the dominant geologic processes. Seismicity in the area indicates that the normal faults are still active (Westaway and Smith, 1989).

METHODS

FIELD MAPPING

The majority of the field mapping was conducted from May to October, 1988. Subsequent field checking of the map continued through October, 1989. The purpose of field mapping was to gather data for descriptive and kinematic analyses of normal faults. Data needed for these analyses were strikes and dips of fault surfaces and adjacent bedding, types of rock deformation in fault zones, patterns of contacts, and descriptions and distribution of rock units. Because the focus of this study was normal faults, the features mapped and described in detail were the range-front faults, the low-angle normal faults, and the rock units involved directly with the low-angle normal faults. Additional data for the structural and sedimentological setting were taken from the work of Galloway (1970), Mendenhall (1975), Dover (1987), and McCalpin (1989). The field data were also used to compile a geologic map of the Richmond quadrangle for the Utah Geological and Mineral Survey (Brummer and McCalpin, 1990)

Parts of the Richmond, Naomi Peak, Mt. Elmer, and Smithfield quadrangles served as 7.5-minute topographic bases on which to record map data. The low-angle normal fault in the Smithfield quadrangle was mapped at a scale of 1:12,000, whereas structures in the Richmond quadrangle were mapped at a scale of 1:24,000.

Aerial photographs of various scales and types provided a basis for mapping. Stereo coverage was obtained for the range front, and field data were recorded on mylar placed on the photographs. Black and white photographs and color photographs at scales of 1:20,000 and 1:15,000, respectively, supplied the most geological information. Infrared high-altitude photographs at a scale of 1:58,000 permitted tracing of trends and patterns of faults and bedding over large areas. Lineaments representing possible faults were mapped on low-sun-angle photographs of the study area. Low-sun-angle photographs provide shadows and high contrast so that structural and

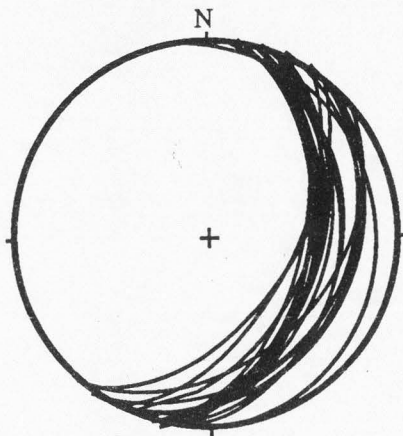
geomorphic surface lineaments may be more readily seen (Cluff and others, 1974). These photographs were taken in the morning during the summer at a scale of approximately 1:12,000. Because of the time of day and year that the photos were taken, only west-facing scarps show up.

Orthophoto quadrangles at a scale of 1:24,000 were used in transferring data from the photographs to the topographic base maps. Data were easily and accurately transferred using the orthophotos because the orthophotos are rectified aerial photographs of 7.5-minute quadrangles.

Additional equipment used in the field consisted of a Brunton compass, altimeter, shovel, rock hammer, hand lens, and a staff ruled in meters.

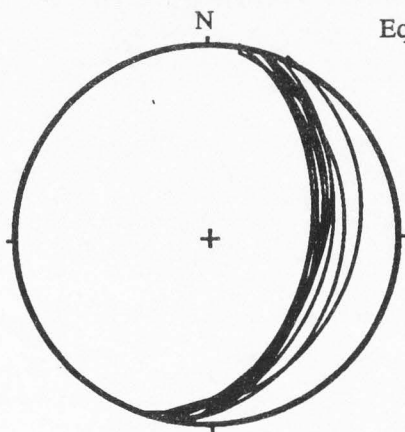
COMPUTER ANALYSES

An Apple Macintosh computer system and software were used to perform graphical analysis of map data. Equal-area, lower-hemisphere stereographic projections were generated using Stereonet, version 4.1, written by Richard W. Allmendinger. Stereograms presented in this study show orientations of bedding planes and faults. The orientations are input as strike and dip measurements (e.g., N 10 E, 35 W) and are displayed as great circles. The first stereograms show similarities among the bedding in the various units of the western flank of the Logan Peak syncline (Fig. 4). The second application of stereonets involved the manipulation of great circles of bedding and faults to show present and restored orientations. A second method of graphical data analysis involved the generation of three-dimensional views of fault traces. The three-dimensional views aid in interpreting relationships among the various high-angle and low-angle normal faults in the study area. This three-dimensional analysis utilized a program called MacSpin, version 2.0, which was produced by D² Software, Inc. of Austin, Texas. This program allows rotation of graphical plots of three-dimensional



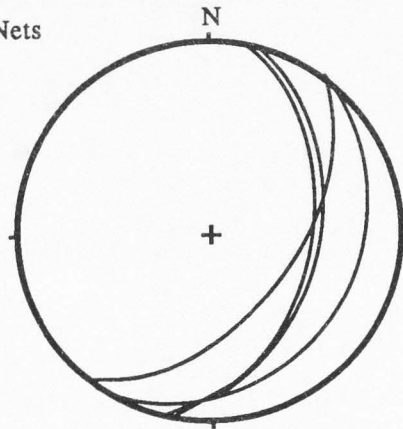
a. composite of all units

Figure 4. Lower-hemisphere stereograms showing great circles of bedding in the west limb of the Logan Peak syncline. Stereograms generated from strike and dip measurements (e.g., N10°E, 30°SE). Rock units included are Mutual Formation, Geertsen Canyon Quartzite, St. Charles Formation, and Garden City Formation.

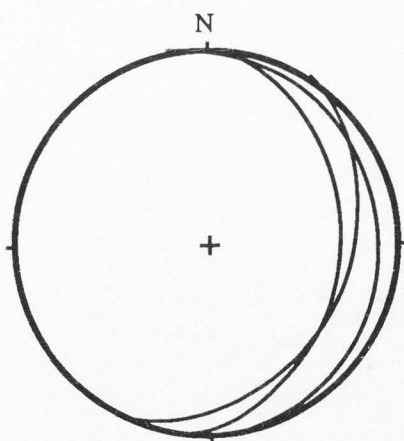


b. Mutual Formation

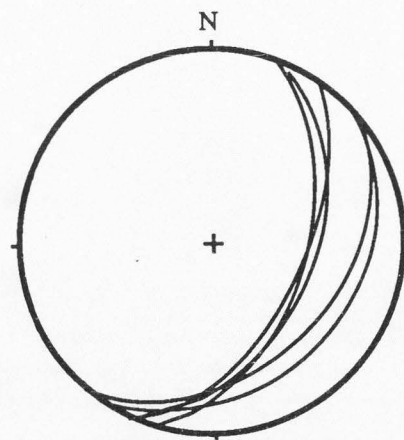
Equal Area Nets



c. Geertsen Canyon Quartzite



d. St. Charles Formation



e. Garden City Formation

data in order to give various vantage points in three-dimensional space. For this study, this program created three-dimensional views of the high-angle and low-angle normal-fault traces. An x-y-z coordinate system provided a framework from which to collect data. The x-y scale (x = north, y = west) was plotted on graph paper that was then placed over the map. Fault traces were then drawn on the graph paper. From the graph paper, x-y coordinates of points along the fault traces were read and recorded. Coordinates for corresponding points on the z axis (elevations) were scaled proportionally from topographic contours and recorded. The data were input, displayed as points, and rotated to show map views, cross-sectional views, down-dip projections of faults, and various oblique views (e.g., Fig. 5).

GEOPHYSICAL SURVEYS

Published and proprietary geophysical data used in this study consist of gravity and seismic-reflection surveys. Resistivity and magnetic survey data also exist for the study area (see Stanley, 1972; Mabey, 1985), but gravity and seismic survey data provide the most useful information for structural interpretations in this study.

Peterson and Oriel (1970), Stanley (1972), and Mabey (1985) performed gravity studies in Cache Valley. Regional studies by Zoback (1983) and Mabey (1987) included interpretations of gravity data from Cache Valley. These studies provided interpretations on basin form, thickness of Cenozoic basin fill, and near-surface locations of concealed high-angle faults. This information was presented in maps and cross sections.

Data from seismic surveys across Cache Valley allowed interpretations to be made concerning subsurface structure, including fault geometry and rock or sediment type (Stanley, 1972; Smith and Bruhn, 1984; Evans, 1990; Evans and Oaks, 1990).

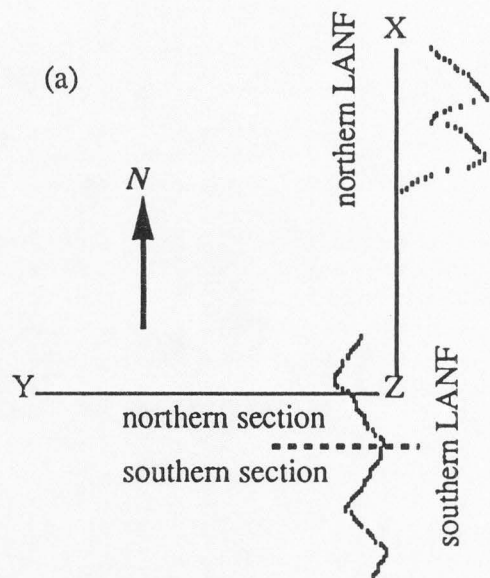
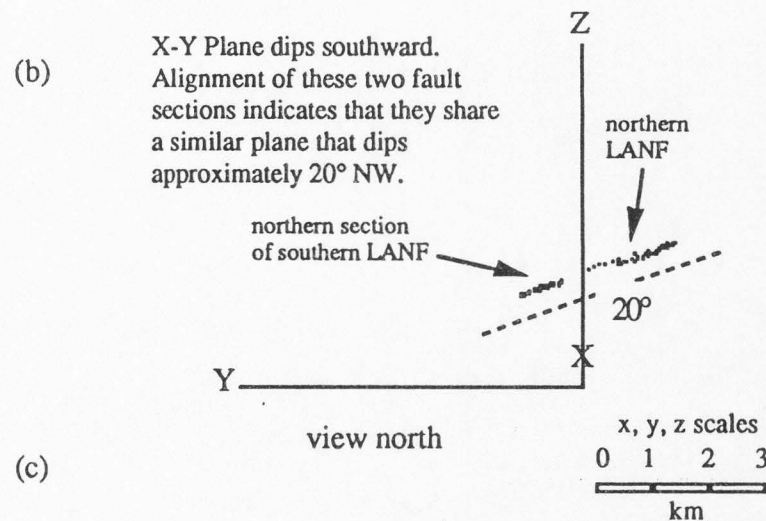
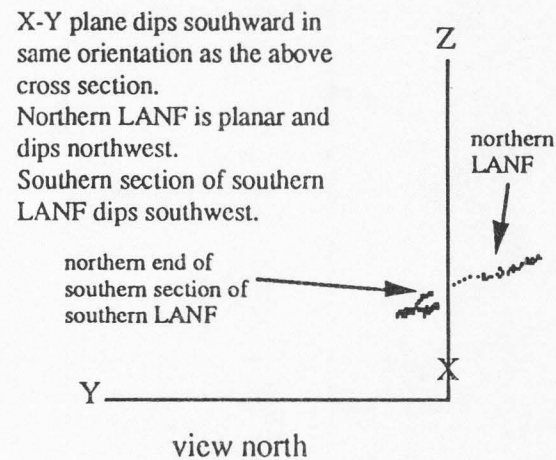


Figure 5. Three-dimensional plots of southern and northern low-angle-normal-fault traces. (a) Map view. (b) Oblique cross-sectional view, northern section of southern low-angle normal fault (LANF). (c) Oblique cross-sectional view, southern section of southern LANF. Views in (b) and (c) indicate that the faults may be parts of a common surface. The surface appears to have a convex shape. Rotation about the Y axis yielded the views in (b) and (c). X-Y plane is at an elevation of approximately 100 m above sea level.



(c)

X-Y Plane dips southward. Alignment of these two fault sections indicates that they share a similar plane that dips approximately 20° NW.



X-Y plane dips southward in same orientation as the above cross section. Northern LANF is planar and dips northwest. Southern section of southern LANF dips southwest.

WELL-LOG DATA

Petroleum drill-hole information was taken from published well logs (Petroleum Information, see References Cited section) and from drill cuttings that were logged for this study (see Appendix section). Information from these sources constrained the amount of offset along normal faults and aided in the determination of stratigraphy and thicknesses of Tertiary and Quaternary units in the basin. Well samples obtained from the Utah Geological and Mineral Survey (UGMS) sample library were logged for two wells in Cache Valley (Amoco Production Company, #1 Lynn Reese, S17, T12N, R1E; and North American Resources, #7-10 Hauser Farms, S10, T13N, R1W) (Fig. 6).

Water-well logs from the Office of the State Engineer in Logan show Quaternary and Tertiary stratigraphy. Geological conclusions from water-well logs are difficult to make because the logs are usually compiled by water-well drillers, not geologists. Terminology used among well drillers is not consistent, nor is it geologically precise.

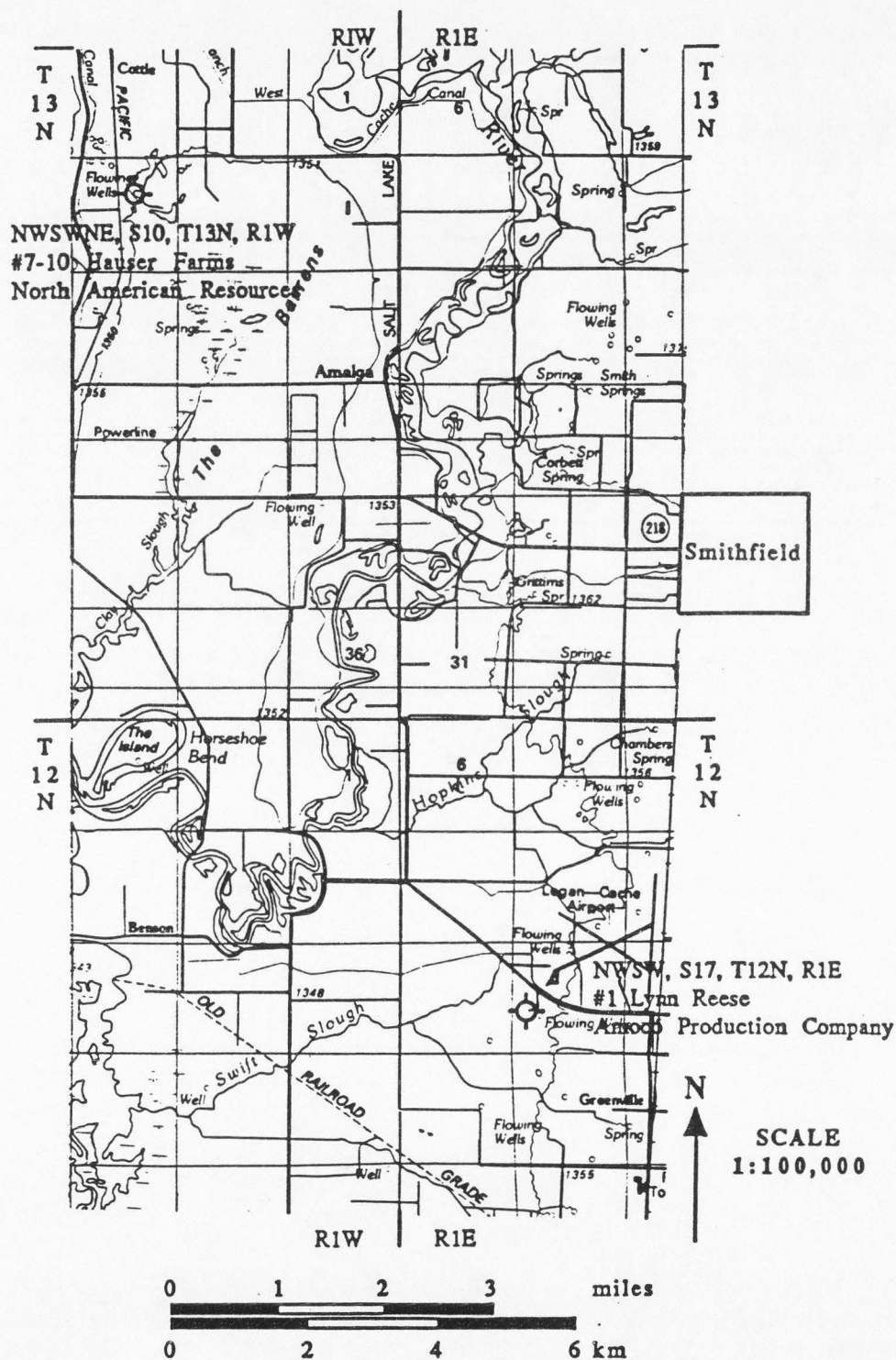


Figure 6. Locations of wells logged for this study. Both wells were drilled and abandoned. Well cuttings from these wells provided information on Cenozoic stratigraphy and depth to bedrock.

DESCRIPTIVE ANALYSIS

Descriptive analysis forms the foundation for discussions and interpretations. The fundamental data described herein are based on direct observation in the field, subsurface exploration including geophysical monitoring and well logging, and laboratory examination of rock specimens. Some of the data presented on the map (Plate 1) are not necessary to understand the structural problems in this report, but are included mainly for map continuity.

BEDROCK STRATIGRAPHY

Five different bedrock formations are directly involved in the low-angle faults. One formation is Tertiary, whereas the other four range from late Precambrian to Early/Middle Ordovician. The units are described according to rock name, color, texture, mineralogy, primary sedimentary structures and secondary rock deformation. Maxey (1941, 1958), Williams (1948), Taylor (1963), Budge (1966), Galloway (1970), Gardiner (1974), Mendenhall (1975), Buterbaugh (1982), Hay (1982), and Deputy (1984) measured stratigraphic thicknesses of units in, or adjacent to, the study area. Because of their work, no new sections were measured for this study.

Mutual Formation

The Mutual Formation, named by Crittenden and others (1952), is a medium- to coarse-grained (1.5 to 0.5 phi) quartzite with numerous small cross-bed sets. Color of the quartzite varies among purple, red, and white; purple-and-white-banded quartzite is common. Mineralogy of the sand-sized grains is quartz. The quartzite is micaceous in places. Joints, fractures, and slickensides are present in the Mutual Formation. Throughout the formation, a conjugate set of joints is oriented generally N83°E, 75°NW and N55°W, 85°SW (orientations given as strike and dip). Spacing of joints and

fractures ranges from 3 cm near fault contacts to as much as 61 cm elsewhere. A slickenside surface striking N28°W was measured on the north side of Smithfield Canyon at an elevation of 1700 m. The surface is undulating with southwestward dips varying from 47° to 0° (horizontal). Other slickenside surfaces in the quartzite on the north side of Smithfield Canyon strike approximately north and dip west at moderate angles (30° to 35°). The fractured quartzite and slickenside surfaces at this location indicate the northward continuation of a thrust fault mapped by Galloway in the Smithfield quadrangle (Plate 1). Bedding throughout the formation is from 8 cm to nearly 91 cm thick and is oriented generally N15°E, 41°SE (Fig. 4b). Interbedded with the quartzite are thin beds of conglomerate and argillite. The conglomerate is composed of rounded pebbles (-1.0 to -6.0 phi) of white quartz and red chert in a quartzite matrix. The lateral extent of the conglomeratic facies was not determined. Thin beds (<30 cm) of green to dark purple argillite are scattered in the upper part of the formation. The dark purple argillite is micaceous. Exposed thickness of the Mutual Formation is approximately 914 m in the southeast corner of the Richmond quadrangle (Mendenhall, 1975). This measurement is not of a complete section because the lower portion of the unit is not exposed. Strike and dip measurements near the upper contact with the Geertsen Canyon Quartzite indicate that the contact may not be conformable in the field area. According to Crittenden and others (1971), near Huntsville, Utah, a thin unit, the Browns Hole Formation, separates the Mutual Formation from the Geertsen Canyon Quartzite. The Browns Hole Formation is not recognized in the study area. The age of the Mutual Formation is late Precambrian (Crittenden and others, 1952). Recent authors have indicated a Late Proterozoic age (Danzl, 1982; Dover, 1985). However, the source of that age was not stated; therefore, late Precambrian is the age used in this report.

Geertsen Canyon Quartzite

The Geertsen Canyon Quartzite, named by Crittenden and others (1971), consists of olive, tan, white, orange-pink, and pink, coarse-grained (1.0 to 0.5 phi) quartzite with shale interbeds near the top of the unit where the formation intertongues with the Langston Formation. Conglomerate in the quartzite is composed of well-rounded pebbles of red chert; and white, gray, and pink quartz. The base of the conglomeratic beds is a sharp boundary with the quartzite, whereas the upper part of the conglomeratic beds is largely gradational with the quartzite. Bedding is difficult to discern in most places. Where seen, bedding reaches 1 m thick. The average strike and dip of bedding is N25°E, 41°SE (Fig. 4c). Thickness of the unit is approximately 777 m (Galloway, 1970). The Geertsen Canyon Quartzite, along with the underlying Mutual Formation, forms steep slopes and cliffs on the west flank of the Bear River Range (Plate 1). Crittenden and others (1971) assigned a Precambrian to Early (?) Cambrian age to the formation. The Geertsen Canyon Quartzite has been referred to as the Brigham Formation in northern Utah (Williams, 1948; Galloway, 1970; Mendenhall, 1975). Crittenden and others (1971) provided a discussion on the change in nomenclature.

The map unit pC-C is undivided quartzite. Jumbled blocks and slabs of Geertsen Canyon and Mutual quartzite compose the unit. The unit is exposed west of the range front in small outcrops. The chaotic nature and the location of the outcrops suggest that they are blocks that broke from bedrock faces farther to the east (Plate 1).

St. Charles Formation

The Upper Cambrian St. Charles Formation consists of an upper member of gray to dark gray, fine- to medium-crystalline dolostone and a lower member of white to yellow, calcareous quartz arenite; shale; and dolostone called the Worm Creek Member

(Richardson, 1913). The upper dolostone has a sugary texture on weathered surfaces and a fetid smell when freshly broken. In the hanging-wall block of the northern low-angle normal fault (LANF), brecciation disrupts bedding at most outcrops. Strike and dip measurements of intact bedding range from N11°W, 12°NE to N31°E, 32°SE (Fig. 4d). Within the hanging wall of the northern LANF, the formation is overlain by the Garden City Formation. Good exposures of the dolostone are around the base of Crow Mountain and on the ridges directly north and south of Nebo Creek in the hanging wall of the northern LANF (Plate 1, east end of section A-A'). North of Crow Mountain are two small outcrops of brecciated dolostone. These outcrops are believed to be blocks that slid down slope from outcrops in the hanging wall of the LANF.

Garden City Formation

The Lower Ordovician Garden City Formation is a medium to dark gray, micritic to medium-crystalline limestone. The basal portion of the unit is siltier than the upper part of the section and contains intraclasts of micritic limestone. Black chert and tan stringers of silt are scattered throughout the unit, which is weakly to moderately vuggy. Bedding is thin (5 to 20 cm) and has a general strike and dip of N32°E, 44°SE (Fig. 4e). Brecciation in the Garden City Formation is confined to specific layers or beds. In places, the brecciated beds are in sharp contact with undeformed beds of limestone. The contact between the Garden City Formation and the underlying St. Charles Formation is found at Crow Mountain and on the ridge tops north and south of Nebo Creek at elevations between 2100 m and 2150 m in the hanging wall of the northern LANF (Plate 1). North of Crow Mountain, near the brecciated blocks of St. Charles dolostone, are two outcrops of brecciated limestone (Plate 1). The blocks have the same origin as do the blocks of St. Charles Formation dolostone.

Salt Lake Formation

Wasatch Formation and Salt Lake Formation are common terms for Tertiary strata in northern Utah (Williams, 1948; Smith, 1953; Adamson, 1955; Adamson and others, 1955). However, Oviatt (1986) pointed out that there are correlation problems involved with the two formations as they are commonly described. Oviatt (1986) avoided the formal terms Wasatch Formation and Salt Lake Formation and used genetic nomenclature for Tertiary rocks in northern Utah. For this report, the formation names are retained, but the member designations of Adamson and others (1955) are abandoned. In place of formal member names, lithologic terms are used to designate the mappable units of the Tertiary formations.

Tertiary sedimentary rocks of importance in this study consist of conglomerates and tuffaceous claystones. Two conglomerate units are differentiated on the basis of structural position: the Wasatch Formation (Tw) and the Salt Lake Formation (Tsl). The older conglomerate, Wasatch Formation, formed unconformably atop the Logan Peak syncline before offset on normal faults (Williams, 1948). The Wasatch Formation is not exposed in the study area, but is present to the east in the Bear River Range (Dover, 1987) and beneath the valley floor covered by later sediments (see Appendix section). The younger conglomerate, Tslc, formed in response to tectonic uplift during normal faulting as evidenced by Tslc that was deposited on the west side of the Bear River Range fault block. Salt Lake Formation conglomerate is not found atop the syncline (Dover, 1987). The tuffaceous unit, Tslt, which consists of lacustrine deposits, appears to interfinger extensively with Tslc along the east side of Cache Valley. Formal stratigraphic nomenclature is not used to describe the units of the Salt Lake Formation. Only two units are recognized at the surface and in drill holes. Conglomerate and tuff interfinger throughout the vertical extent of the formation (see

Appendix section). Therefore, no direct correlation could be made to the members described by Adamson (1955) and Adamson and others (1955). Only the two units exposed in the study area, Tslc and Tslt, are described below.

Salt Lake Formation conglomerate is a thick, clast-supported conglomerate consisting of subrounded to well-rounded coarse sand to boulders in a tuffaceous, white to gray, sandy groundmass. Clasts in the conglomerate are green argillite; purple, white, red, and pink quartzite; brown to white sandstone; crystalline, weathered dolostone; black chert; oolitic and fossiliferous micritic limestone; and crystalline limestone. Clast composition varies from south to north in the study area. East of Smithfield, the conglomerate contains mostly gray carbonate clasts. As the outcrops are traced northward, quartzite clasts become more abundant in the conglomerate (e.g., outcrops at Richmond Knoll). This gradational change reflects, in part, the change in Precambrian and Paleozoic parent material from south to north along the range front (Plate 1). In addition, Tslc probably contains reworked clasts of Tw. Clast composition also has structural importance concerning the southern LANF. Quartzite clasts are not present in Tslc that is structurally and topographically above the bedrock quartzite from Hyde Park Canyon to Smithfield Canyon. The absence of quartzite clasts in the hanging-wall conglomerate immediately adjacent to the quartzite/conglomerate contact, along with other evidence, supports the interpretation that the conglomerate is in fault contact with the underlying quartzite. Through a comparison of the parent material and the clast composition, one may approximate the amount of displacement along the southern LANF (see Kinematic Analysis section). Primary structures are difficult to find in the conglomerate. Where bedding planes can be found, the strike is generally N30°W to N60°W, and dips are 6° to 12° to either the east or the west. Imbricated cobbles in the conglomerate in Dry Canyon show a paleocurrent direction to the southwest. Large areas of colluvium, landslide deposits, and pediment gravel cover the

Salt Lake Formation (McCalpin, 1989; Brummer and McCalpin, 1990). These surficial units have not been included on Plate 1 so that the older structural features may be more easily seen and interpreted. Lack of marker beds hindered detailed stratigraphic analyses of the Salt Lake Formation conglomerates. Good exposures of the conglomerate exist along the north side of High Creek (SW/4, S5, T14N, R2E and NE/4, S7, T14N, R2E), on the slopes of Richmond Knoll (S13, T14N, R1E), on ridge tops north and south of City Creek (S31, T14N, R2E and S6, T13N, R2E), at the mouth of Oxkiller Hollow at an elevation near 1585 m (NE/4, S24, T14N, R1E), and in Dry and Hyde Park Canyons. A small travertine deposit is in the conglomerate at an elevation of 1945 m along an east-west ridge directly north of City Creek (S31, T14N, R2E) (Plate 1, point A). On the hanging-wall block of the northern LANF are remnants of Salt Lake Formation conglomerate. These remnants indicate that Tslc at one time covered the bedrock slopes at higher elevations. The age and topography of the conglomerate change northward across Smithfield Canyon possibly due to inferred high-angle normal fault D (Plate 1). The conglomerate at the surface in the hanging wall of fault D is thought to be younger than the conglomerate in the hanging wall of the southern LANF because the conglomerate on the north side of the canyon is interpreted to depositionally overlap fault D which, in turn, cuts the southern LANF. On the basis of topography, the conglomerate in the hanging wall of the southern LANF appears to be more resistant, and thus possibly older, than the conglomerate in the hanging wall of fault D.




The tuffaceous unit, which interfingers with Tslc, is a light tan to olive gray, tuffaceous claystone with beds and lenses of gray volcanic ash. The claystone is blocky when fresh, but becomes weakly fissile when weathered. This unit is poorly to moderately consolidated and is horizontally bedded. Northeast of Richmond Knoll, an exposure of this claystone contains gray ash in small pods (6 cm to 26 cm in diameter) that resemble rip-up clasts. Tslt is covered in most places, but three or four exposures

were mapped and sampled at the mouths of High Creek and Oxkiller Hollow and south of the mouth of Cherry Creek (Plate 1). The contact between the conglomerate and the tuffaceous unit is exposed in NW/4, S7, T14N, R2E along an irrigation canal. The conglomerate truncates horizontal beds of tuff in what appears to be a cut-and-fill structure (Fig. 7). Fault D may truncate Tslt near the mouth of Smithfield Canyon.

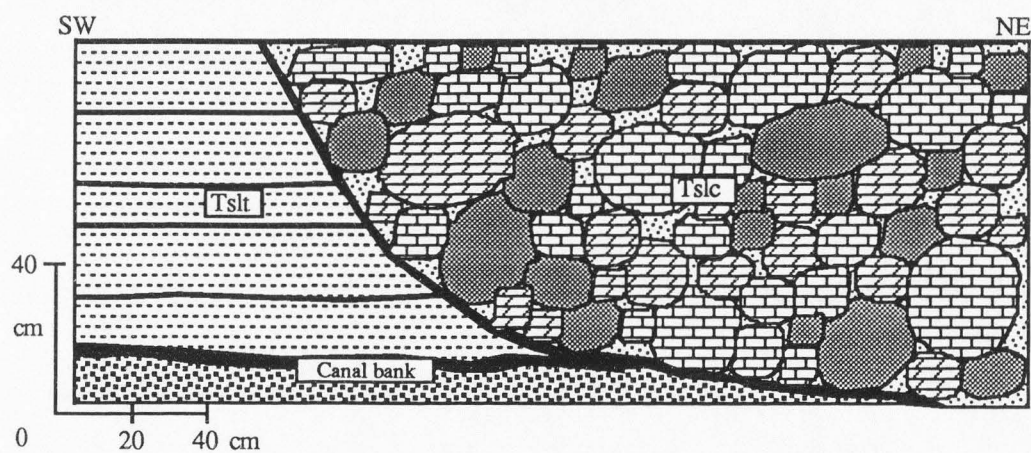
Mineralogical analyses were made on samples taken from outcrops and drill cuttings. Surface samples of claystone and ash were ground in a plate grinder, then were washed in water and decanted to remove the clay-sized particles. After the samples were dried and sieved, a magnetic separator was used to separate the different mineral constituents. Observation of the constituents with a binocular microscope showed that glass shards with stretched vesicles are the main components of the tuffaceous samples. Hornblende, biotite, magnetite, and muscovite exist in lesser amounts. Binocular-microscope analysis of drill cuttings from two Cache Valley wells (Fig. 6) indicated that marcasite, calcite, bitumen, and quartz are scattered throughout the tuffaceous unit, whereas clinoptilolite is restricted to a bed approximately 1060 m below the surface in the Amoco well (see Appendix section). Fossils scattered in the tuffaceous sediments are ostracods, gastropods, and pyritized pelecypods.

Exposed thickness of the Salt Lake Formation is approximately 366 m (Mendenhall, 1975). This thickness represents only a small part of the formation because the lower portion of the section is not exposed. A more accurate estimate of thickness of the formation was gained from well samples taken from a well near the Logan airport (Amoco Production Company, #1 Lynn Reese, S17, T12N, R1E) (Fig. 6 and Appendix section). The contact between Wasatch Formation and the younger Salt Lake Formation may be gradational through about 6 meters (-870 to -876 m). Tslc and Tslt are inferred to interfinger on the basis of the well logs and depositional environment. The contact between Tw and the younger Tertiary units is placed about

Figure 7. Contact between the tuff (Tslt) and conglomerate (Tslc) units of the Salt Lake Formation. Conglomerate on the right truncates horizontal beds of tuff on the left. Lithologies of clasts in the conglomerate member represented by symbols:

limestone  dolostone  quartzite 

Exposure is located along an irrigation canal in NW/4, S7, T14N, R2E.



2231 m below the surface of the valley where the deepest cuttings of Tslt were logged (see Appendix section). The contact between the Salt Lake Formation and the Quaternary deposits is placed about 335 m below the surface where the shallowest cuttings of Tslt were logged. Approximately 1896 m of Tslc and Tslt were logged between the contact with Quaternary sediments and the contact with the Wasatch Formation. The Wasatch Formation, about 110 m thick, rests unconformably on at least 125 m of purple quartzite in the drill hole.

The depositional environment of Tslc in the study area is interpreted to be alluvial fans consisting of material derived from adjacent fault-block highlands. The tuffaceous sediments of Tslt are water-laid volcanoclastic sediments deposited in a down-faulted lake basin. The two units interfinger near the basin-range boundary. Danzl (1982) presented similar interpretations of deposits in northern Cache Valley near Oneida Narrows, Idaho.

The Tertiary rocks in, and adjacent to, the study area range from Eocene to Pliocene. Williams (1964) used potassium-argon dates and paleontologic evidence to infer a Miocene to Pliocene age for the tuffaceous sediments (Tslt) of the Salt Lake Formation in Cache Valley (see also Yen, 1947; Brown, 1949). Tslt and Tslc are inferred to be coeval. In a more recent study, Danzl (1982) concluded that the age of similar sediments near Oneida Narrows is Miocene to Pliocene. The basal conglomerate of the Wasatch Formation is probably lower Eocene (Williams, 1948).

GEOLOGIC STRUCTURES

Structures in the area studied are the Logan Peak syncline, high-angle normal faults, low-angle normal faults, and thrust faults. These structures are described according to their geometries, orientations, map patterns, and field relationships.

Logan Peak Syncline

Precambrian and lower Paleozoic rock units strike north to northeast and dip moderately east in the west limb of the Logan Peak syncline. General strike and dip of beds in the west limb is N19°E, 40°SE (Fig. 4a). The axis of the syncline, which is east of the study area, plunges gently to the south to southwest (Williams, 1948). Due to the orientation of the fold relative to the range-front normal faults, progressively older rocks are exposed from south to north along the range front (Plate 1).

Normal Faults

A normal fault or normal-slip fault is defined as a fault with a hanging wall that moved down relative to the footwall. Generally, normal faults are thought to have average surface dips of 60° to 70°. In the past, faults with dips much less than 45° with normal dip-slip displacement have been assigned many names, but rarely has low-angle normal fault been used. For this report, low-angle normal fault is used to describe a normal-slip fault with a present surface dip of less than 45°. High-angle normal fault is commonly used in the literature to describe a normal-slip fault with a dip greater than 45°. This connotation for a high-angle normal fault will be used in this report also. Gravity fault was used in earlier literature to describe many normal faults. By using the term gravity fault, geologists implied that the primary driving force in normal faulting was gravity.

High-Angle Normal Faults. The pattern of high-angle normal faults in the study area is quite different from the pattern of normal faults to the south near Logan, Utah. The range-front fault zone east of Logan is a narrow zone (~1 km east to west) made up of one major fault, the East Cache fault (see McCalpin, 1989), whereas the range-front fault zone in the study area is a wide zone (~ 6.5 km east to west) made up of at least six high-angle normal faults (faults A-F, Plate 1). Near the mouth of Logan Canyon, the East Cache fault is west of the boundary between the rather flat valley floor and the

faceted bedrock spurs at the range front (Fig. 8). This distinct boundary changes farther to the north, east of Hyde Park, Utah. The range-bounding East Cache fault apparently bifurcates, distributing the displacement between at least two high-angle normal faults (faults E and F) (see McCalpin, 1989). Fault splay E created a boundary between the faceted Paleozoic bedrock and the low hills of Tertiary conglomerates and tuffaceous claystones, whereas fault splay F formed a scarp in Tertiary rocks against which Pleistocene Lake Bonneville formed a shoreline (Fig. 9).

The high-angle normal faults in the study area generally strike within a few degrees east or west of north. Dips of the faults are difficult to determine at the surface because of the Quaternary cover. However, surface dips were measurable where the faults had been exposed by trenching, excavation, or stream erosion. High-angle normal faults are exposed in gravel pits at the mouth of High Creek (NW/4, S13, T14N, R1E and NE/4, S23, T14N, R1E). These normal faults, which are in fault zone C, define graben 20 m to 30 m wide in Provo-level deltaic sediments (Fig. 10 and Fig. 11). Across the graben, the faults dip both east and west, and dips range from 55° to 75° . These faults formed late in the deposition of Provo-level deltas of Lake Bonneville (~13,000-14,000 years ago; McCalpin, 1989). Because the faults have no surface expression, they cannot be traced to the north or south.

Near the mouth of Dry Hollow, fault E appears to bifurcate (fault splays E_1 and E_2). Fault E_1 is exposed at the mouth of Dry Hollow in a prospect pit within carbonate bedrock approximately 10 m to 20 m east of the range front. Deformation in the fault zone of E_1 consists of limonitically altered carbonate gouge and breccia, and breccia with slickensides that are oriented $N9^{\circ}E$, $72^{\circ}NW$ and $N16^{\circ}E$, $80^{\circ}NW$. Small faults within the gouge zone have dips of 35° to 45° west and strikes that are near north. Hot fluids apparently moved along the fault zone because porous, tufa-like deposits of calcium carbonate exist in the fault zone. Fault E_2 , west of E_1 , is at the face of the

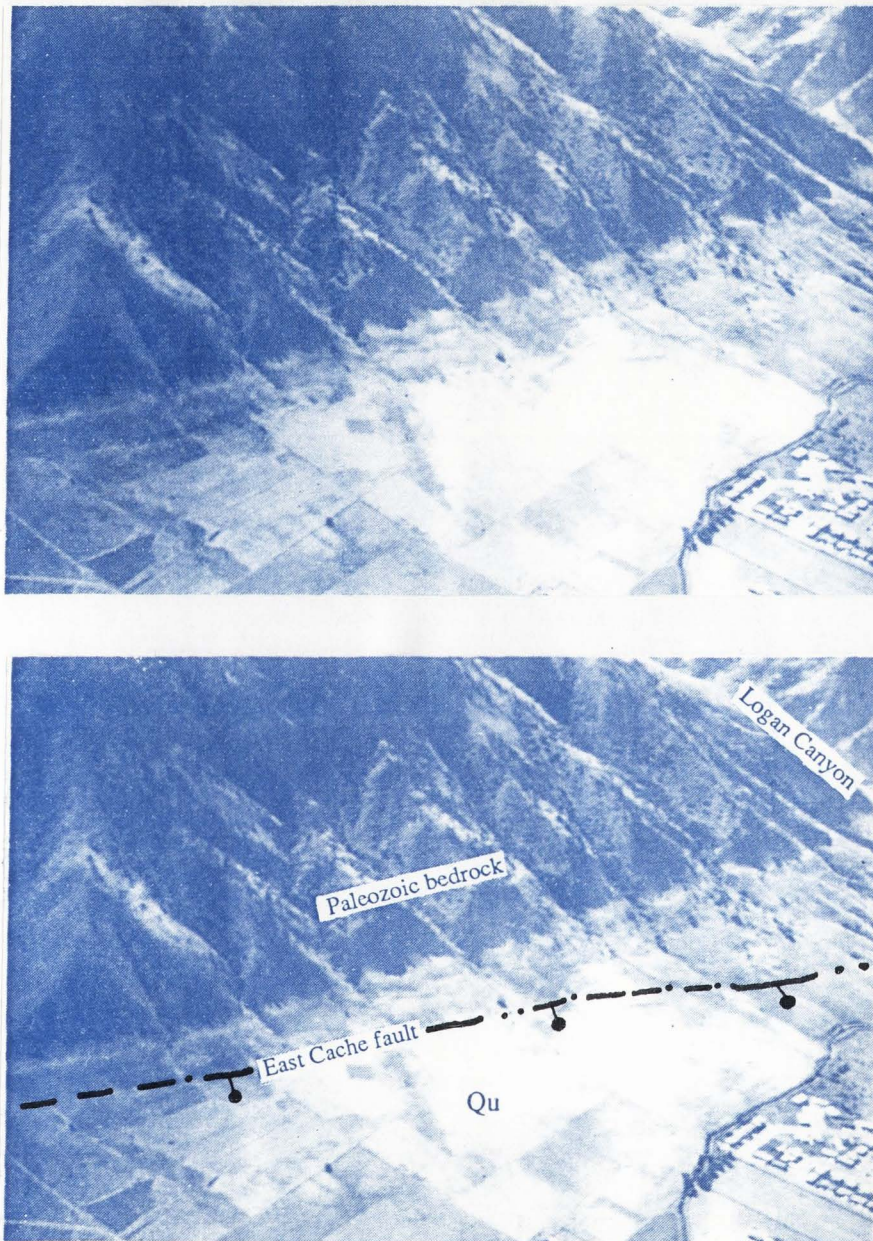


Figure 8. Oblique aerial photograph of the range front near Logan, Utah. View is southeast. The high-angle East Cache fault is responsible for the sharp boundary between the steep range front and the flat valley floor. Heavy line indicates position of fault scarp in unconsolidated Quaternary deposits (Qu); location is approximate based on the work of Lowe (1987) and McCalpin (1989). Photograph used with permission of R. Q. Oaks, Jr.

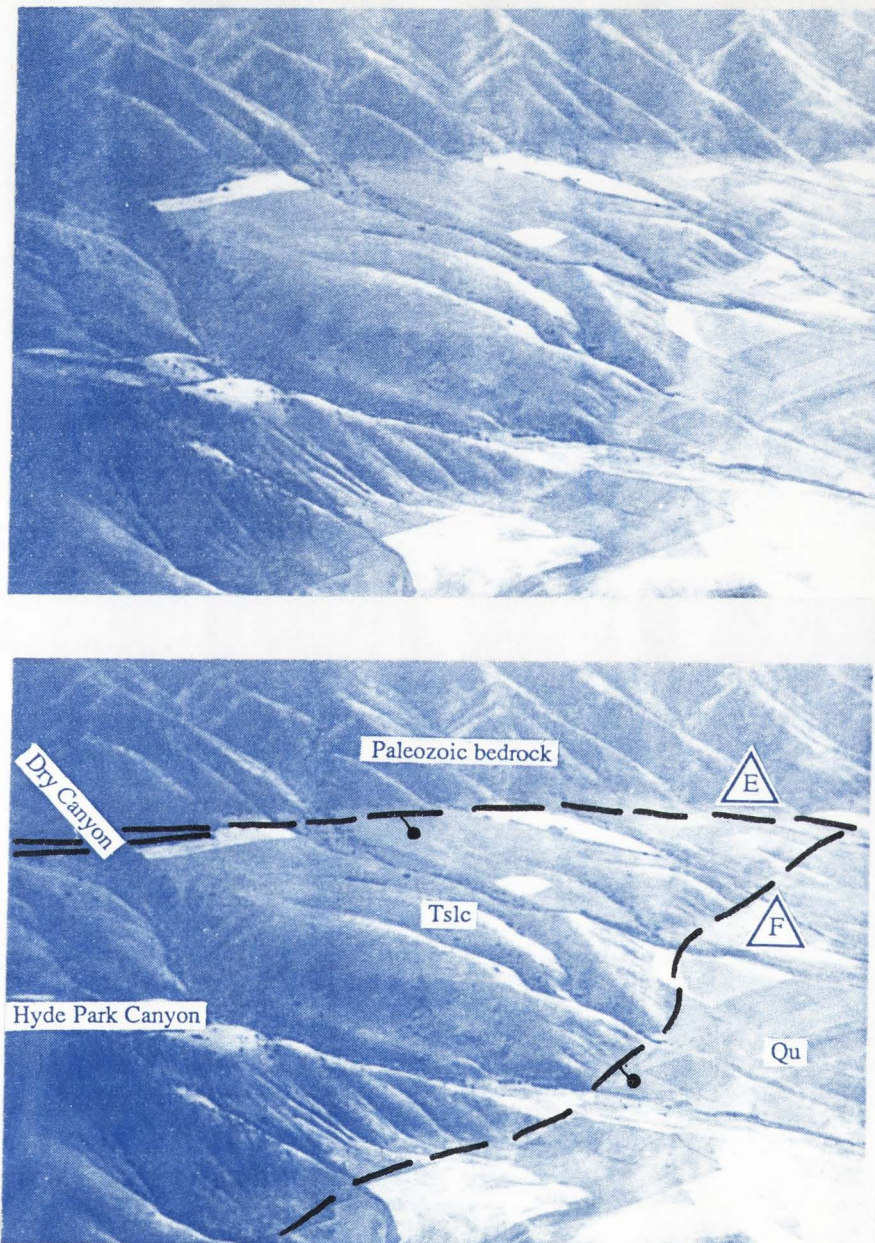


Figure 9. Oblique aerial photograph of the range front near Hyde Park, Utah. View is southeast. The East Cache fault in this area splays (faults E and F). The low hills of Salt Lake Formation conglomerate (Tslc) are bounded on the east and west by the normal-fault splays. Heavy lines indicate approximate positions of East Cache fault traces based on field data from this study and from McCalpin (1989). Undifferentiated Quaternary deposits (Qu) are eastward of the low hills of conglomerate. Photograph used with permission of R. Q. Oaks, Jr.



Figure 10. Small graben in gravel pit south of High Creek near Richmond, Utah. View is south-southwest. Faults offset Provo-level deltaic sediments in the lower part of the exposure. At the top of the exposure, the same faults are truncated by later Provo-level sediments. Pit located at point C on Plate 1.

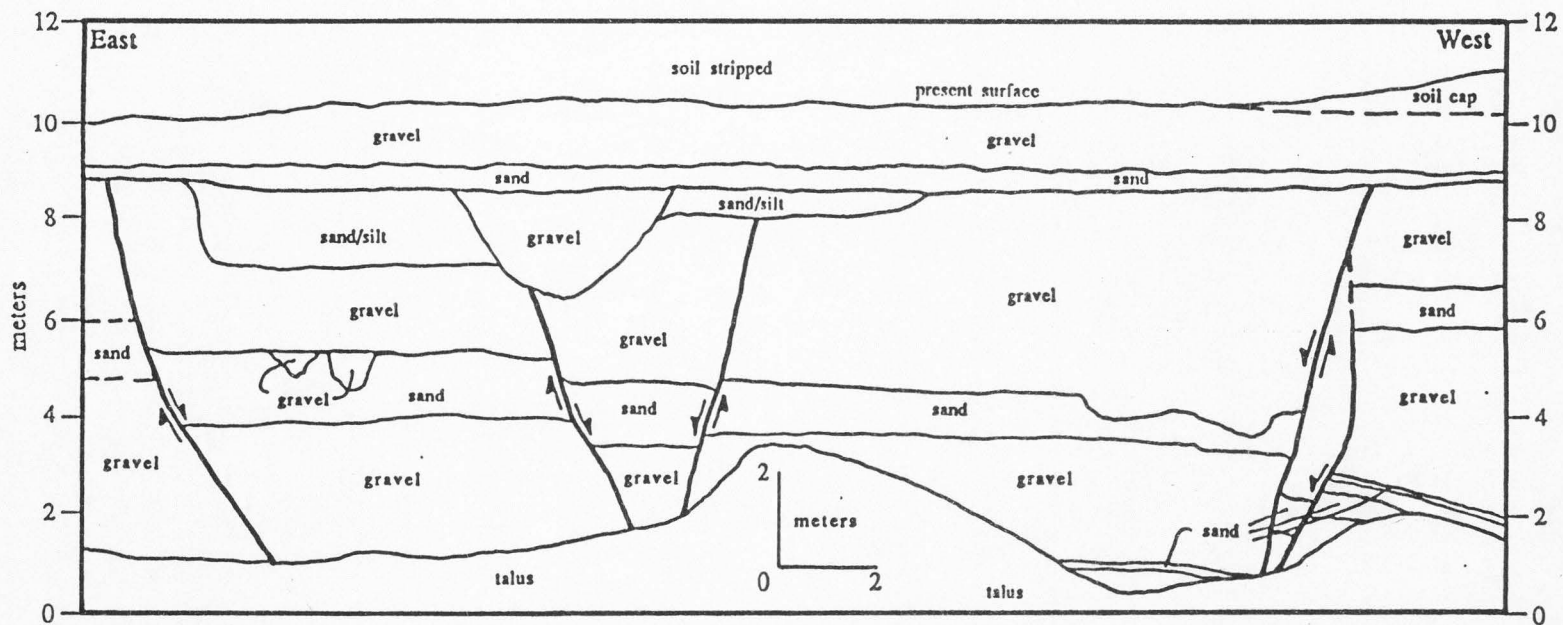


Figure 11. Field sketch of a small graben exposed in a gravel pit north of High Creek. Commercial gravel pit located at the southwest edge of Richmond Knoll, north of High Creek. View is south. Graben located in Provo-level deltaic sediments at point D on Plate 1. Sketch from Brummer and McCalpin (1988, unpublished data).

mountain near the contact between the bedrock faceted spur and Tslc (Plate 1). Fault E₂ placed Tslc in the west down against Cambrian carbonates in the east. The altered fault zone of fault E (splays E₁ and E₂, inclusive) is traceable northward from Dry Hollow to the ridge south of Thurston Hollow based on the limonitic alteration in the soil and in the bedrock float. Pediment gravel on the ridge south of Thurston Hollow covers the contact between Tslc and the underlying Cambrian carbonates. On the north-facing slope of Thurston Hollow, the Tertiary-Cambrian contact is exposed, is depositional, and dips 25° west. The depositional contact between Tertiary and Cambrian rocks at Thurston Hollow indicates that fault E₂ dies out in that area. Fault E₁ appears to die out in the same area. As fault E died out northward, its displacement was probably transferred to fault F.

The westward stepping out of the East Cache fault at this point may be due to an anomaly in the bedrock through which fault E could not propagate northward from near Hyde Park Canyon. McCalpin (1989) described this area as a segment boundary between the northern and middle segments of the East Cache fault.

The western splay of the East Cache fault, fault F, strikes northwest from where the East Cache fault bifurcates. Fault F is not traceable northward from Crow Mountain. This may indicate that fault F connects with fault B, is cut off by fault B, or is concealed and undetectable. There is no conclusive evidence for any of these interpretations. Fault F, in most places, is the boundary between Tertiary and Quaternary sediments and in some places is evidenced by a scarp. Because of later Quaternary sedimentation, the fault is concealed or inferred along much of its trace (McCalpin, 1989).

Faults A and B extend northward from near Crow Mountain. Fault A is mapped west of Richmond (Plate 1). Mendenhall (1975) mapped this concealed fault on the basis of the western-most outcrops of Precambrian and Paleozoic bedrock and the

differences in depths to bedrock encountered in water wells. On the basis of gravity data, Mabey (1985) mapped a fault near, or coincident with, fault A. Fault B created an escarpment in the Tertiary rocks against which Lake Bonneville formed a shoreline. Minor segmentation of fault B possibly occurred at the mouth of High Creek (Plate 1). Faults A and B are mapped as concealed and/or questionable along their traces.

In the Richmond quadrangle, on the ridge between Oxkiller Hollow and Praters Hollow, fault D strikes approximately N25°E and dips about 70°NW. Here, the fault displaced quartzite of the Mutual Formation against quartzite of the Mutual Formation. Evidence for the fault at this location is a small scarp (<1 m), slickensides in loose blocks of quartzite, and altered and brecciated quartzite. Northeast of Oxkiller Hollow, Mendenhall (1975) mapped the fault as the boundary between conglomerate of the Salt Lake Formation and quartzite of the Mutual Formation. South of Oxkiller Hollow, fault D is not easily traceable. The relationship of Tertiary rocks faulted against older rocks northeast of Oxkiller Hollow, a slight break in slope near the contact between Tslc and older rocks south of City Creek, a change in topography north to south across the mouth of Smithfield Canyon, and the similarity in strike to fault B were used in this study as evidence for mapping fault D south of Oxkiller Hollow. Mendenhall (1975) mapped the fault southward of Oxkiller Hollow to show that it cut to the surface through Tslc. However, field mapping for this study does not support Mendenhall's interpretation. Southward from Oxkiller Hollow, the fault is not mapped as the contact between Tslc and older rocks because there are no breccia or gouge zones, slickensides, or other deformation structures present where the contact is exposed. The fault is probably very near the mapped depositional contact and may only be covered by an unknown thickness of younger Salt Lake Formation sediments. Because fault D is not exposed at its southern end, its relationship to fault F is uncertain. On Plate 1, fault D is shown to merge with fault F. There is no conclusive evidence for this interpretation.

The dips of the high-angle normal faults at depth may differ from the dips observed at the surface. Smith and Bruhn (1984), Evans and Oaks (1990), and Evans (1990) documented subsurface dips on the East Cache fault from 70° near the surface to approximately 50° at a depth of approximately 3.5 km. The dip angles were interpreted from seismic-reflection profiles. The lessening of dip with depth may indicate a listric geometry for the East Cache fault. However, Evans (1990) indicated that the high-angle normal faults in the area are probably only slightly curved because sedimentary reflectors in the hanging wall exhibit low dips. If the slight curvature of the East Cache fault continues to depth, the fault would reach a 20° angle at approximately 7 km depth.

Ages of faulting are somewhat difficult to determine. The range-front faults offset the Miocene/Pliocene sedimentary rocks in several places, whereas Provo-level deltaic sediments (~13,000 to 14,000 years old) are not offset. Many of the faults have probably accommodated numerous periods of movement. A further interpretation regarding the onset of high-angle normal faulting in the study area is based on the relative positions of the Eocene Wasatch Formation and the Miocene/Pliocene Salt Lake Formation (Brummer and Evans, 1989). The Wasatch Formation was originally deposited in the higher elevations of the Bear River Range, whereas the Salt Lake Formation was deposited as a basin-filling unit. The difference in positions indicates that Cache Valley had to form sometime between the Eocene and the Miocene/Pliocene. Oaks and others (1989) presented some evidence that normal faulting had occurred east of the study area in the Bear River Range before deposition of the Wasatch Formation.

Low-Angle Normal Faults. The structures of greatest interest in this study are two low-angle normal faults. The southern low-angle normal fault was mapped from Hyde Park Canyon north to Smithfield Canyon. Near Dry Canyon, the fault is planar, strikes approximately $N10^\circ W$, and dips an average of $20^\circ SW$. The hanging wall contains Tslc, whereas the footwall contains Mutual Formation quartzite (Plate 1). The

conglomerate is deformed only within 1 m above the fault contact. Alteration of the conglomerate at the contact is represented by limonitic and hematitic alteration, minor amounts of metallic sulfide minerals (mainly chalcopyrite), weak silicification, brecciated conglomerate, and yellowish gouge (Fig. 12). The gouge and breccia contain few clasts of Mutual Formation quartzite. The main constituents of the conglomerate are carbonate clasts. Because of the alteration and mineralization, prospectors, in the early 1900's, developed two or three small prospect pits along the fault contact on the north side of Dry Canyon (Plate 1). The yield from these pits must have been poor because the pits were abandoned after only a small amount of digging. On the north side of Dry Canyon, along the fault, are several small springs or seeps. Footwall deformation consists of fractured and brecciated, purple to white Mutual Formation quartzite. Fracture density is greatest near the fault contact. Loose blocks of quartzite show polished slickenside surfaces. On the north side of Dry Canyon, altered purple quartzite and green argillite are present in mine tailings near 1768 m along the fault (Plate 1, point B). This deformation indicates that the conglomerate/quartzite contact is a fault and not a depositional contact as mapped by Williams (1948) and Galloway (1970). Bedding in the footwall is difficult or impossible to define and measure due to the high degree of fracturing in the quartzite. If the fault continues southward from Hyde Park Canyon, it is covered by younger Tslc. If the fault does not continue southward, it may have died out. The southern LANF originally may have continued northward for an unknown distance across Smithfield Canyon. If so, then it has been downdropped by fault D and has subsequently been buried by younger Salt Lake Formation sediments. These statements are based on the available geologic data and are evaluated in the Interpretations section.

Exposed on the ridges north and south of Nebo Creek is the northern LANF (Plate 1). This fault is planar, strikes north to northeast (up to N25°E to N30°E), and

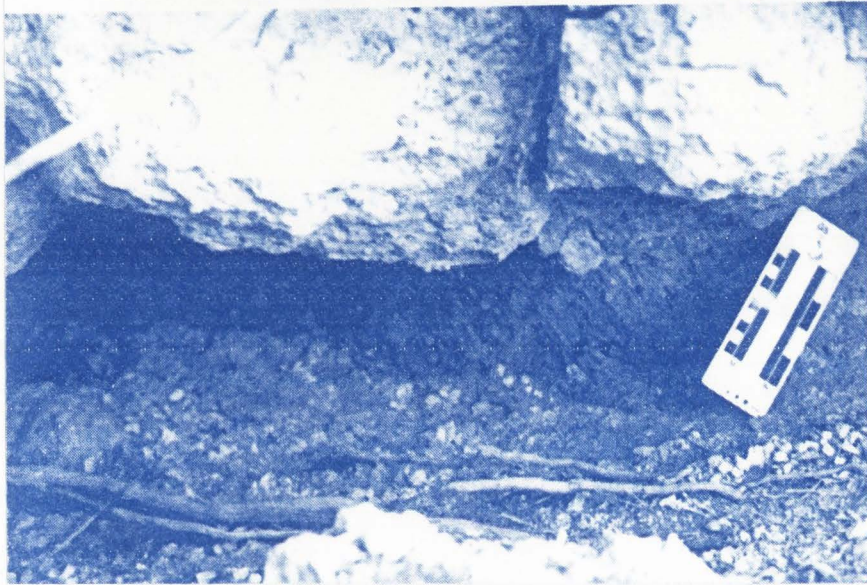


Figure 12. Gouge zone in conglomerate of the Salt Lake Formation along the trace of the southern low-angle normal fault. Photo taken at prospect pits at point B on Plate 1.

dips approximately 22°NW. The fault trace is easily visible on the south-facing slopes due to contrasting vegetation (Fig. 13). East-dipping St. Charles Formation and Garden City Formation carbonates in the hanging wall lie above east-dipping quartzites of the Mutual Formation and Geertsen Canyon Quartzite in the footwall. Breccia and yellowish-gray carbonate gouge are at the fault contact. In the hanging wall, the St. Charles Formation is brecciated at most outcrops. Brecciation in the Garden City Formation is less extensive and appears to be confined to specific layers or beds. Undeformed beds are in sharp contact with intensely brecciated beds. Footwall deformation consists of slickenside surfaces on loose blocks of quartzite and fractured and brecciated quartzite near the fault. Tslc covers this low-angle fault both to the north and to the south, and Tslc remnants overlie bedrock within the LANF (Plate 1).

Two ages of low-angle normal faulting are interpreted. The southern fault placed Tertiary rocks down against older quartzites, whereas the northern fault placed Cambrian and Ordovician rocks down against older quartzites with Tertiary rocks depositionally overlapping the Cambrian and Ordovician hanging-wall rocks. The difference in ages of faulted hanging-wall rocks shows that the southern LANF is probably younger than the northern LANF. Computer analyses of the low-angle-fault traces show that the two faults may share a common structural surface, which is convex westward (Fig. 5). Because the ages of faulted rocks are different and because kinematic reconstructions are difficult to complete based on the assumption that the two faults are connected, the two low-angle faults are interpreted to be two separate faults.

Smithfield Canyon appears to mark a transition in geology and topography. East of Hyde Park, McCalpin (1989) observed that pediment surfaces rise abruptly northward from where the East Cache fault splays (faults E and F). The transfer of slip from fault E to fault F possibly resulted in the apparent southward tilt of the wedge of Salt Lake Formation conglomerate between those two faults (see also McCalpin, 1989).

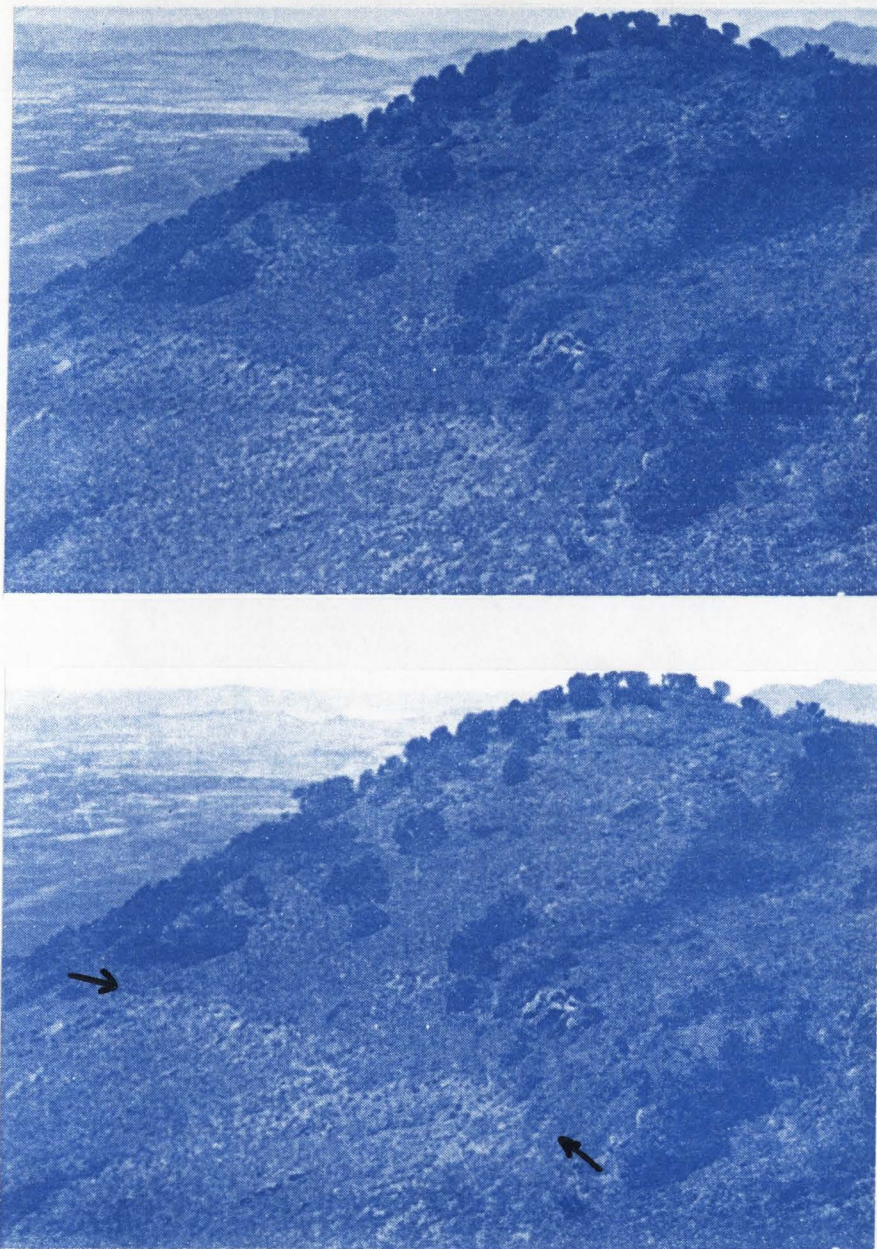


Figure 13. Fault contact on southern ridge of the northern low-angle normal fault. Contact represented by the change in vegetation. Arrows delineate the fault trace. Ordovician/Cambrian rocks lie above Cambrian/Precambrian quartzites. View is northwest from point E on Plate 1.

The hanging wall of fault E, which makes up the southern tip of the conglomerate wedge, would have been placed downward relative to the northern part of the conglomerate wedge, which is in the footwall of fault F. Southward tilting of the conglomerate wedge would have caused the northern end of the wedge near Smithfield Canyon to be topographically higher than the southern end. Subsequent erosion of the conglomerate wedge would have exposed progressively older and seemingly more resistant conglomerate northward to Smithfield Canyon. Faulting and erosion may help explain why the southern LANF is exposed only between Hyde Park Canyon and Smithfield Canyon. South of Hyde Park Canyon, the southern LANF may be covered by conglomerate that is younger than the conglomerate that was displaced by the southern LANF. At Smithfield Canyon, fault D may have cut the southern LANF. This interpretation suggests that the southern LANF is older than faults D, E, and F because the faulting and tilting of the conglomerate wedge by those high-angle normal faults would have occurred after the southern LANF formed (see Low-Angle Normal Faults section for other interpretations of the southern LANF). Northward across Smithfield Canyon, the contact between the Salt Lake Formation and the underlying Mutual Formation changes from a fault contact to a depositional contact and steepens from 20° to about 35°. This change could be explained by fault D. Fault D may have cut the two low-angle normal faults. Then, younger Tslc may have covered the hanging wall of fault D and fault D itself. The Tslc in the hanging wall of fault D does not form slopes as steep as does the Tslc in the hanging wall of the southern LANF, which would suggest that there is a greater degree of lithification in the southern Tslc due to cementation and/or compaction.

Thrust Faults

Galloway (1970) mapped several west-dipping thrust faults in the Smithfield quadrangle. The dips range from 20° to 30° west, and strikes range from 0° to $N20^{\circ}E$. One thrust fault is of particular interest because it is apparently truncated by the northern LANF. In most places in the study area, the thrust fault dips approximately 25° west (Galloway, 1970) and forms the contact between the Mutual Formation and the Geertsen Canyon Quartzite (Plate 1). Slickensides and fractured quartzite mark the thrust fault in the Richmond quadrangle on the north side of Smithfield Canyon. Undulating slickenside planes strike approximately $N28^{\circ}W$ and dip from 0° to $47^{\circ}SW$. The fault is not traceable northward beyond the northern LANF.

Galloway (1970) and Mendenhall (1975) mapped bedding-plane thrust faults in the study area. These faults dip eastward in the same orientations as the bedding in the western limb of the Logan Peak syncline. Galloway (1970) mapped these structures in the St. Charles and Garden City formations, whereas Mendenhall (1975) mapped an extensive trace of one of these thrusts in the Geertsen Canyon Quartzite just below the contact with the Langston Formation. Except for beds that are locally discordant or cut by one of these faults, the criteria used by these geologists to map these bedding-plane thrust faults are not distinctly stated. None of these thrust faults have been included in Plate 1.

GEOPHYSICAL SURVEYS

Published and proprietary geophysical data were used to make interpretations. In this section, the basic survey data are presented as written descriptions and as maps and diagrams. Bouguer gravity maps show a large, negative gravity anomaly in Cache Valley (Fig. 14; Peterson and Oriel, 1970; and Mabey, 1985). Southern Cache Valley contains a narrow, elongated gravity low, whereas, near Lewiston, Utah, Cache Valley has a southwest-trending, elongated gravity high extending south from Mt. Smart,

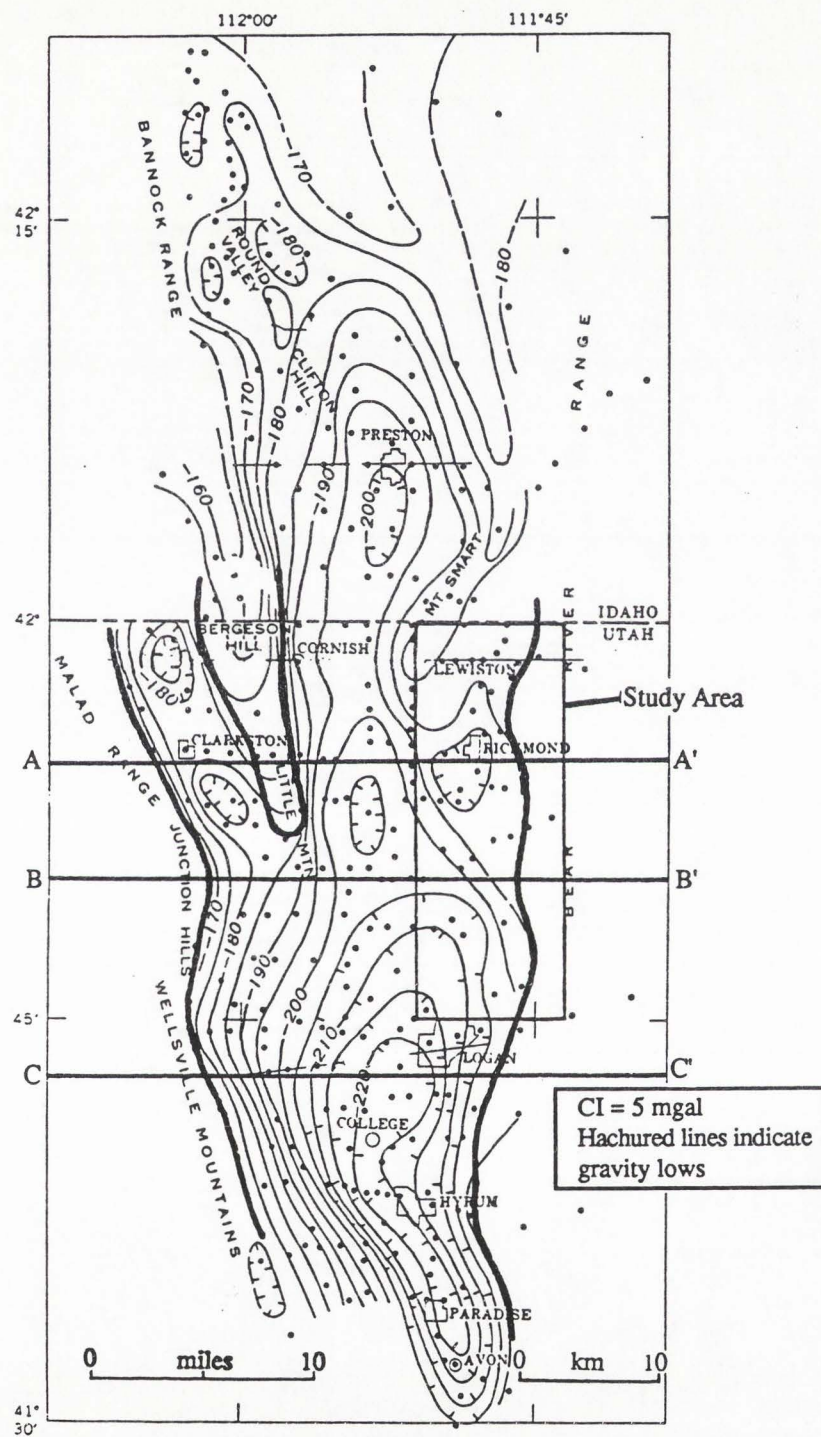


Figure 14. Bouguer gravity map of Cache Valley, Utah-Idaho. Dots indicate gravity stations used by Peterson and Oriel (1970). Cross-section lines used in Figure 15 indicated above. Heavy lines represent the approximate boundary between bedrock and less dense, unconsolidated sediments. Modified from Peterson and Oriel (1970).

Idaho. Three gravity profiles drawn east to west across Cache Valley (Fig. 14, sections A-A', B-B', C-C') indicate that the deepest part of the basin near Logan, Utah, is near the valley-range margin, whereas the maximum basin depth near Richmond is approximately 12 km from the range front (Fig. 15). The width of the range-front fault zone is reflected in the distance of the deep basin from the range front (see Normal Fault section). Sheriff (1989) used gravity data to determine the maximum depth to anomalous masses beneath the surface with the equation

$$h = \frac{\Delta G}{0.04185(\Delta\rho)} \quad (1)$$

In equation 1, h is the maximum depth in meters to the anomalous mass, $\Delta\rho$ is the density difference, and ΔG is the gravity difference in milligals calculated from the highest and lowest readings in and along the margin of Cache Valley (see Fig. 15). A density difference of 0.2 g/cc was assumed as the difference between Precambrian/Paleozoic quartzite and Tertiary conglomerate in the study area. For this study, h in equation 1 represents the thickness of Quaternary and Tertiary basin fill that overlies a large block of Precambrian/Paleozoic bedrock (see also Zoback, 1983). The assumption made in this case is that the anomalous mass of Precambrian/Paleozoic bed at depth beneath Tertiary and Quaternary basin fill is there because of offset on normal faults at the valley margins. On the basis of this assumption, h in equation 1 approximates the amount of throw on normal faults that bound the valley. The thicknesses of basin fill determined from gravity data are roughly similar to the thickness of Quaternary and Tertiary fill logged in the Amoco well. The two gravity profiles nearest the well, B-B' and C-C', indicate from 3.82 km to 5.62 km of basin fill, respectively (Fig. 14 and Fig. 15). Approximately 2.36 km of Quaternary and Tertiary basin fill were logged in the Amoco well (see Appendix section). The discrepancy in

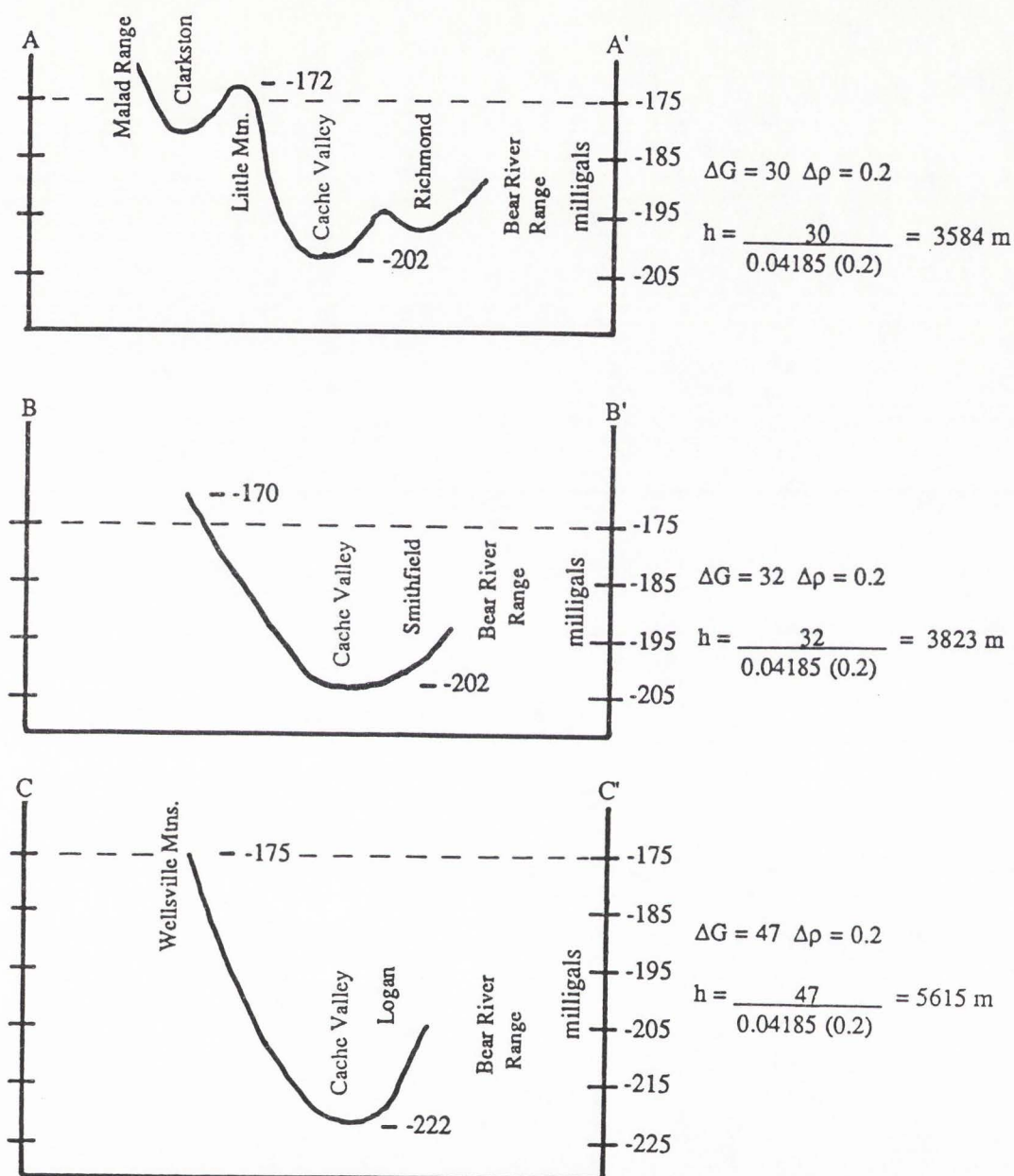


Figure 15. Gravity profiles from Figure 14. Calculations of offset by faults bounding Cache Valley are based on the gravity difference in milligals (ΔG) and the density difference ($\Delta \rho$). Density difference of 0.2 g/cc between Precambrian/Paleozoic bedrock and Tertiary/Quaternary sediments was assumed. Depth in meters (h) was determined with the method outlined by Sheriff (1989). Depth (h) is a maximum value that approximates the offset by faults. Actual offsets may be less. Gravity difference (ΔG) in each profile figured from the lowest value in Cache Valley and the highest value found along the side of the valley.

thicknesses between those calculated from gravity data and that from the log may be explained by the fact that the gravity data provide a maximum thickness (h in equation 1). The actual thickness is probably less than that which was calculated in equation 1 (Sheriff, 1989). The assumed density difference may also be too small. A greater density difference would yield smaller values for h in equation 1. Calculations based on equation 1 suggest that the thickness of Cenozoic basin fill decreases northward from near Logan, Utah (Fig. 15).

A local gravity low is centered on Richmond, Utah, which suggests that the town is situated on a mass of low-density sediment or rock. A steep gravity gradient is present on the west side of the valley from near Clifton Hill to the south end of Little Mountain and along the east side of the Wellsville Mountains to at least as far south as Avon, Utah. South of Little Mountain, the steep gradient has a northwest trend. There, the gravity gradient is gentler than to the north or south (Fig. 14).

Seismic-reflection data presented by Smith and Bruhn (1984), Evans and Oaks (1990), and Evans (1990) suggest net slip on range-bounding faults and subsurface attitudes of inferred fault planes. A seismic-reflection profile across the East Cache fault zone in the southern part of Cache Valley shows three 60° west-dipping reflectors, representing possible faults, crossing prominent east-dipping reflectors that are probably stratigraphic layers (Smith and Bruhn, 1984). Evans (1990) and Evans and Oaks (1990) reported dips greater than 45° near the surface. Seismic data also reveal 914 m to 1219 m of Cenozoic basin fill on the west side of the range-front fault zone near Richmond (J. P. Evans, 1990, written commun.). The thickness of the basin fill determined from gravity data is directly related to the net offset on range-bounding normal faults as evidenced by seismic profiles (Evans, 1990). Evans (1990) documented net slip on the East Cache fault system from 7.6 km at the southern end of Cache Valley to 2.5 km near the Utah-Idaho border.

INTERPRETATIONS

KINEMATIC ANALYSIS

Kinematic analysis involves the interpretation of deformational movements that take place during the formation and deformation of rocks (Davis, 1984). Deformation may be described as either rigid- or nonrigid-body movements. Kinematic analysis for this report is concerned solely with rigid-body deformation. Rigid-body movements are translation and rotation, which involve changes in position, but not changes in size or shape of a rock body.

Rigid-body translations are expressed using displacement vectors. The vectors describe three parameters: 1) distance of transport, 2) direction of transport, and 3) sense of transport (Davis, 1984). These three parameters are used to describe the displacements along the normal faults being studied.

Analyzed first is the northern LANF southeast of Richmond, Utah. Net dip slip on this fault is approximately 3.4 km based on the offset of the Cambrian-Ordovician contact (Fig. 16). Because observed slickensides were not in place, the amount of oblique-slip motion, if any, could not be determined. If pure dip slip is assumed, the direction of transport would be approximately N80°W to N60°W on the basis of the strike of the fault. The southern LANF east of Hyde Park, Utah, yields less information with which to perform kinematic analysis. Dip slip probably occurred in a direction of approximately N80°W. Observed slickensides are on loose boulders; therefore, the presence of oblique slip on this fault could not be determined. The amount of dip slip is difficult to infer due to the lack of distinct bedding in the Salt Lake Formation conglomerate in the hanging wall. A range of dip-slip amounts may be approximated on the basis of the location of parent material for the carbonate clasts in the conglomerate.

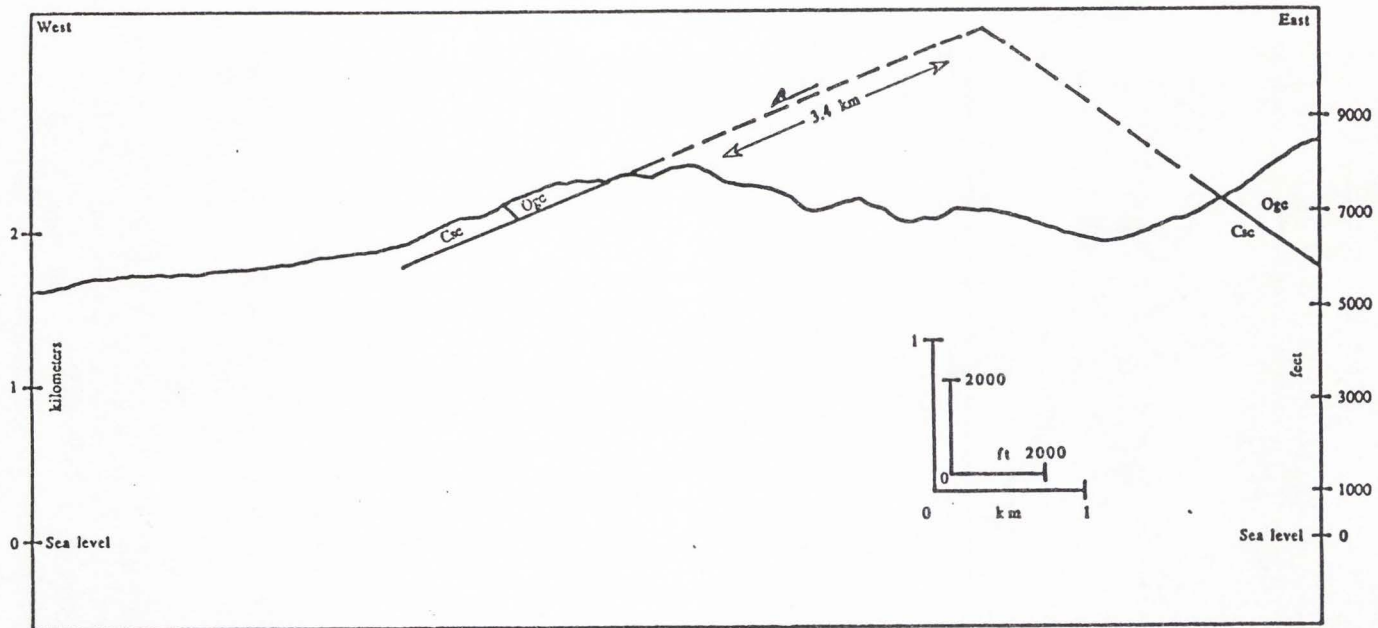


Figure 16. Amount of dip slip on the northern low-angle normal fault. Determination based on the offset of the Ordovician-Cambrian contact as shown. Cross-section line shown on Figure 17.

Middle Cambrian carbonate units are probably the parent units. If the Tertiary conglomerate formed on top of, or immediately down slope from, the parent units, dip slip would be 1 km to 3 km on the basis of the position of the basal and upper contacts of the Middle Cambrian carbonate sequence.

Because most of the high-angle normal faults in the area are concealed, little is known about direction and sense of transport. The exposure of fault E at Dry Hollow shows grooves that rake 75°SW and 17°NE on slickensides that strike $\text{N}16^{\circ}\text{E}$, 80NW and $\text{N}9^{\circ}\text{E}$, 72NW , respectively. The rake measurements indicate that there has been oblique-slip motion on some of the normal faults in the area. Throw can be approximated by using well-log data and map data. Because normal faulting in the area began in the Tertiary, displacement of Tertiary units provides information concerning the amount of throw across the fault zone on the east side of Cache Valley. Well-log and map data show that the Tertiary Wasatch Formation rests on the Ordovician Swan Peak Formation at high elevations in the Bear River Range and buried beneath 1 to 2 km of valley fill (Dover, 1987; Petroleum Information). Detailed analysis of well logs and map data indicated that the Tertiary-Ordovician contact is 1001 m below sea level in the #1 Lynn Reese well on the west side of the fault zone (see Appendix section) and approximately 1890 m above sea level on the east side of the fault zone in Cowley Canyon (Fig. 17). The closest exposure of the Wasatch Formation-Swan Peak Formation contact east of the Lynn Reese well lies at an elevation of 1890 m above sea level. The elevation of the contact varies from place to place and reaches a present-day maximum of approximately 2590 m in the Bear River Range near Tony Grove Lake. Because the base of the Wasatch Formation rises westward to its erosional pinchout near the crest of the range, the elevation of 1890 m indicates that throw on the east side of Cache Valley due to both high-angle and low-angle normal faulting is at least 2.9 km.

Throw on individual high-angle normal faults is more difficult to constrain. Water-well data are the best means presently available with which to constrain throw on individual concealed normal faults. The depth to the top of the Salt Lake Formation was needed to construct structure cross sections and to constrain throw on individual faults. Plate 1 shows the locations of water wells and the inferred depths to the top of the Salt Lake Formation that were used in this report.

Individual thrust faults in the area, as described by Galloway (1970), accommodated approximately 3 m to 244 m of eastward displacement. The thrust fault that was cut by the northern LANF displaced the Mutual Formation approximately 244 m eastward (Galloway, 1970). Moreover, structural reconstructions based on the position of the Mutual Formation show that there may have been up to 900 m of dip slip on a single thrust fault (section C-C', Plates 2 and 3).

The amount of extension in the Basin and Range province is not well constrained (Zoback and others, 1981). Extension across a single basin has been estimated at 5% to 15%, whereas extension across the province is estimated to average 10% to 35% (Stewart, 1978; Zoback and others, 1981). Proffett (1977) documented an extreme case of extension of more than 100% in western Nevada. An estimation of extension across faults in the study area was not attempted.

Rigid-body rotations may be possible along faults in the area. Kinematic interpretations regarding rotational movement are discussed in the section below.

HYPOTHESES

Several hypotheses concerning the origin of low-angle faults with normal-slip motion have been published. In order to explain the origin of the low-angle faults in the study area, each of these hypotheses is tested, evaluated, and accepted or rejected according to the data from the study area. The hypotheses are evaluated based on

similarities in orientation (strike and dip) of the faults, age of deformation, types of deformation in the fault zone, and local structural setting. If none of the published hypotheses apply to the current geologic setting, then new hypotheses must be proposed. The hypotheses may be grouped into the following five categories: folded thrust fault, rotated high-angle normal fault, gravity slide, low-angle normal fault, and listric normal fault.

Folded Thrust Fault

This hypothesis was proposed by Curry (1938, 1954) to explain the origin of turtleback faults in Death Valley. Curry believed that the low-angle faults with normal-slip displacement were thrust faults that were once planar, but were subsequently arched or folded. In these examples, Cenozoic rocks have been faulted down onto Precambrian metamorphic rocks. Curry's interpretation was that the thrust faults originally dipped east and accommodated westward-directed thrusting. Arching and folding of the thrust faults reversed the eastward dips so that the faults now dip 20° to 30° westward west of the fold crest (Curry, 1954; Drewes, 1959; Hunt and Mabey, 1966). The warping of the thrust faults facilitated later low-angle faults with apparent normal-slip motion. The fault surfaces have subsequently been exposed by local erosion through the hanging wall.

Curry's hypothesis requires that observed low-angle faults with apparent normal-slip motion dip in the opposite direction from which they originally formed. If the low-angle normal faults in the study area were to have the same origin as the turtleback faults, the observed westward-dipping faults would have formed as eastward-dipping thrust faults that accommodated westward-directed motion. Subsequent arching on the west flank of the Bear River Range would have reversed the dip of the faults. Thrust faults would have formed during regional thrusting associated with the Sevier

Orogeny (Jurassic to early Tertiary). Evidence required to test the folded thrust-fault hypothesis is westward-directed thrusting discordant to bedding, pre-folding eastward dips of thrust faults on the west flank of the Logan Peak syncline, east-dipping thrust or reverse faults on the east side of the Bear River Range, and age of thrusting.

In the study area, eastward-dipping thrust faults exist (Galloway, 1970; Mendenhall, 1975). However, these faults are bedding-plane thrusts which, if arched to reverse the dips, would not be similar to the low-angle normal faults in the study area because the observed low-angle normal faults are discordant to bedding. Regional thrusting during the Sevier Orogeny was eastward-directed (Hintze, 1979; Levy and Christie-Blick, 1989). East of the southern LANF are two gently west-dipping thrust faults that displaced the Mutual Formation eastward. If the low-angle normal faults in the west flank of the Logan Peak syncline were originally east-dipping thrust faults that were arched to produce westward dips as bedding was folded, then a reconstruction of pre-folding orientations should indicate the original dips of the hypothesized folded faults. A simple rotation that restored bedding to near horizontal also restored the low-angle normal faults to high angles (Fig. 18). Gentle, pre-folding, eastward dips of faults were not generated in the restoration. If arching of east-dipping thrust faults had occurred on the east side of the Bear River Range, the faults would probably be represented now as high-angle reverse faults. No east-dipping thrust or reverse faults are shown to exist on the east side of the Bear River Range (Dover, 1985; Dover, 1987). Because thrust faulting in the region continued only to about the early Eocene (Levy and Christie-Blick, 1989), late Tertiary units should not be displaced by thrust faults. Evidence of this is the presence of Wasatch Formation (Eocene ?) that covers thrust faults on the central and eastern parts of the Bear River Range (Dover, 1985) and the presence of faulted Salt Lake Formation (Miocene/Pliocene) in the hanging wall of the southern low-angle fault.

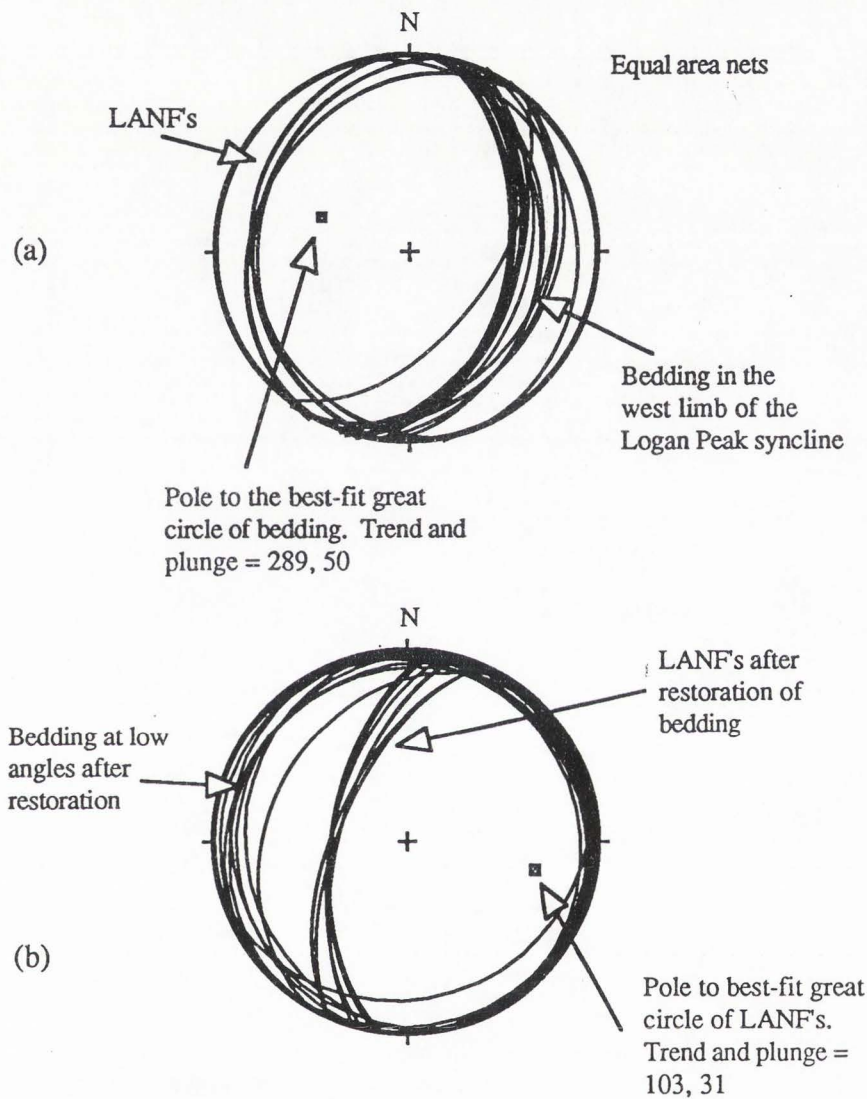


Figure 18. Stereograms of present and restored bedding. (a) Present orientations of LANF's and bedding in the west limb of the Logan Peak syncline. If the faults existed before folding, their original orientations can be determined by restoring to zero the average dip of bedding. Present dip of bedding averages $N19^{\circ}E, 40^{\circ}SE$. (b) Restored orientations of bedding and LANF's. East-dipping beds were rotated 40° counterclockwise about the average azimuth of bedding to their approximate pre-folding orientations. LANF's after restoration of bedding are oriented approximately $N13^{\circ}E, 59^{\circ}NW$.

The folded thrust-fault hypothesis is rejected because regional thrusting that is discordant to bedding is eastward directed on westward-dipping faults, pre-folding orientations of faults are not east dipping, and thrust or reverse faults on the east side of the Bear River Range are west dipping. It is highly unlikely that a thrust fault displaced the Salt Lake Formation in the hanging wall of the southern low-angle fault because thrust faulting had probably ended by the time the Salt Lake Formation was deposited.

Rotated High-Angle Normal Fault

A simple model to explain younger rocks faulted onto older rocks involves extension along high-angle and low-angle normal faults. One explanation involving extensional tectonics is that an observed low-angle normal fault may have originally formed as a high-angle normal fault that has subsequently been rotated to lower angles by later faulting or folding. The factors which are most important in determining if rotation has occurred are the orientations of hanging-wall bedding before and after hypothesized rotation. An examination of the attitudes of hanging-wall bedding is therefore essential to proving or disproving the rotation hypothesis. The hypothesis also requires that younger normal faults that have steeper surface dips than the low-angle normal faults in question exist either in the footwall or the hanging wall of the older fault.

Subhypothesis 1. Rotation of an older fault may occur due to younger faulting in the footwall of that older fault. Proffett (1977) depicted this relationship graphically (Fig. 19). Armstrong (1972) reinterpreted low-angle faults in the Egan Range of eastern Nevada as rotated high-angle normal faults. Previous to Armstrong's work, the low-angle faults in the Egan Range had been considered Mesozoic thrust faults (Fritz, 1968). His new interpretations were based on the restoration of Tertiary bedding in the hanging-wall block of the fault back to a pre-faulting orientation (near horizontal). In

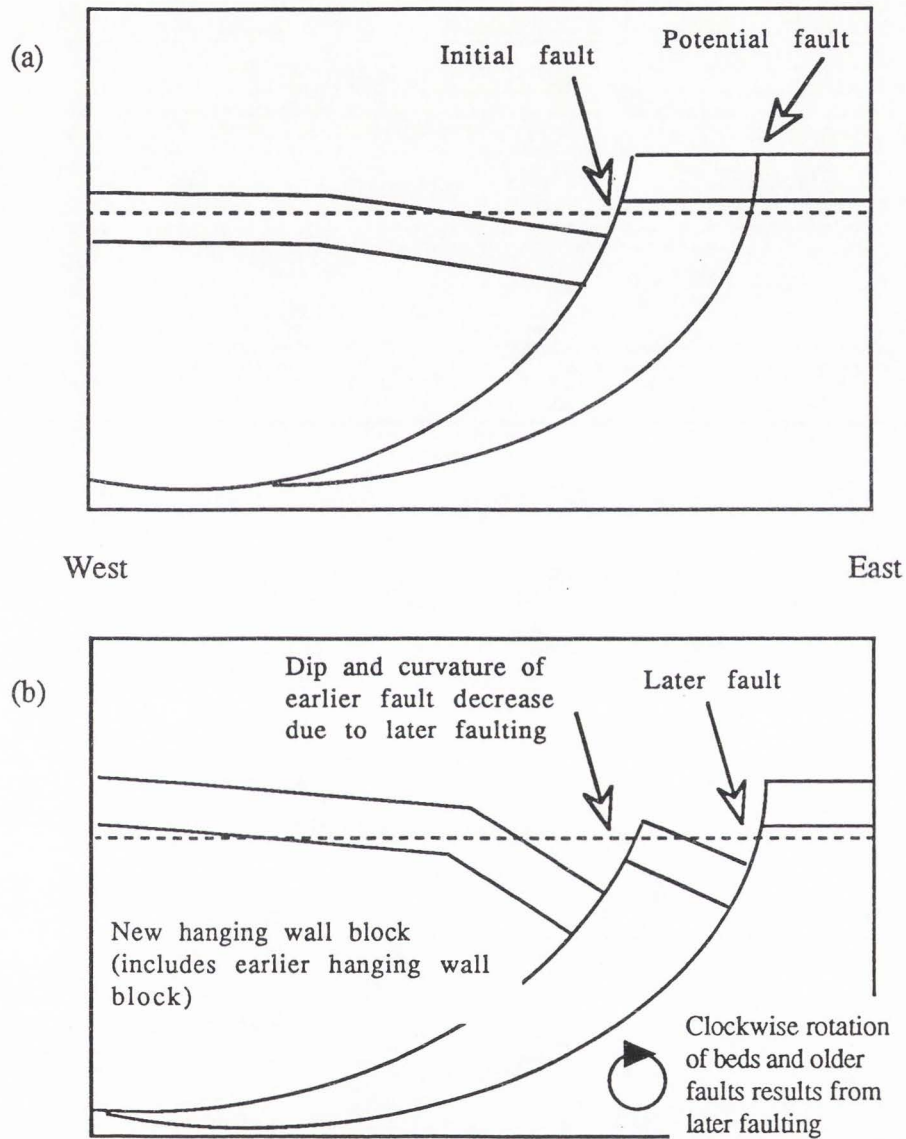


Figure 19. Reduction of fault-plane dip due to tilting by a later fault in the footwall block of an older fault. In (a), a potential fault exists in the footwall of the existing listric normal fault. Movement along the later fault tilts the earlier fault and bedding planes in the new hanging-wall block (b). Sense of rotation due to these west-dipping faults is clockwise. A listric geometry may not be essential for rotation to occur. Diagrams modified from Proffett (1977).

western Nevada, Proffett (1977) documented normal faults with steep to gentle dips at the surface. He found that the oldest faults are the most gently dipping, whereas the youngest faults are the most steeply dipping. His interpretation of this observation was that faulting along a listric normal fault in the footwall of an older normal fault reduces the dip of the older fault (Fig. 19). Rotation of the hanging-wall block is also supported by the fault-ward dip of bedding that was originally horizontal. A curved normal fault (i.e., a listric normal fault) is not essential to this hypothesis because two or more planar faults may also produce rotated bedding and faults.

In the study area, evidence for this hypothesis is not strong. The hypothesis requires that younger west-dipping normal faults exist east of the observed low-angle normal faults. From the mapping of Dover (1987; Fig. 17), no west-dipping high-angle normal faults can be inferred in the area directly east of the low-angle normal faults. From air photos, Cluff and others (1974) did map faults to the east of the low-angle normal faults. The faults mapped by Cluff and others may exist; however, field evidence for these faults was not found during mapping for this study. This hypothesis also requires that bedding in the older hanging wall be rotated along a younger fault. Stereonet manipulations were used to show pre-rotation orientations of hanging-wall bedding. The restoration of bedding was accomplished by first plotting the great circles of present orientations of bedding planes and faults (Fig. 20a/c). All of the great circles were then rotated 40° clockwise about the average azimuth direction of the low-angle normal faults to show the orientations of faults and associated hanging-wall bedding as they would have been before the hypothesized rotation along a younger normal fault (Fig. 20b/d). Forty-degree rotation was used to restore faults with 20° dips to 60° dips. Sixty degrees was selected as the average dip of a high-angle normal fault (Davis, 1984).

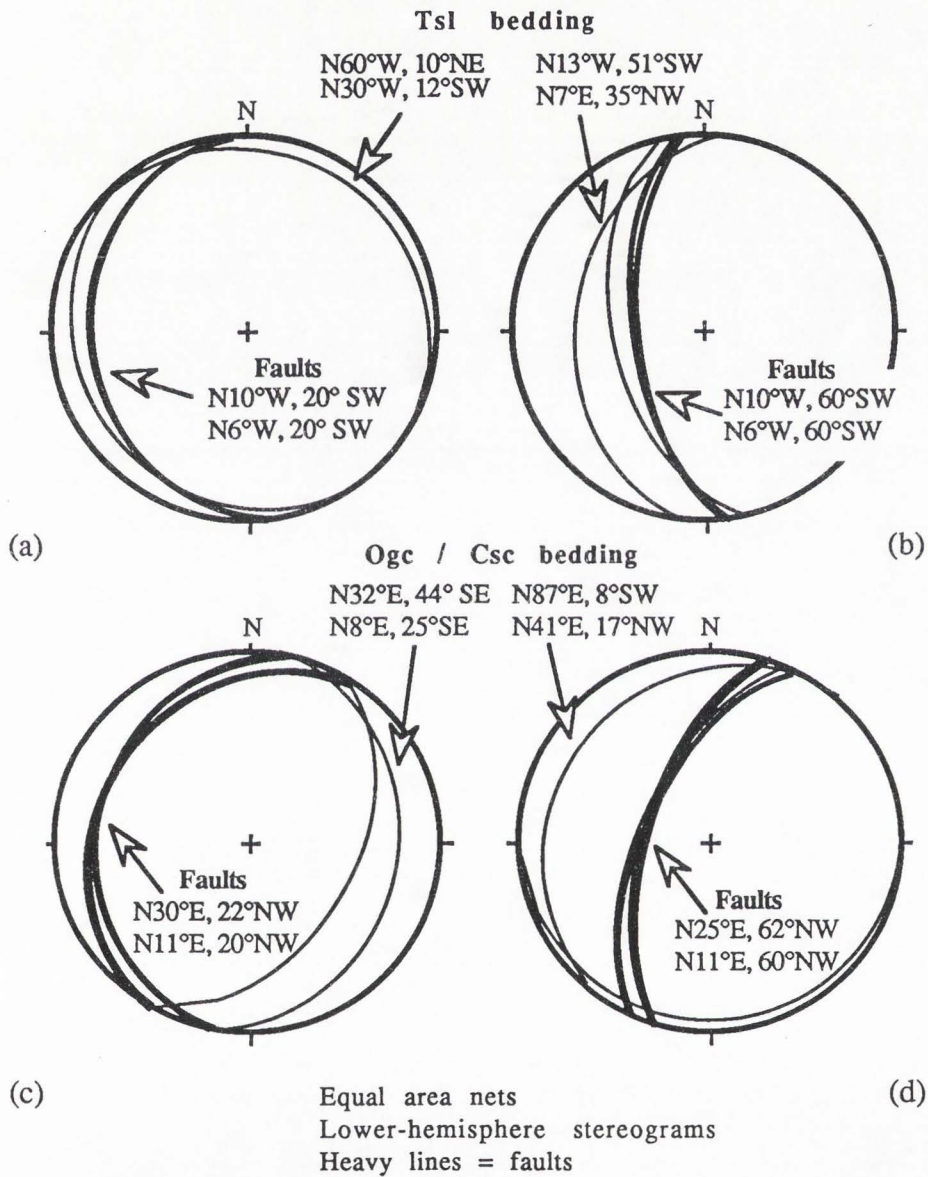


Figure 20. Restoration of low-angle normal faults to hypothesized high-angle normal faults. In both cases, faults and bedding were rotated 40° clockwise about the azimuth of one of the low-angle normal faults. (a) and (b) Southern low-angle normal fault stereograms; (a) Orientations at present; (b) Orientations after rotation. (c) and (d) Northern low-angle normal fault stereograms; (c) Orientations at present. (d) Orientations after rotation.

In the hanging-wall block of the northern LANF, Cambrian and Ordovician beds presently dip east at angles very similar to the beds in the footwall, which are part of the west limb of the syncline (compare Fig. 4b/c to 4d/e). Because all Paleozoic units in the study area were originally part of the syncline, and because normal faulting is interpreted to be younger than the folding of the syncline, restored orientations of bedding in the hanging wall are expected to be similar to the present bedding orientations in the west limb of the syncline. By restoration of the present 20° dip of the low-angle normal fault to the average dip of a high-angle normal fault (60°), one can see that the orientations of restored bedding are not similar to the present orientations of footwall bedding in the west limb of the syncline (compare Fig. 20b/d to Fig. 4b/c). The bedding in the hanging wall of the northern LANF is presently in the same orientation as the bedding in the footwall block which indicates that no fault-related rotation has occurred.

In the southern LANF, indistinct bedding in the hanging-wall block hinders an interpretation concerning the rotation hypothesis for this fault. Strike of bedding in the conglomerate varies greatly from northwest to northeast, but dip is generally less than 20° either east or west. Restoration of the two most reliable strike and dip measurements from the Salt Lake Formation conglomerate in the Richmond area indicates that the bedding planes probably dip too steeply for unrotated bedding. (Fig. 20a/b).

Subhypothesis 2. A second possibility is that rotation of an older fault occurred due to younger faulting in the hanging wall of that older fault. However, rotation of the older fault is difficult to achieve in this scenario. For rotation of faults to occur in this subhypothesis, the footwall side of the younger fault must be pushed upward. Upward movement on the footwall block may result in folding of beds and preexisting faults immediately adjacent to the younger fault. The amount of upward displacement relative to downward displacement along the faults in the study area is not known. This

uncertainty makes this subhypotheses even more difficult to test. Moreover, on the basis of stereonet manipulations, hanging-wall bedding has not been rotated (Fig. 20).

Because hanging-wall bedding has not been rotated by later faults and because no normal fault with large offset exists in the footwall blocks of the low-angle normal faults, both subhypotheses are rejected. There is no evidence for folding that post-dates large-offset normal faulting. Therefore, folding is not thought to be a factor in fault rotation.

Gravity Slide

A large, intact mass of rock that slides down a topographic gradient by the influence of gravity is referred to as a gravity slide. Wise (1963), Anderson (1971), Armstrong (1972), and Beutner (1972) implied that there are three basic requirements for gravity sliding. First, as the term gravity slide implies, a gravity potential or gradient must exist. This potential may be generated by uplift along faults or by the formation of folds (Moore and others, 1968). Failure by sliding depends on, secondly, a free face and thirdly, a preexisting plane of weakness. The generation of a free face by normal faulting takes away any buttressing along the newly formed footwall, releases confining pressure, and facilitates failure (Wise, 1963; Armstrong, 1972; Beutner, 1972). A preexisting plane of weakness should also exist. The weak plane may be a preexisting fault (Beutner, 1972), or joint; or the weak plane may be a weak stratigraphic unit such as shale (Wise, 1963). For sliding to occur, the toe of this weak plane must be exposed either by uplift (Anderson, 1971), or by erosion, or by a combination of the two. The subhypotheses presented below were evaluated on the basis of the three requirements discussed above.

Descriptions of the various documented glide blocks reveal some similarities in deformation. Brecciation in the glide block or hanging-wall block is the most

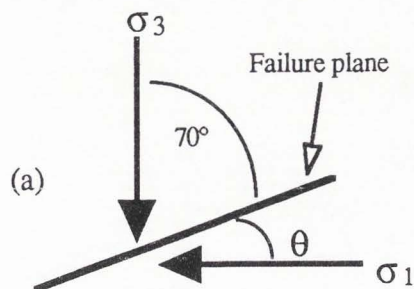
widespread type of deformation (Longwell, 1951; Moores, 1968; Armstrong, 1972; Beutner, 1972; Krieger, 1977). Examples described by Beutner (1972) show megabreccia that grades vertically into intact bedding within the glide blocks. Intense brecciation is common in the glide blocks within 15 m of the failure plane (Moores, 1968; Armstrong, 1972; Beutner, 1972). Brittle deformation in the glide blocks is also shown by shattered and fractured rocks (Moores and others, 1968; Armstrong, 1972). The glide blocks described by Longwell (1951), Moores (1968), and Beutner (1972) are 100 m to 300 m thick, and have surface areas ranging from 2.6 to 20.7 km².

Deformation in the footwall is usually much less severe. The footwall may not be deformed at all (Moores, 1968), or may be deformed only near the failure plane (Armstrong, 1972; Beutner, 1972). In the examples documented by Beutner (1972), powdery, white to rusty quartz (granulated quartzite) is within 1 m of the failure plane, followed downward by 1 to 3 m of brecciated quartzite. Below the brecciated quartzite is undeformed quartzite.

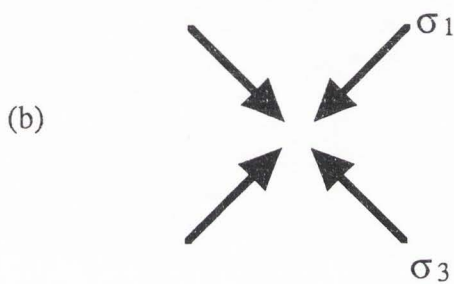
The age of deformation in most of these examples is Tertiary (Anderson, 1971). The faults have surface dips that vary from 5° to 60° (Anderson, 1971; Beutner, 1972).

Deformation in the hanging wall and the footwall blocks described above is quite similar to the deformation in the low-angle normal-fault blocks in the study area (see section on Low-Angle Normal Faults).

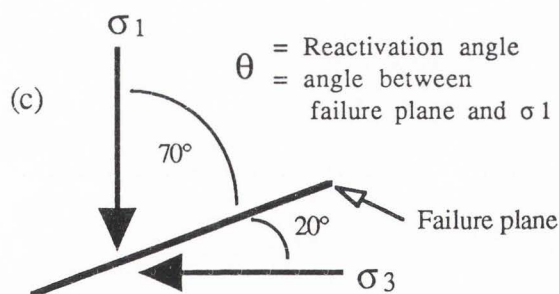
Subhypothesis 1. Evaluated in this section is the subhypothesis of reverse gravitative movement on preexisting thrust-fault surfaces (Dahlstrom, 1970; Beutner, 1972; Sprinkel, 1979; Mattox and Weiss, 1987). Reactivation of thrust faults as low-angle normal faults requires that principal stresses be reoriented. During compressional tectonism, the greatest principal stress axis is horizontal, whereas the least principal stress axis is vertical (Anderson, 1951). Principal stress axes during extensional tectonism are oriented just opposite (Fig. 21). For the reactivation hypothesis to be



Orientations of principal-stress axes typical of compressional tectonics.



Principal-stress axes in a transitional state between compressional and modern Basin and Range extensional tectonics. This pre-Basin and Range stress state may have caused the low-angle normal faults in the study area.



Orientations of principal-stress axes typical of modern Basin and Range extensional tectonics. Reactivation of a pre-existing thrust fault relies on the alignment of σ_3 in the same general direction in which σ_1 was oriented during compressional tectonics.

Figure 21. Reorientation of principal stress axes during the transition from compressional to extensional tectonism. (a) For thrust faulting, greatest principal stress axis is horizontal. For the fault in (a) to be reactivated as a low-angle normal fault, the principal stresses must be inverted as in (c). The transition from compressional tectonics to modern Basin and Range tectonics may have involved intermediate stress states such as that in (b).

valid, the horizontal axes must have approximately the same bearing before and after stress reorientation. Bradshaw and Zoback (1988) discussed rotation of stress axes, but attributed the rotation of axes to refraction of stresses off rock layers at depth, not to a shift in the regional stress system. Jaroszewski (1984) discussed non-typical orientations of stress axes and their influence on fault geometry.

Fault reactivation in the study area may have occurred. However, simple mechanical constraints should be considered to determine if gravity sliding is possible in the study area. Sibson (1985) used basic frictional-failure criteria to show that reactivation of a thrust fault as a low-angle normal fault is unlikely unless certain conditions are met in the system (see also Bradshaw and Zoback, 1988). The first condition is that the coefficient of friction (μ) be low, i.e., $\mu < 0.55$. The second condition is that the effective least principal stress (σ_3') be tensile, i.e., $\sigma_3' < 0$. Sibson considered a triaxial stress state with effective principal compressive stresses: $\sigma_1' > \sigma_2' > \sigma_3'$. Within this stress field is a cohesionless plane (e.g., a preexisting fault) lying at an angle θ to σ_1' . In the examples presented by Sibson (1985), effective principal stresses are used. Effective principal stresses are those that have been adjusted to account for the presence of any fluid pressure. Sibson drew upon Amontons' first law,

$$\tau = \mu\sigma_n, \quad (2)$$

as the basis for his arguments on reactivation of a preexisting, cohesionless fault plane. In equation 2, τ and σ_n are the shear and normal stresses, respectively, and μ is the coefficient of friction (Sibson, 1985; Hatcher, 1990). To account for the presence of fluid pressure (P_f) in the fault zone, Equation 2 may be rewritten as

$$\tau = \mu(\sigma_n - P_f), \quad (3)$$

in which $(\sigma_n - P_f)$ is the effective normal stress (σ_n'). Equation 3 states that renewed shearing or sliding on a cohesionless plane due to gravity will occur when shear stress is great enough to overcome friction and effective normal stress. Failure in this example is dependent on the angle of inclination of the plane, the frictional properties of the rock types above and below the fault plane, the mass of the block above the fault plane, and the amount of fluid pressure involved (Fig. 22). As the angle of inclination increases, the gravity potential of the block above the plane increases, which in turn increases shear stress and decreases normal stress. The frictional value, which cannot be measured directly, depends on the rock types involved and is a ratio of shear to normal stress. For cohesive material, the coefficient of friction is equal to the slope of the Mohr envelope (Ragan, 1973). An increase in the mass of the block above the plane will result in an increase in the force directed downward on the plane. Fluid pressure in the fault zone decreases normal stress, which allows failure to occur at lower shear stress (Hubbert and Rubey, 1959). These failure criteria may be represented by

$$\tau = mg \sin \phi \quad (4)$$

$$\sigma_n = mg \cos \phi \quad (5)$$

$$\sigma_n' = (mg \cos \phi) - P_f, \quad (6)$$

in which m is the mass of the block, g is acceleration due to gravity, ϕ is the angle of internal friction or the angle of inclination of the failure plane, and σ_n' is the effective normal stress that accounts for fluid pressure, P_f . These relationships are illustrated graphically (Fig. 22).

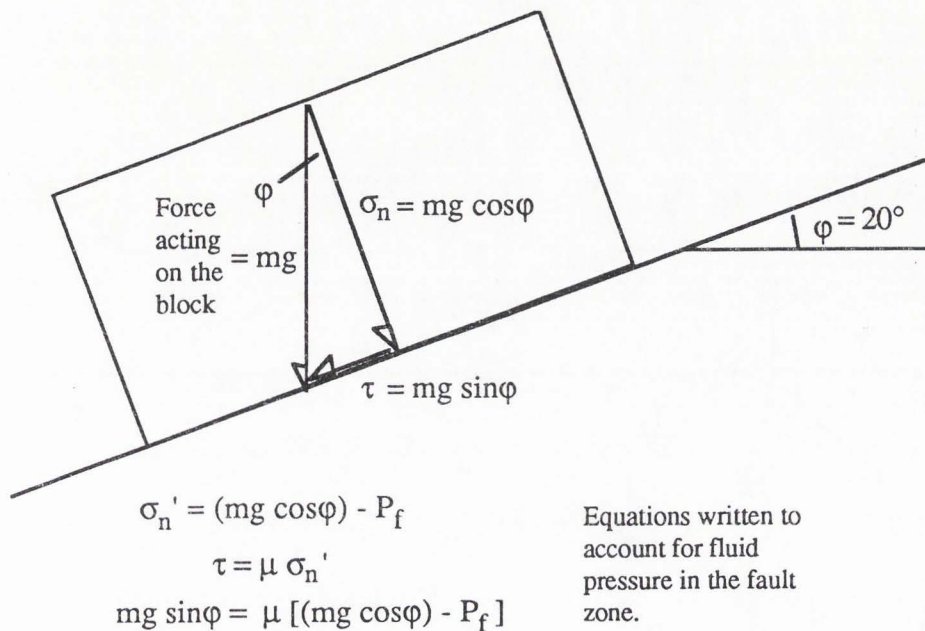


Figure 22. Shear and normal stresses acting on a sliding block on a cohesionless plane. Movement of the block depends on its mass (m), the angle of the plane (ϕ), friction coefficient (μ), fluid pressure acting on the failure plane (P_f), and gravity (g). Equations above indicate the conditions that must be met to induce sliding of the block on the plane. For sliding to occur, shear stress must exceed the combined effects of friction and effective normal stress on the plane. Modified from Ragan (1973).

Equations 4 and 5 are substituted into equation 2 to give

$$\mu = \frac{\sin \varphi}{\cos \varphi} = \tan \varphi . \quad (7)$$

Sibson's derivation from equation 2 showed the stress ratio needed for reactivation on a cohesionless plane,

$$R = \frac{\sigma_1'}{\sigma_3'} = \frac{1 + \mu \cot \theta}{1 - \mu \tan \theta} , \quad (8)$$

which can be graphically depicted. In equation 8, σ_1' and σ_3' are the effective principal stresses (Sibson, 1985). From Figure 23, one can see that for reactivation angles (θ) greater than about 50° , R is negative ($R < 0$). This means that σ_3' is negative (i.e., σ_3' must be tensile). The coefficient of friction (μ) varies inversely with the reactivation angle θ (Fig. 24). For a typical reactivation angle of a low-angle fault ($\theta = 60^\circ$), the coefficient of friction is ~ 0.55 (Fig. 24). This value for μ is fairly low, which means that failure could occur at low shear stress. Higher reactivation angles yield lower friction values (Fig. 24). However, the μ values required for reactivation are too low when compared to the average μ value for rocks, which is 0.75 to 0.85 (Byerlee, 1978; Sibson, 1985). The preceding friction values are for rock sliding on rock. Because most natural fault zones contain gouge and breccia, the friction values required for failure will be lower than rock-on-rock friction values (Shimamoto and Logan, 1981a; 1981b). Shimamoto and Logan (1981a) documented the effect of clay minerals on the frictional-failure properties of fault gouge. In the laboratory, kaolinite, illite, chlorite, and bentonite showed coefficients of friction of 0.66, 0.48, 0.42, and 0.22,

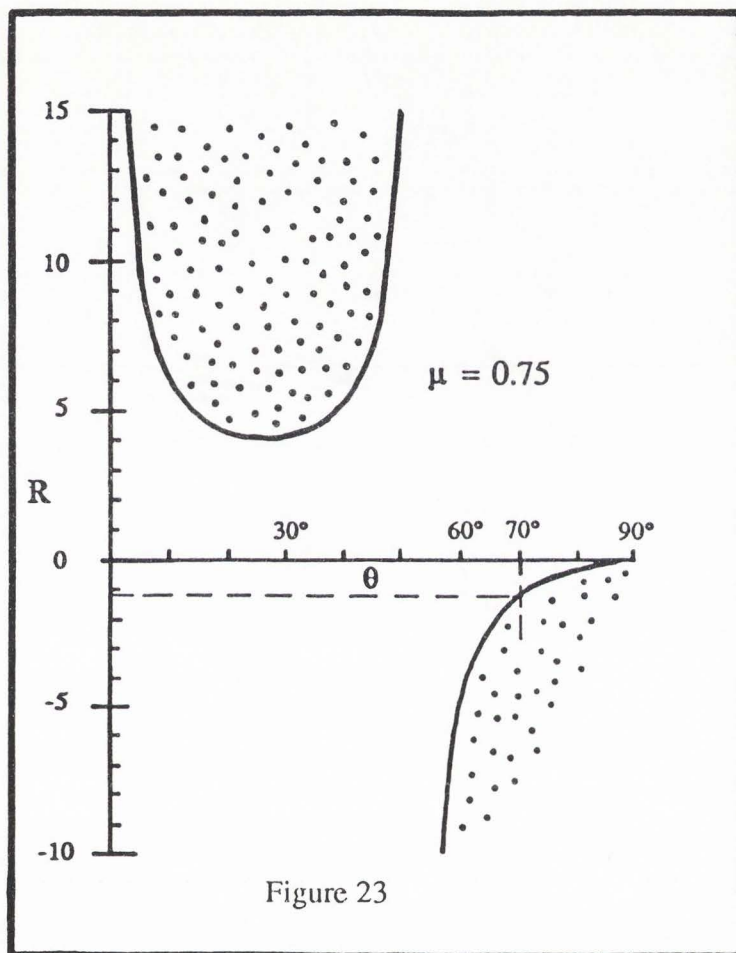


Figure 23

Figure 23. Variance of the stress ratio for reactivation (R) with reactivation angle (θ).

An average coefficient of friction (μ) is assumed for rocks. The stress ratio for reactivation required for a 70° reactivation angle is negative, which indicates that least effective principal stress must be tensile. Failure occurs within the dotted areas. Modified from Sibson (1985).

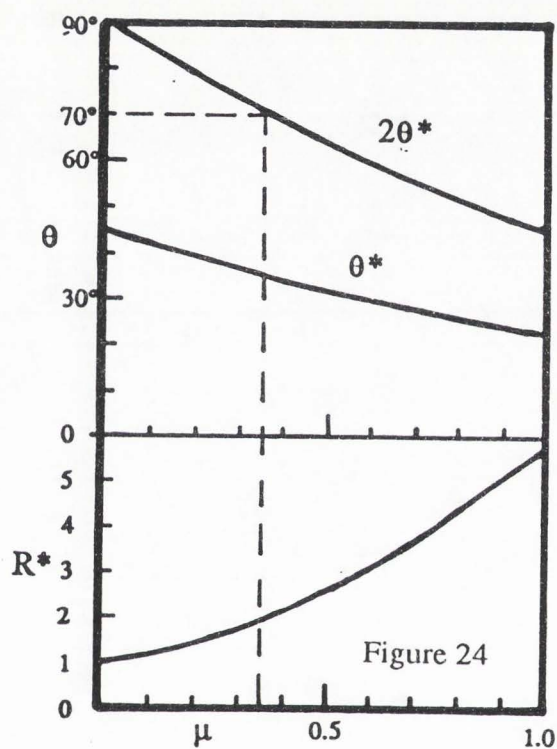


Figure 24. Variance of the coefficient of friction (μ) with reactivation angle (θ). Coefficient of friction at a reactivation angle of 70° is 0.36, which is much lower than the average values of μ for real rock tests (see Byerlee, 1978). R^* = minimum positive stress ratio for reactivation; θ^* = optimum reactivation angle. Modified from Sibson (1985).

respectively. The point should be made that natural fault gouges rarely consist entirely of clay minerals. Therefore, the exact effect of clay in gouges in the geological environment is not well understood. Clay-bearing fault gouge with the proper type of clay minerals in the proper amounts does facilitate failure at lower shear stresses than if rock were sliding on rock. Shimamoto and Logan (1981b) also documented the effects of non-clay gouges on the sliding behavior of rocks. Their conclusions were, among others, that Mohs' hardness of a mineral can be used as a parameter to predict the failure behavior of a monomineralic gouge and that the failure behavior of a mixed-mineral gouge can be predicted by using the frictional values from the monomineralic constituents involved. Minerals of intermediate hardness, such as calcite and dolomite, produced higher friction coefficients than did harder minerals such as quartz and feldspar. Because even small displacements generate gouge, rock-on-rock sliding models are limited in their geological applications (Shimamoto and Logan, 1981b). Many of the friction values for the non-clay gouges are as high as, or higher than, the solid rock values reported by Byerlee (1978; Shimamoto and Logan, 1981b).

A third limitation for frictional reactivation is that the allowable stress states induce failure only on the preexisting fault and not in the surrounding intact rock (Sibson, 1985). The optimum stress state is represented by a schematic Mohr diagram in Figure 25a. This Mohr diagram shows that failure or reactivation occurs only on the plane that has a pole oriented at an angle α to σ_1 defined as

$$\alpha = 45 + (\varphi / 2), \quad (9)$$

where φ is the angle of internal friction (Fig. 25a). A further increase in deviatoric stress will allow failure on preexisting planes with orientations between A and B defined by 2α (Fig. 25b). This is not an optimum condition for reactivation because failure is

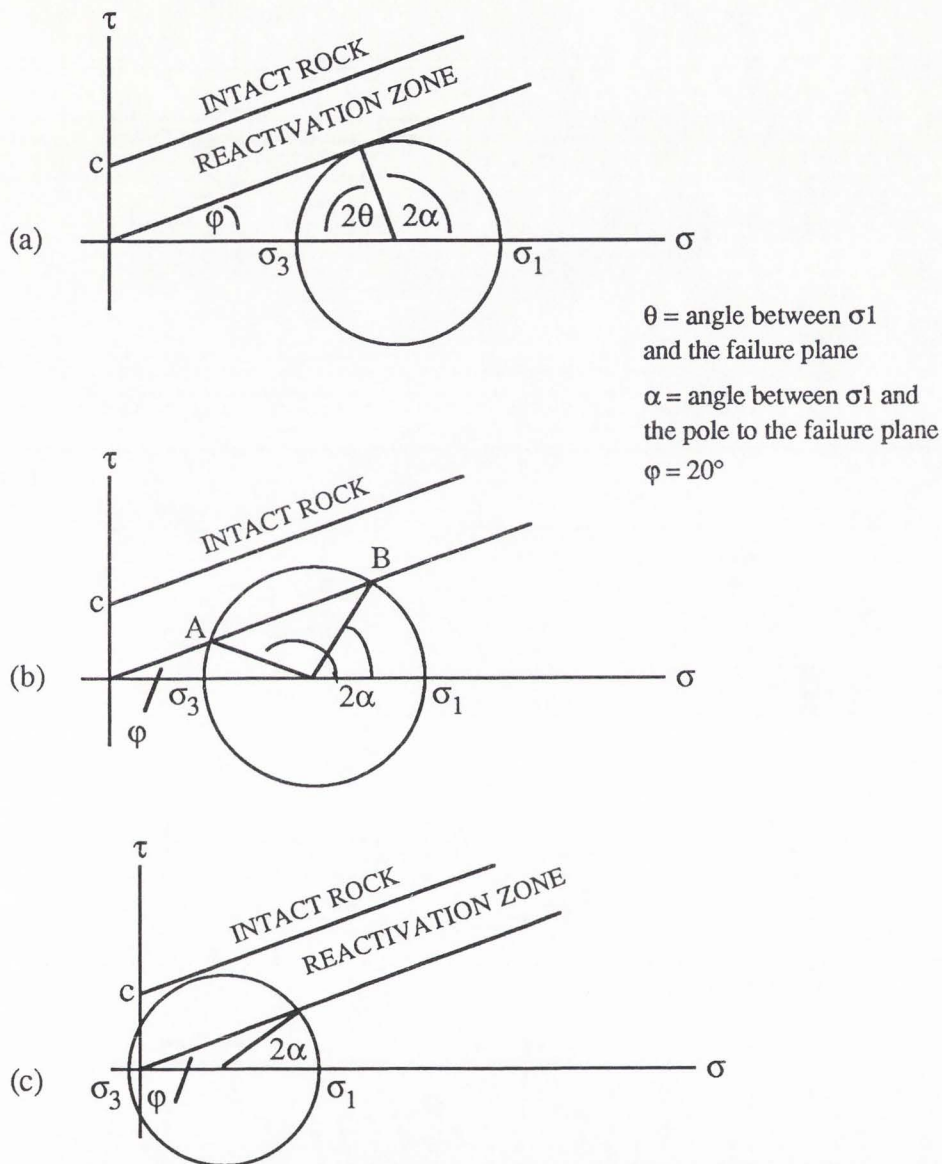


Figure 25. Schematic Mohr diagrams showing stress states for fault reactivation. (a) Optimum stress state for the reactivation of one fault only. (b) Stress state that will allow reactivation of any plane with an orientation between A and B which is defined by 2α . This is a non-optimum case for the reactivation of one fault with a specific orientation. (c) Stress state required for reactivation of low-angle faults in the study area. In (c), least principal stress is tensile. Examples are based on a cohesionless failure plane. Modified from Sibson (1985).

possible not only on the preexisting fault of interest, but also on any weak plane with an orientation defined by the angle 2α . Failure could occur on any plane within the failure field. There would be no preference of one plane over another.

Data from the study area may be applied to Sibson's reactivation arguments. If stress reorientation and fault reactivation are assumed for the low-angle normal faults in the study area, a reactivation angle of $\sim 70^\circ$ is yielded (Fig. 21). A 70° reactivation angle (θ) indicates that a coefficient of friction of ~ 0.36 (Fig. 24) and a negative stress ratio for reactivation are needed for reactivation of low-angle faults in the study area (Fig. 23). The two conditions above require that effective least principal stress be negative (i.e., σ_3' be tensile). The schematic Mohr diagram representing the stress state needed for reactivation of the low-angle faults in the study area is shown in Figure 25c. Figure 25c does not represent the actual stress state that existed to form the low-angle structures in the study area. It merely shows a stress state that would produce failure in an area with faults similar to those in the study area. Figure 25c was constructed by using Sibson's guidelines and the 20° dip angle of one of the low-angle normal faults from the study area. Under the stress state shown in Figure 25c, least effective principal stress is negative. Negative least effective principal stress is not a common stress state for real rock (Jaroszewski, 1984). Sibson's model outlines the requirements for rock-on-rock failure and not for failure in fault gouge. On the basis of x-ray diffraction analyses of fault gouge samples from the low-angle normal faults, the mineralogy in the gouges is calcite, dolomite, quartz, and possibly illite. The fourth mineral, tentatively identified as illite, was in only one of the samples. Because the sample with the illite was collected from a fault zone with weak to moderate argillization, some clay minerals might be present. The other three minerals were expected because the rocks in the hanging-wall and footwall blocks are dolostones, limestones, and quartzites. Monomineralic gouges composed of calcite, dolomite, and quartz have experimental

friction coefficients of 0.74, 0.78, and 0.70, respectively (Shimamoto and Logan, 1981b). These coefficients are very similar to, if not higher than, the values required for rock-on-rock failure (see Byerlee, 1978). Gouges also add cohesion to the fault, whereas in Sibson's model, the failure plane was cohesionless. Cohesion added to Sibson's model would make reactivation even more difficult. Equation 3 may be rewritten to account for cohesion,

$$\tau = C + \mu(\sigma_n - P_f), \quad (10)$$

in which C is cohesion. Equation 10 indicates that more stress is required for failure than in equation 3 due to the effect of cohesion on the fault plane. The amount of fluid pressure in the gouge of the low-angle normal faults is unknown. If fluid pressure in the fault zone were increased due to an event such as seismic shaking, then reactivation might be possible (see also Sibson, 1985).

In addition to the mechanical limitations, each of the three requirements for a gravity slide must be considered in the evaluation of this subhypothesis. In the study area, the existence of a gravity potential and a free face depends largely on when the high-angle normal faults formed the early range front. Erosion probably did not play a large part in generating a gravity potential and free face. For there to be a gravity potential and free face to allow failure along low-angle planes in the present field area, high-angle normal faulting would have had to precede low-angle normal faulting. The wedge of conglomerate included in the southern LANF was possibly tilted by high-angle normal faults after low-angle normal faulting. High-angle normal faults cut across the low-angle normal faults near the Bonneville shoreline. Earlier episodes of motion must be inferred from cross-sectional reconstructions of geologic history. Brummer and Evans (1989) inferred that fault D extended southward beneath the Salt Lake Formation

and across the toe of the northern LANF. Their interpretation was that the concealed high-angle normal fault generated a gravity potential and free face during an early episode of high-angle normal faulting. Subsequent relief allowed westward sliding into the Cache Valley basin. The location and age of fault D are reinterpreted in this report. Fault D is younger than the low-angle normal faults and is responsible for the surface against which the younger conglomerates of the Salt Lake Formation were deposited north of Smithfield Canyon. Earlier episodes of motion on faults B and F could have generated the gravity potential needed for basinward sliding. There is little field evidence to support or refute recurrent motion on the high-angle normal faults. The third requirement, a preexisting plane of weakness, is represented in this subhypothesis by a preexisting thrust fault. The thrust faults shown on Plate 2 have orientations very similar to the southern LANF and lie structurally below that LANF. On the north side of Smithfield Canyon, the thrust fault has a steeper dip where the northern LANF offsets it. Sprinkel (1979) stated that evidence for a reactivated thrust fault was low-angle normal faults where high-angle normal faults are common, reverse drag along normal faults, and younger rocks on older rocks with large stratigraphic gaps. Sprinkel (1979) also suggested that reactivation was indicated by the low angle and planar nature of the fault surfaces and by severe brecciation of the hanging-wall rocks. Only the reverse-drag evidence seems convincing for an argument for reactivated thrust faults. Even so, reverse drag is often generated along normal faults. Furthermore, reverse drag was not observed during mapping for this report.

In summary, the mechanical limitations and geological evidence do not support the reactivated-thrust-fault hypothesis. Mechanical limitations reveal that reverse gravitative movement may not be possible in the study area because the inferred coefficient of friction is too low and effective least principal stress is tensile. A coefficient of friction of ~ 0.36 would be needed for reactivation. This coefficient is too

low for average values of intact rock (~ 0.85 ; Byerlee, 1978) and for carbonate/quartzite fault gouge in the study area (0.70 to 0.78; Shimamoto and Logan, 1981b). Sibson (1985) added a further comment that reactivation of listric faults requires very high fluid pressure, or an abnormally low frictional coefficient, or principal stress trajectories that deviate greatly from vertical and horizontal. Field relations of Tertiary rocks over pre-Cenozoic bedrock do not support preexisting thrust faults. A gravity potential and free face may have existed to allow failure. However, other field evidence makes the reactivation subhypothesis an unlikely explanation. The evidence used by Sprinkel (1979) and presented above just as easily or better describes a normal fault. Galloway (1970) mapped west-dipping thrust faults east of the southern LANF (Plate 1). The orientation of the thrust fault cut by the northern LANF is very similar to the southern LANF, but is not similar to the northern LANF. The southern LANF displaced the Salt Lake Formation (Miocene/Pliocene). If reactivation took place, eastward thrusting and westward reverse gravitative motion had to occur after the Salt Lake Formation was deposited. There is no evidence in the area to suggest that thrusting occurred after the deposition of the Salt Lake Formation. Gravity sliding on a preexisting thrust fault is unlikely for the southern LANF. The ages of faulted rock in the northern LANF are compatible for the age of regional thrusting. However, the thrust fault that is cut by the northern LANF dips 20° to 25° steeper than the northern LANF. If reverse movement were to have occurred, it would have been expected to have been along the preexisting, 47° west-dipping thrust fault. The mechanical limitations and the geologic evidence combine to make the reactivated-thrust-fault subhypothesis invalid.

Subhypothesis 2. Gravity-slide subhypothesis 2 (GS2) examines three other possible preexisting weaknesses that may have allowed westward sliding on the low-angle normal faults: weak stratigraphic units, joints, and bedding planes. Weak rock such as shale is not present in the fault zones of either of the low-angle normal faults.

Besides, bedded shale would probably be east dipping as part of the west limb of the Logan Peak syncline. As such, it would be discordant to the fault surfaces. Joints in the footwall quartzite are not favorably oriented. The joints would need to be dipping about 20° west similar to the existing faults. Measured joint sets show orientations of $N83^\circ E$, $75^\circ NW$ and $N55^\circ W$, $85^\circ SW$. Because the northern LANF is discordant to bedding, a bedding plane weakness is ruled out for that fault. For the southern LANF, the original surface on which the Salt Lake Formation was deposited may have provided a weakness that allowed the conglomerate to slide westward after uplift on a high-angle normal fault generated a gravity potential and free face. Schematic block diagrams depict the structural evolution based on the premises of this hypothesis (Plate 3). Alignment of the top of the hanging-wall block with the toe of the weak contact may have allowed the block of conglomerate to slide westward onto the top of the hanging-wall block. Recurrent movement on the high-angle normal fault must be inferred from these reconstructions because only the latest episode of movement is currently evidenced at the surface. This hypothesis fits the field data and cannot be discredited at this time. The depositional contact between the conglomerate and older bedrock could have provided a weak plane that allowed westward sliding after a free face was generated.

Listric Normal Fault

Listric normal faults decrease in dip with increasing depth to produce a concave-up geometry in a longitudinal cross section (Fig. 26). The low-angle faults in the study area may be parts of listric normal faults. However, hanging-wall rocks should be rotated when moved along a curved surface, and there should be evidence of curved fault surfaces. Surface data do not support the requirement of rotated hanging-wall bedding (Fig. 20; see also Rotated High-Angle Normal Fault section). Furthermore, interpretations of subsurface data indicated that faults in the area do not have much of a

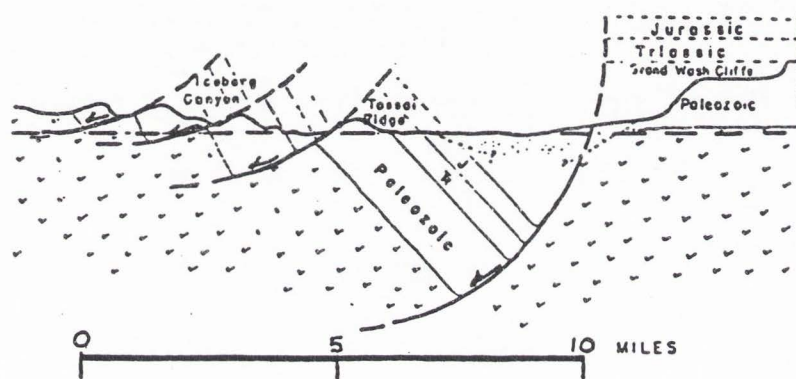


Figure 26. Dip of listric normal faults at surface. Dip of a listric normal fault is dependent upon the structural level at which the fault is viewed. Modified from Longwell (1945).

listric shape, nor is there significant rotation of Tertiary beds (Evans, 1990). Therefore, the low-angle normal faults in the study area do not appear to be parts of listric normal faults.

Low-Angle Normal Fault

Low-angle normal faults form the "hard way" according to Anderson (1971, p. 54). This means that the faults did not form along any apparent preexisting plane of weakness and that the faults were not rotated, but actually formed as normal faults with low dip angles in response to extensional tectonism. The local geologic settings of the low-angle normal faults described by Longwell (1945) and Anderson (1971) are vastly different from the setting of the study area. Because of the great differences, no comparison or analysis of those faults was warranted here. Wernicke (1981) proposed that some large low-angle normal faults in the Basin and Range province extend deep into the lithosphere to merge with a nearly horizontal fault zone. The structures he described cover large areas and have horizontal offsets of approximately 20 km. Therefore, no comparison was made between those low-angle normal faults and the faults in the study area.

Mechanically, low-angle normal faults are unusual. Low-angle normal faults were not predicted in Anderson's (1951) typical normal-fault scheme, but then again, neither were high-angle reverse faults predicted in his typical thrust-fault scheme. Reverse faulting seems to be fairly well documented and accepted within the geologic community and low-angle normal faulting is becoming better documented and accepted in the Basin and Range province even though the precise mechanics involved in the faulting are not well understood. The above statements are not proof that low-angle normal faulting occurs, but are presented to indicate that low-angle normal faults may occur even though they are not predictable by any current models.

Subhypothesis 1. The possibility should be considered that a low-angle normal fault formed when a free face was generated by earlier high-angle normal faulting. This low-angle-normal-fault subhypothesis (LANF1) is similar to the gravity-slide hypotheses except that a preexisting plane of weakness is not required for failure. Failure would have to be accomplished entirely by the application of extensional forces to intact rock. The best way to test this subhypothesis is to reconstruct the structural evolution by use of schematic cross sections (Plate 3). These reconstructions are based on projection of the present surface data back in time. The reconstructions reveal events that must have occurred to result in the present surface geology. Two episodes of high-angle normal faulting took place before low-angle normal faulting. Uplift along the high-angle faults and erosion of Wasatch Formation and older bedrock contributed to the formation of the Salt Lake Formation. In the diagrams, newly deposited Salt Lake Formation conglomerates cover the toe of the potential failure plane. An open-air free face is not shown, but the conglomerate would probably be unconsolidated and would not impede a sliding block. Episodes of high-angle normal faulting followed after the low-angle normal faulting. Inferred in the reconstructions is that the two low-angle normal faults cut both Precambrian/Paleozoic bedrock and Tertiary sediments. Because both faults formed during the same stage and cut similar rocks, they are inferred to be the same fault. Fault D created two structural levels of low-angle normal faults. Plate 3 indicates that this subhypothesis is possible for the origins of both low-angle normal faults in the study area.

Subhypothesis 2. A free face may not be necessary for the formation of low-angle normal faults. Low-angle normal faults may develop as confined bedrock is fractured at low angles in response to an extensional stress state. Again, the best way to test this subhypothesis (LANF2) is to reconstruct the faulting history (Plate 3). Low-angle normal faulting followed an initial episode of high-angle normal faulting in this

subhypothesis. The evolution based on this subhypothesis is similar to Subhypothesis 1. At least three episodes of high-angle normal faulting followed the low-angle normal faulting. In this reconstruction, the low-angle normal faults evolve parallel to each other in time, and both low-angle normal faults cut Precambrian/Paleozoic bedrock. Because the faults cut rocks of similar ages, they might be connected in the subsurface. The surface and near-surface data support this subhypothesis. Low-angle normal faulting without a free face seems to be a valid interpretation of the geologic data.

Subhypothesis 3. The first episode of normal faulting in the reconstructions for subhypotheses 1 and 2 was high-angle normal faulting that generated a deep basin after deposition of the Wasatch Formation. A third subhypothesis (LANF3) examines the possibility that the first episode of normal faulting was low-angle normal faulting that represented a pre-Basin and Range style of normal faulting. Hypothesized pre-Basin and Range extension involved a stress state with principal stress axes that were neither horizontal nor vertical. A stress state of this nature may have been an intermediate state in the transition from compressional tectonism to extensional tectonism (Fig. 21). Such a stress state may have resulted in faults with unusual geometries that formed between Sevier Orogeny thrusting and modern Basin and Range high-angle normal faulting. If this subhypothesis is assumed, then low-angle normal faults might be indicative of a pre-Basin and Range style of normal faulting. Zoback and others (1981) provided a discussion of the Cenozoic evolution of stress states and tectonic styles in the Basin and Range province. Although the discussion of Zoback and others (1981) applied to changing stress states within the period of extensional tectonism, their logic may be applied to the transition of stress states from compressional to extensional tectonism. The transition from compressional tectonism to extensional tectonism probably took place about 30 to 40 million years ago. Zoback and others (1981) recognized two stages of extensional tectonism. The early phase, in which the least principal stress axis was

directed generally WSW-ENE, lasted from about 30 million years ago to 10 million years ago. The later phase, which has controlled extension in the province since about 10 million years ago, has a least principal stress axis that is horizontal and is directed approximately WNW-ESE to E-W (Zoback, 1989). The change from the early phase to the later phase was time transgressive and not abrupt. Because of this gradual transition, structures indicative of both phases may have formed concurrently in localized settings (Zoback and others, 1981). Younger faults with a distinct style and trend truncating older faults with a different style and trend and strata related to the later stage lying unconformably on older, faulted strata provide good evidence for two distinct phases of faulting (Zoback and others, 1981). The local geology associated with the northern LANF in the study area satisfies both of the above conditions. The hanging wall of the northern LANF is truncated by faults B and D (Plate 1 and Plate 3) and is overlain by the Salt Lake Formation which was deposited in response to tectonic uplift. On the basis of the strike of the northern LANF, the least principal stress axis would have been oriented approximately WNW during the early phase of extensional tectonism. From the current data, one cannot state what the exact orientations of the principal stress axes were. However, on the basis of the time period when the faulting occurred, one may infer that the axes were in a transitional state. A reconstruction of the structural evolution based on two phases of extension explains the northern LANF well. Low-angle normal faulting probably occurred in response to an intermediate stress state during the transition from compressional to modern extensional tectonism (Late Eocene to Early Miocene [?]). The principal stress axes would have continued to rotate and eventually would have established themselves in their presently accepted orientation (i.e., least principal stress axis is horizontal and is directed WNW-ESE). This new stress state resulted in high-angle normal faulting. Because the hanging wall of the southern LANF contains faulted Salt Lake Formation conglomerate and the hanging wall

of the northern LANF does not, parallel evolution of the two low-angle faults is not concluded. The first sediments of the Salt Lake Formation may have been deposited in a shallow basin that was formed during the first episode of low-angle normal faulting. This initial sedimentation was followed by a second episode of low-angle normal faulting. This interpretation is supported by the Tslc in the hanging wall of the southern LANF that is thought to be older than the Tslc that depositionally overlaps the northern LANF (see Descriptive Analysis section). The faulted Salt Lake Formation conglomerates in the southern LANF are interpreted to be part of the lower section of the Salt Lake Formation conglomerates. After the formation of the southern LANF, high-angle normal faulting of modern Basin and Range extension ensued. Plate 3 indicates that an episode of high-angle normal faulting occurred between the formation of the two low-angle normal faults for Subhypothesis 3. This interpretation was based on an assumption made early in the research that all of the Salt Lake Formation conglomerates were a direct result of uplift on high-angle normal faults. However, this assumption is not necessarily correct. Uninterrupted low-angle normal faulting makes the explanation of Subhypothesis 3 simpler than the interpretation involving two episodes of low-angle normal faulting interrupted by an episode of high-angle normal faulting. The reconstruction of the evolution for Subhypothesis 3 works well with the geologic field data and with the hypothesized stress states. In light of the discussion of possible stress states responsible for low-angle normal faults, Subhypotheses 1 and 2 are not so attractive because they do not involve two distinct phases of normal faulting as described by Zoback and others (1981). Zoback and others (1981) implied that two distinct stress states are needed to generate two different styles of faults. Therefore, of the three subhypotheses for low-angle normal faults, Subhypothesis 3 is the most likely. The interpretation involving two episodes of low-angle normal faulting followed by episodes of high-angle normal faulting is the favored interpretation within Subhypothesis 3.

STRUCTURAL EVOLUTION

More than one hypothesis is valid based on the arguments presented previously. Because of this, more than one reconstruction of the structural evolution is possible. The Cenozoic structural history is dominated by several stages of uplift and erosion as evidenced by the thick sequence of faulted, coarse-clastic sedimentary rocks of Tertiary age. The structural interpretations presented here differ from those presented in earlier studies (Galloway, 1970; Mendenhall, 1975; Brummer and Evans, 1989). For simplification, the valid hypotheses will be referred to below by their abbreviated names: gravity-slide subhypothesis 2 = GS2, low-angle-normal-fault subhypothesis 1 = LANF1, low-angle-normal-fault subhypothesis 2 = LANF2, low-angle-normal-fault subhypothesis 3 = LANF3. In order to maintain consistency in the discussion of the structural evolution among the four hypotheses, eight stages of development are proposed (Plate 3). The diagrams depict the sequences of events that might have occurred to produce the geological relationships observed at the surface presently (stage 8). The ages listed for some of the stages could only be approximated by bracketing between stages with known ages. Data do not exist to allow for a determination of the amount of degradation during intermediate stages. The diagrams in stage 8 were projected back in geologic time on the basis of the known throw on normal faults and age relations among faults. Additional data used were bedding contacts and structures exposed at the surface, and subsurface data.

A reconstruction of the geologic history begins with pre-normal faulting formation of the Logan Peak syncline. During the Sevier Orogeny (Jurassic to early Tertiary), units were thrust eastward from their original site of deposition. As a consequence of this thrusting, the units in the allochthon were arched or folded into synclines and anticlines (stage 1). After the thrusting and folding, degradation ensued.

This degradation was followed by deposition of the Wasatch Formation (Eocene) unconformably across the Logan Peak syncline (stage 2). In Plate 3, erosion and deposition are shown by dashed lines.

For GS2, LANF1, and LANF2, stage 3 involved high-angle normal faulting after the Wasatch Formation was deposited (late Eocene [?]). The northern LANF was formed during stage 3 of LANF3 after deposition of the Wasatch Formation. The low-angle normal faulting generated a shallow basin into which the first Salt Lake Formation sediments were shed. A deep basin generated by high-angle normal faults is not essential for LANF3 (see also discussion under Subhypothesis 3 in Low-Angle Normal Fault section).

As a consequence of the uplift of stage 3, coarse-clastic sediments were shed off the highlands into a basin to the west (proto-Cache Valley) (stage 4). The coarse-clastic sediments (Salt Lake Formation conglomerates) consisted of bedrock clasts from the west limb of the Logan Peak syncline and reworked Wasatch Formation sediments. Degradation during stage 4 may have occurred between the late Eocene and early Miocene.

For GS2 and LANF1, recurrent movement on faults B and F probably generated free faces (stage 5). Low-angle normal faults formed during stage 5 for LANF2 and LANF3. For LANF3, the formation of the southern LANF represents the second phase of low-angle normal faulting. The southern LANF of LANF3 may have formed at a higher structural level than the northern LANF did. Events of stage 5 may have taken place during the early to middle Miocene.

Free faces generated during stage 5 facilitated failure by sliding or faulting (stage 6). In GS2, failure was also aided by the hypothesized weak contact between the Tertiary conglomerate and the Precambrian-Paleozoic rocks. Degradation during stage 6

followed stage 5 for LANF2 and LANF3. Stage 6 may have occurred during the middle to late Miocene.

During stage 7 for all hypotheses, degradation and deposition of the Salt Lake Formation continued. Normal fault D formed during stage 7 according to LANF1, LANF2, and LANF3. Fault D may be partially responsible for the southward tilting of the hanging-wall block of the southern LANF. The northern extent of the southern LANF was cut by fault D and was covered by later Salt Lake Formation sediments in the hanging wall of fault D. The age of events in stage 7 is probably late Miocene to Pliocene.

Stage 8 contributed more high-angle normal faulting and degradation to the features observed today in the study area. All four hypotheses provide for recurrent movement on faults E and F which may have tilted the hanging-wall block of the southern LANF. Fault A may have formed in the same period in which fault C formed. Degradation, which continues to the present, followed the uplift on the high-angle normal faults. Stage 8 possibly began in the late Pliocene. The latest movement on high-angle normal faults was 13,000 to 14,000 years ago as evidenced by Provo-level deltaic sediments that are offset at fault C (McCalpin, 1989).

CONCLUSIONS

ORIGINS

The analyses and interpretations presented in this study indicate four possible origins for the low-angle normal faults in the study area. The hypotheses that are not valid for the study area are folded thrust fault, rotated-high-angle-normal-fault subhypotheses 1 and 2, gravity-slide subhypothesis 1, and listric-normal-fault subhypotheses 1, 2, and 3. Therefore, the remaining hypotheses for the origin are gravity-slide subhypothesis 2 (GS2), and low-angle-normal-fault subhypotheses 1 (LANF1), 2 (LANF2), and 3 (LANF3). GS2 for the southern LANF entails the westward sliding of Tertiary conglomerate on its own lower, depositional contact. It is not known or provable whether that lower contact actually provided a weak discontinuity that was preferred over fracturing of intact rock. Reconstructions showed that gravity sliding along that contact was possible for the origin of the southern LANF. However, geologic simplicity may argue against GS2. One would expect that because the deformation, orientation and ages are similar for the two low-angle normal faults that their origins would be attributable to the same explanation. Neither of the gravity-slide subhypotheses could explain the origin of the northern LANF. Explanations that do account for both low-angle normal faults are more attractive and more favorable. Each of the low-angle-normal-fault subhypotheses accounts for the origins of both faults. LANF1 is virtually identical to GS2 except that a preexisting weak plane is not required for failure, and that slippage occurred within quartzites rather than at their upper contact. Schematic reconstructions shown on Plate 3 indicated that LANF1 was valid for the study area. LANF2 proposed that the low-angle normal faults formed solely by fracturing intact rock. LANF2 required no free face and no preexisting weak plane. In LANF2, low-angle normal faults formed after an initial episode of high-angle normal

faulting. Because a free face did not have to be generated after the initial stage of degradation, an episode of high-angle normal faulting is eliminated, which makes this interpretation somewhat simpler. Cross-sectional reconstructions based on LANF2 showed that LANF2 is plausible for the origins of the low-angle normal faults. However, LANF1 and LANF2 did not consider the principal stresses necessary for formation of low-angle and high-angle normal faults. The discussion by Zoback and others (1981) suggested that two distinct stress states were needed to generate two different styles of normal faults. Because LANF1 and LANF2 do not account for two distinct stress states, the validity of these two subhypotheses is questionable. The explanation for the origin of the low-angle normal faults that appears most satisfactory is LANF3. LANF3 accounts for both high-angle and low-angle normal faults and the principal stresses that would have generated two distinct styles of normal faults. Schematic reconstructions also support the conclusion that LANF3 is the best explanation.

REGIONAL APPLICABILITY

Field descriptions of the study area and of low-angle faults from throughout the Basin and Range province indicate many local variables which result in many different models to illustrate structural origin. Because of this, no one model will account for all low-angle normal faults in Basin and Range province. When studying low-angle normal faults, one should evaluate the local data carefully, then draw upon models from the published literature or form new models to explain the local structures.

REFERENCES CITED

- Adamson, R. D., 1955, The Tertiary Salt Lake Group in Cache Valley, Utah-Idaho [M.S. thesis]: Logan, Utah, Utah State Agricultural College, 59 p.
- Adamson, R. D., Hardy, C. T., and Williams, J. S., 1955, Tertiary rocks of Cache Valley, Utah and Idaho, *in* Eardley, A. J., ed., Tertiary and Quaternary geology of the eastern Bonneville Basin: Utah Geological Society Guidebook to the Geology of Utah, number 10, p. 1-22.
- Anderson, E. M., 1951, The dynamics of faulting and dyke formation with applications to Britain: Edinburgh, Oliver and Boyd, 206 p.
- Anderson, R. E., 1971, Thin skin distension in Tertiary rocks of southeastern Nevada: Geological Society of America Bulletin, v. 82, no. 1, p. 43-58.
- Armstrong, R. L., 1968, Sevier Orogenic Belt in Nevada and Utah: Geological Society of America Bulletin, v. 79, no. 4, p. 429-458.
- 1972, Low-angle (denudation) faults, hinterland of the Sevier Orogenic Belt, eastern Nevada and western Utah: Geological Society of America Bulletin, v. 83, no. 6, p. 1729-1754.
- Bailey, R. W., 1927, The Bear River Range fault, Utah: American Journal of Science, v. 13, p. 497-502.
- Baker, A. A., 1964, Geology of the Orem quadrangle, Utah: U. S. Geological Survey Geologic Quadrangle Map GQ-241, scale 1:24,000.
- Best, M. G., and Hamblin, W. K., 1978, Origin of the northern Basin and Range province: Implications from the geology of its eastern boundary, *in* Smith, R. B., and Eaton, G. P., eds., Cenozoic tectonics and regional geophysics of the western Cordillera: Geological Society of America Memoir 152, p. 313-340.
- Beutner, E. C., 1972, Reverse gravitative movement on earlier overthrusts, Lemhi Range, Idaho: Geological Society of America Bulletin, v. 83, no. 3, p. 839-846.
- Bradshaw, G. A., and Zoback, M. D., 1988, Listric normal faulting, stress refraction, and the state of stress in the Gulf Coast basin: Geology, v. 16, no. 3, p. 271-274.
- Brown, R. W., 1949, Pliocene plants from Cache Valley, Utah: Washington Academy of Sciences Journal, v. 39, no. 7, p. 224-229.
- Brummer, J. E., and Evans, J. P., 1989, Evidence for the onset of extensional tectonics, western Bear River Range, Utah: Geological Society of America Abstracts with Programs, v. 21, no. 5, p. 60.

- Brummer, J. E., and McCalpin, J., 1990, Geologic map of the Richmond quadrangle, Cache County, Utah: Utah Geological and Mineral Survey Open-File Report 174, scale 1:24,000.
- Budge, D. R., 1966, Stratigraphy of the Laketown Dolostone, north-central Utah [M.S. thesis]: Logan, Utah, Utah State University, 86 p.
- Burton, S. M., 1973, Structural geology of the northern part of Clarkston Mountain, Malad Range, Utah-Idaho [M.S. thesis]: Logan, Utah, Utah State University, 54 p.
- Buterbaugh, G. J., 1982, Petrology of the Lower Middle Cambrian Langston Formation, north-central Utah and southeastern Idaho [M.S. thesis]: Logan, Utah, Utah State University, 166 p.
- Byerlee, J. D., 1978, Friction of rocks: *Pure and Applied Geophysics*, v. 116, p. 615-626.
- Cluff, L. S., Glass, C. E., and Brogan, G. E., 1974, Investigation and evaluation of the Wasatch fault north of Brigham City and Cache Valley faults, Utah and Idaho: A guide to land-use planning with recommendations for seismic safety: Report prepared for the U.S. Geological Survey under contract no. 14-08-001-13665 by Woodward-Lundgren and Associates, Oakland, California, 147 p.
- Crittenden, M. D., Jr., Sharp, B. J., and Calkins, F. C., 1952, Geology of the Wasatch Mountains east of Salt Lake City: Parleys Canyon to the Traverse Range, *in* Marsell, R. E., ed., *Geology of the central Wasatch Mountains, Utah*: Utah Geological Society Guidebook to the Geology of Utah, number 8, p. 1-37.
- Crittenden, M. D., Jr., Schaeffer, F. E., Trimble, D. E., and Woodward, L. A., 1971, Nomenclature and correlation of some Upper Precambrian and basal Cambrian sequences in western Utah and southeastern Idaho: *Geological Society of America Bulletin*, v. 82, no. 3, p. 581-602.
- Curry, H. D., 1938, "Turtleback" fault surfaces in Death Valley, California: *Geological Society of America Bulletin Abstracts*, v. 49, p. 1875.
- 1954, Turtlebacks in the central Black Mountains, Death Valley, California: *California Division of Mines Bulletin* 170, ch. IV, p. 53-59.
- Dahlstrom, C. D. A., 1970, Structural geology in the eastern margin of the Canadian Rocky Mountains: *Canadian Petroleum Geology Bulletin*, v. 18, p. 332-406.
- Danzl, R. B., 1982, Stratigraphy and depositional environment of the Tertiary Salt Lake Group near Oneida Narrows, southeastern Idaho: *Northwest Geology*, v. 11, p. 22-30.
- Davis, G. H., 1984, *Structural geology of rocks and regions*: New York, John Wiley and Sons, 492 p.

- Deputy, E. J., 1984, Petrology of the Middle Cambrian Ute Formation, north-central Utah and southeastern Idaho [M.S. thesis]: Logan, Utah, Utah State University, 124 p.
- Dickinson, W. R., Goodlin, T. C., Grover, J. A., Mark, R. A., and Shafiqullah, M., 1987, Low-angle normal-fault system along the range front of the southwestern Galiuro Mountains in southeastern Arizona: *Geology*, v. 15, p. 727-730.
- Dover, J. H., 1985, Geologic map and structure sections of the Logan 30' x 60' quadrangle, Utah and Wyoming: U.S. Geological Survey Open-File Report 85-216, scale 1:100,000.
- 1987, Geologic map of the Mount Naomi Roadless Area, Cache County, Utah, and Franklin County, Idaho: U.S. Geological Survey Miscellaneous Field Studies Map MF-1566-B, scale 1:100,000.
- Drewes, H., 1959, Turtleback faults of Death Valley, California: a reinterpretation: *Geological Society of America Bulletin*, v. 70, no. 12, pt. 1, p. 1497-1508.
- Evans, J. P., 1990, Structural setting of seismicity in northern Utah: Utah Geological and Mineral Survey Open-File Report (in press).
- Evans, J. P., and Oaks, R. Q., Jr., 1990, Geometry of Tertiary extension in the northeastern Basin-and-Range Province superimposed on the Sevier Fold and Thrust Belt, Utah, Idaho, and Wyoming: *Geological Society of America Abstracts with Programs*, v. 22, no. 6, p. 10.
- Fenneman, N. M., 1931, *Physiography of Western United States*: New York, McGraw-Hill Book Co., 534 p.
- 1946, Physical divisions of the United States: U.S. Geological Survey Map, scale 1:7,000,000.
- Fritz, W. H., 1968, Geologic map and sections of the southern Cherry Creek and northern Egan Ranges, White Pine County, Nevada: Nevada Bureau of Mines Map 35.
- Galloway, C. L., 1970, Structural geology of eastern part of the Smithfield quadrangle, Utah [M.S. thesis]: Logan, Utah, Utah State University, 115 p.
- Gardiner, L. L., 1974, Environmental analysis of the Upper Cambrian Nounan Formation, Bear River Range and Wellsville Mountain, north-central Utah [M.S. thesis]: 121 p.
- Gray, W. E., 1975, Structural geology of the southern part of Clarkston Mountain, Malad Range, Utah [M.S. thesis]: Logan, Utah, Utah State University, 43 p.
- Hatcher, R. D., Jr., 1990, *Structural geology: principles, concepts, and problems*: Columbus, Ohio, Merrill Publishing Company, 531 p.
- Hay, H. W., Jr., 1982, Petrology of the Middle Cambrian Blacksmith Formation, north-central Utah [M.S. thesis]: Logan, Utah, Utah State University, 157 p.

- Hintze, L. F., 1979, Geologic history of Utah: Brigham Young University Geology Studies, v. 20, pt. 3, 181 p.
- Hose, R. K., and Danes, Z. F., 1973, Development of the Late Mesozoic to Early Cenozoic Structures of the Eastern Great Basin, *in* De Jong, K. A., and Scholten, R., eds., Gravity and Tectonics: New York, John Wiley and Sons, p. 429-441.
- Hubbert, M. K., and Rubey, W. W., 1959, Role of fluid pressure in mechanics of overthrust faulting, Part 1: Geological Society of America Bulletin, v. 70, p. 115-166.
- Hunt, C. B., and Mabey, D. R., 1966, Stratigraphy and structure of Death Valley, California: U. S. Geological Survey Professional Paper 494-A, 162 p.
- Jaroszewski, W., 1984, Fault and fold tectonics: Chichester, England, Ellis Horwood Limited, 565 p.
- Krieger, M. H., 1977, Large landslides, composed of megabreccia, interbedded in Miocene basin deposits, southeastern Arizona: U. S. Geological Survey Professional Paper 1008, 25 p.
- Levy, M., and Christie-Blick, N., 1989, Pre-Mesozoic palinspastic reconstruction of the eastern Great Basin (western United States): Science, v. 245, p. 1454-1462.
- Longwell, C. R., 1945, Low-angle normal faults in the Basin and Range Province: American Geophysical Union Transactions, v. 26, pt. 1, p. 107-118.
- 1951, Megabreccia developed downslope from large faults (Arizona-Nevada): American Journal of Science, v. 249, no. 5, p. 343-355.
- Lowe, M.V., 1987, Surficial geology of the Smithfield quadrangle, Cache County, Utah [M.S. thesis]: Logan, Utah, Utah State University, 143 p.
- Mabey, D. R., 1985, Geophysical maps of the Mount Naomi Roadless area, Cache County, Utah and Franklin County, Idaho: U.S. Geological Survey Miscellaneous Field Studies Map, MF-1566-C, scale 1:100,000.
- 1987, Subsurface geology along the Wasatch Front, *in* Gori, P. L., and Hays, W. W., eds., Assessment of regional earthquake hazards and risk along the Wasatch Front, Utah: U.S. Geological Survey Open-File Report 87-585, v. 1, p. C1-C39.
- Mattox, S. R., and Weiss, M. P., 1987, Reactivation of a Cretaceous thrust surface by Basin and Range extension, southwestern Gunnison Plateau, central Utah: The Mountain Geologist, v. 24, no. 3, p. 55-65.
- Maxey, G. B., 1941, Cambrian Stratigraphy in the northern Wasatch region [M.S. thesis]: Logan, Utah, Utah State Agricultural College, 64 p.

- 1958, Lower and Middle Cambrian stratigraphy in northern Utah and southeastern Idaho: Geological Society of America Bulletin, v. 69, no. 6, p. 647-688.
- McCalpin, J., 1989, Surficial geologic map of the East Cache fault zone, Cache County, Utah: U.S. Geological Survey Miscellaneous Field Studies Map MF-2107, scale 1:50,000.
- McDonald, R. E., 1976, Tertiary tectonics and sedimentary rocks along the transition: Basin and Range province to plateau and thrust belt province, Utah, *in* Hill, J. G., ed., Geology of the Cordilleran hingeline: Rocky Mountain Association of Geologists Symposium, p. 281-317.
- Mendenhall, A. J., 1975, Structural geology of eastern part of Richmond and western part of Naomi Peak quadrangles, Utah-Idaho [M.S. thesis]: Logan, Utah, Utah State University, 45 p.
- Mitchell, G. C., and McDonald, R. E., 1986, History of Cenozoic extension in central Sevier desert, west central Utah, from COCORP seismic reflection data: discussion: American Association of Petroleum Geologists Bulletin, v. 70(8), p. 1015-1021.
- Moore, E. M., 1968, Miocene-Pliocene sediments, gravity slides, and their tectonic significance, east-central Nevada: Journal of Geology, v. 76, no. 1, p. 88-98.
- Moore, E. M., Scott, R. B., and Lumsden, W. W., 1968, Tertiary tectonics of the White Pine-Grant Range region, east-central Nevada, and some regional implications: Geological Society of America Bulletin, v. 79, no. 12, p. 1703-1726.
- Oaks, R. Q., Jr., Runnells, T. R., and Avery, C. E., 1989, Tectonic factors influencing deposition of the fluvial and lacustrine Wasatch Formation (Eocene), north-central Utah: Geological Society of America Abstracts with Programs, v. 21, p. A366.
- Oviatt, C. G., 1986, Geologic map of the Honeyville quadrangle, Box Elder and Cache Counties, Utah: Utah Geological and Mineral Survey Map 88, scale 1:24,000.
- Peterson, D. L., and Oriel, S. S., 1970, Gravity anomalies in Cache Valley, Cache and Box Elder Counties, Utah, and Bannock and Franklin Counties, Idaho: U.S. Geological Survey Professional Paper 700-C, p. C114-C118.
- Petroleum Information: Well-completion card file, Utah Geological and Mineral Survey.
- Proffett, J. M., Jr., 1977, Cenozoic geology of the Yerington district, Nevada, and implications for the nature and origin of Basin and Range faulting: Geological Society of America Bulletin, v. 88, no. 2, p. 247-266.
- Ragan, D. M., 1973, Structural geology - an introduction to geometrical techniques (2nd edition): New York, John Wiley and Sons, 208 p.

- Richardson, G. B., 1913, Paleozoic section in northern Utah: *American Journal of Science*, 4th ser., v. 36, p. 406-416.
- Sheriff, R. E., 1989, *Geophysical methods*: Englewood Cliffs, N. J., Prentice Hall, 605 p.
- Shimamoto, T., and Logan, J. M., 1981a, Effects of simulated clay gouges on the sliding behavior of Tennessee Sandstone: *Tectonophysics*, v. 75, p. 243-255.
- 1981b, Effects of simulated fault gouge on the sliding behavior of Tennessee Sandstone: Nonclay gouges: *Journal of Geophysical Research*, v. 86, no. B4, p. 2902-2914.
- Sibson, R. H., 1985, A note on fault reactivation: *Journal of Structural Geology*, v. 7, no. 6, p. 751-754.
- Smith, N., 1953, Tertiary stratigraphy of northern Utah and southeastern Idaho: *Intermountain Association of Petroleum Geologists, 4th Annual Field Conference Guidebook*, p. 73-77.
- Smith, R. B., and Bruhn, R. L., 1984, Intraplate extensional tectonics of the eastern Basin-Range: Inferences on structural style from seismic reflection data, regional tectonics, and thermal-mechanical models of brittle-ductile deformation: *Journal of Geophysical Research*, v. 89, no. B7, p. 5733-5762.
- Sprinkel, D. A., 1979, Apparent reverse movement on previous thrust faults along the eastern margin of the Basin and Range Province, north-central Utah: *Basin and Range Symposium, Rocky Mountain Association of Geologists and Utah Geological Association*, p. 135-143.
- Stanley, W. D., 1972, Geophysical study of unconsolidated sediments and basin structure in Cache Valley, Utah and Idaho: *Geological Society of America Bulletin*, v. 83, p. 1817-1830.
- Stewart, J. H., 1978, Basin and Range structure in western North America: A review, *in* Smith, R. B., and Eaton, G. P., eds., *Cenozoic tectonics and regional geophysics of the western Cordillera*: *Geological Society of America Memoir* 152, p.1-31.
- Taylor, M. E., 1963, The lower Devonian Water Canyon Formation of northeastern Utah [M.S. thesis]: Logan, Utah, Utah State University, 63 p.
- Wernicke, B., 1981, Low-angle normal faults in the Basin and Range Province: Nappe tectonics in an extending orogen: *Nature*, v. 291, p. 645-648.
- Westaway, R., and Smith, R. B., 1989, Source parameters of the Cache Valley (Logan), Utah, earthquake of 30 August, 1962: *Bulletin of the Seismological Society of America*, v. 79, no. 5, p. 1410-1425.
- Williams, J. S., 1948, Geology of the Paleozoic rocks, Logan quadrangle, Utah: *Geological Society of America Bulletin*, v. 59, p. 1121-1164.

- 1958, Geologic atlas of Utah: Cache County: Utah Geological and Mineralogical Survey Bulletin 64, 98 p.
- 1964, The age of the Salt Lake Group in Cache Valley Utah-Idaho: Utah Academy of Sciences, Arts and Letters Proceedings, v. 41, pt. 2, p. 269-277.
- Wise, D. U., 1963, Keystone faulting and gravity sliding driven by basement uplift of Owl Creek Mountains, Wyoming: American Association of Petroleum Geologists Bulletin, v. 47, no. 4, p. 586-598.
- Yen, T., 1947, Pliocene fresh-water mollusks from northern Utah: Journal of Paleontology, v. 21, no. 3, p. 268-277.
- Young, J. C., 1960, Structure and stratigraphy in north central Schell Creek Range, in Boettcher, J. W. and Sloan, W. W., Jr., eds., Guidebook to the Geology of east-central Nevada, p. 158-172.
- Zoback, M. L., 1983, Structure and Cenozoic tectonism along the Wasatch fault zone, Utah: Geological Society of America Memoir 157, p. 3-27.
- 1989, State of stress and modern deformation of the northern Basin and Range province: Journal of Geophysical Research, v. 94, no. B6, p. 7105-7128.
- Zoback, M. L., Anderson, R. E., and Thompson, G. A., 1981, Cainozoic evolution of the state of stress and style of tectonism of the Basin and Range province of the western United States: Philosophical Transactions, Royal Society of London, ser. A, 300, p. 407-434.

Am...
El...
Si...
Ca...

APPENDIX

Amoco Production Company
 #1 Lynn Reese
 S17, T12N, R1E, NWSW
 Cache County, Utah

Logged by: Jon Brummer
 Date: 12/88 to 2/89
 Elevation of KB: 1361 m
 Total depth from KB: 2487 m

	Depth from KB meters	Elevation meters	Observations
			sample size = 1/4 of a packet = ~10 g
Qu	27-37	1334-1324	unconsolidated, poorly sorted/rounded quartz sand, medium-sized sand
	37-40		light gray, fine sand and silt, numerous dark grains of limestone (?)
	52-55		limestone, quartzite
	70-91		limestone, some quartzite (some clasts abraded/rounded)
	107-122		limestone, chert, red quartz (some clasts abraded/rounded)
	149-152		gray carbonate, clear/white quartz sand (little or no CaCO ₃ cement)
	165-168		gray carbonate, clear/red quartz sandstone
	332-335	1029-1026	gray limestone covered with white carbonate film
Qu			
	344-348	1017-1014	white, fine silt/tuff with carbonate and quartzite clasts
Qu-Tsl (?)			
Tslc	366-369	995-992	gray carbonate - some broken grains, some rounded grains; cemented, fine grained sandstone - white to pink; a few pieces of gray tuff
	405-408		same as above - calcareous and tuffaceous

	427-430	blocky (1/4" to 1/2" blocks), gray clayey silt with some larger grains, crumbles easily
	442-457	same as above - tuffaceous
Tslt	457-466	white tuff with high % of black bitumen; tuff not well consolidated
	466-485	blocky, gray clayey silt - similar to 427-430
	485-488	blocky, clayey material with black brittle bitumen
	488-524	blocky, gray clayey silt - similar to 427-430
	524-533	clast-supported, blocky, gray, clayey material
	533-634	blocky, gray, clayey silt - similar to 427-430
Tslc	634-646	no matrix, mostly granule-sized dark gray to light gray/brown carbonate; a few light gray tuff clasts; a few calcite and quartz fragments; some clasts rounded, but many are broken and angular
	643-698	similar to 634-646, but has light gray, clayey silty matrix; matrix coats clasts
Tslt	744-753	large sand-sized clasts of silty clayey tuffaceous material; bits of bitumen; clasts not indurated
	753-789	similar to 744-753, but has angular clasts of carbonate and quartzite (about 2%)
	844-853	clasts of silty, clayey tuffaceous material; a few clasts of fine sandstone; marcasite (pyrite?) in sandstone
	866-872	clasts of silty, clayey tuffaceous material, with gray carbonate clasts; fine quartz sandstone clasts (white/clear cement); ostracod in sandstone clast; 0.5% quartz and quartzite

884-890	similar to the above (866-872)
902-908	bits of pyritized mollusc shell; higher % of gray carbonate than previously above; still large amount of gray/white tuffaceous material
921-927	similar to the above (902-908); more dark clasts than the above (carbonates)
Tslt 951-957	sandstone clasts (~10%); carbonate clasts (~5%); rest is gray tuffaceous material
Tslt 975-982	<5% carbonate; gray tuff dominates
1000-1006	gray/light gray tuff; 2-3% carbonate; 5-8% sandstone clasts
1024-1030	gravel-sized (5-9 mm), tuff clasts that are moderately well indurated; minor carbonate and sandstone
1042-1055	mostly tuff; some sandstone and minor carbonate; clast sizes=2-3 mm
1055-1067	white/yellow/tan, platy material (x-ray analysis indicated zeolite - clinoptilolite); some quartz grains included; 0.5% tuff present;
1067-1073	similar to the above, but has more carbonate, sandstone and gray tuff; a few dark green, clayey, blocky clasts; zeolite still dominant
1073-1085	even amounts of zeolite, carbonate and tuff; minor black, brittle bitumen
1085-1091	less yellow zeolite, more gray tuff and crystalline carbonate; pyrite as incrustations on carbonate clasts; a few quartz and chalcedony clasts; very small % of red sandstone clasts
1091-1097	similar to the above; gastropod shells
1097-1103	tuff, gray carbonate; increasing amount of quartz (quartzite) that is red, pink, white and clear, and sandstone that is red/pink; 0.5%-1.0% yellow zeolite still present

	1110-1122	quartz sandstone, tuff, carbonate in approximately equal amounts; quartz sandstone is more white/clear than red
	1125-1128	mostly gray tuffaceous material with some gray carbonate and clear quartz mixed in
Tslt	1137-1140	similar to 1125-1128; ~0.5% green, soft, clayey material; brownish/tan quartz fragments
Tslc	1152-1158	mostly dark gray carbonate with minor tuff and quartz
Tslc	1174-1177	same as the above (1152-1158)
	1186-1189	fine fragments - mostly dark gray carbonate with minor tuff and quartz; still some yellow zeolite material (very low %)
	1204-1207	mainly fine crystalline, dark limestone; poorly sorted sandstone with white matrix/cement is minor; gray tuff - minor; round/subround clear quartz, bitumen present
	1216-1219	mostly gray tuff; lesser amounts of carbonates; bitumen present
	1219-1222	mainly fine crystalline, dark limestone; poorly sorted sandstone with white matrix/cement is minor; gray tuff - minor; high % of round/subround clear quartz
	1231-1234	fine/medium sand-sized clasts high % of clear quartz ostracods gray carbonates, minor tuff
	1247-1250	equal amounts of gray carbonate and gray tuff
	1262-1265	fine/medium sand-sized clasts clear quartz gray carbonate, minor tuff
	1277-1280	fine/medium sand-sized clasts clear quartz gray carbonate, minor tuff

Tslt (?)		
1292-1295		fine/medium sand-sized clasts high % of clear quartz ostracod gray carbonates, tuff dominate
1308-1311		gray tuff; smaller amounts of carbonates, minor quartz
1311-1314		gray tuff, minor carbonates
1323-1326		gray tuff; minor carbonates; ostracods
1341		gray tuff; gray carbonate (85% tuff, more tuff than at 1359)
1359		gray tuff; gray carbonate (mostly tuff)
Tslt 1372		tuff and limestone (more tuff than limestone)
Tslc		
1387-1390		mainly limestone with quartzite (quartzite resembles Geertsen Canyon quartzite); lesser tuff, sandy matrix; minor marcasite
1399-1402		limestone mainly with lesser amounts of tuff and minor quartz and marcasite
1402		limestone; quartz; some tuff
Tslt		
1427		gray tuff
1433		mostly gray tuff 1 gastropod 1 ostracod tuff has dark minerals: (biotite/hornblende)
1448		gray tuff with marcasite
1460-1463		white matrix-supported sand with lots of small marcasite cubes
1463		tuffaceous, sandy material (Salt Lake Formation)

	1600's		sandy tuff
Tslc	2231	-870	gray carbonate; gray tuffaceous clasts, 1-2 % (Salt Lake Formation)
Tw (?)	2237-2240	-876 to -879	no red clasts, but carbonates and yellowish quartz sandstone is present; lacks tuff
Tw	2253-2362	-892 to -1001	red clasts (Wasatch Formation); gray carbonate, quartz, quartz sandstone
Osp	2362-2487	-1001 to -1126	Purple quartzite
	2487	-1126	Total depth in purple quartzite; reported as Swan Peak Formation in drilling reports

Amoco Production Company
#1 Lynn Reese
S17, T12N, R1E, NWSW
Cache County, Utah

Samples available
only from 2347.0 m to
2350.9 m

Log of side core

Depth from KB meters	Observations Wasatch Formation
2347.0-2347.1	reddish tinged quartz sandstone; some is almost quartzitic
2347.1-2347.3	2.0-1.0 phi, quartz sandstone; angular clasts; micaceous; well indurated, calcareous and poorly sorted; possibly arkosic although little feldspar noticed
2347.3-2349.1	same as the above (2347.1-2347.3)
2349.1-2349.4	similar to the above, but coarser; still angular and poorly sorted
2349.7-2350.0	similar to 2347.1-2347.3
2350.6-2350.9	poorly sorted, angular, dark red to gray metallic stained, sand to pebble-sized chert and quartz (conglomerate; not cemented) (Wasatch Formation)

North American Resources
 #7-10 Hauser Farms
 S10, T13N, R1W, NWSWNE
 Cache County, Utah

Logged by: Jon Brummer
 Date: 12/88 to 2/89
 Elevation of KB: 1352 m
 Total depth from KB: 1624 m

Depth from KB meters	Elevation meters	Observations
Qu 154-162		sample size = 1/4 of a packet = ~10 g light colored (white) sandy silt/clay
Qu (?) 180-189	1172-1163	white clay
<hr/>		
Tslt (?) 189-243.8	1163-1108	light gray clayey tuff; many mollusc fossils (pelecypods, gastropods)
472-482		light gray clayey tuff; about 1% quartz and carbonate chips (Salt Lake Formation)
628-637		2.0 to 0.5 phi, quartz sand; some carbonate clasts - angular and poorly sorted; and few tuff clasts; unconsolidated, loose sand
1158		white quartzite (5%); white, soft clay-mud (drilling mud?)
1170-1173		white, opaque material - easily crushable, crystalline, non-calcareous (composition unknown); zeolite (?)
1186-1189		mostly gray clayey material (tuff); pyrite minor
1201-1204		gray, clayey, blocky tuff; quartz grains present
1204-1250		gray tuff as above (1201-1204); some calcite fragments
1311		white material (see 1170)
1350-1353		gray, clayey tuff
1353-1363		95% white/gray, broken quartz pieces
1378-1381		clear/white quartz dominates; tuff and carbonate in equal amounts; white to very

		pale green clasts that are brittle; 1-2 pyrite cubes present
Tslt (?)		
1393-1399		white quartz - 95%; a few tuff clasts; clasts broken/angular; pyrite scattered
1411-1414		sandy tuffaceous sediment (Salt Lake Formation)
1414-1417	-63 to -66	similar to the above, but has mica flakes scattered throughout (Salt Lake Formation)
Tslt		
pCm (?)		
1417-1420	-66 to -69	white quartzite; minor carbonate
1439-1442		white quartz - 99%; 2-3 white tuff clasts
1466-1469		white quartz - 100%
1487-1491		white quartz - 100%
1500-1503		equal mixture of white quartzite and gray tuff clasts; fossil debris
1521-1524		white quartz (quartzite) - 99%; 2-3 tuff clasts
1533-1536		white quartzite - 100%
1548-1551		white quartzite - 65%; red, indurated sandstone - 25% to 35%
1567-1570		white quartzite - 98%; a few gray tuff clasts
1576-1579		similar to above (1567-1570)
1591-1594		quartz, dark gray tuff (?) clasts
1600-1603		white quartzite with a green tinge
1624	-273	Total depth; pC (?) quartzite

Plate 1. Geologic map of faults along the west side of the Bear River Range in northern Utah.

MAP EXPLANATION

Quaternary	Qu	Undivided surficial units; deposits consist of fluvial, deltaic, and lacustrine sediments; most units related to Lake Bonneville
Tertiary	Tslc	Salt Lake Formation - conglomeratic unit; polymictic, clast-supported pebble to boulder conglomerate
	Tslt	Salt Lake Formation - tuffaceous unit; tan to gray tuffaceous claystone with beds and lenses of volcanic ash
Devonian	Du	Undivided Devonian units; Water Canyon and Jefferson Formations; dolostones, limestones, and sandstones
Silurian	Sl	Laketown Dolomite; gray dolostone
Ordovician	Ou	Undivided Ordovician units; Garden City Fm, Swan Peak Fm, and Fish Haven Fm; limestone, dolostone, shale, and quartzite
	Ogc	Garden City Formation; gray, micritic to medium-crystalline limestone; Black chert and tan silt scattered throughout; part of a fault block
Cambrian	Csc	St. Charles Formation; gray, fine- to medium-crystalline dolostone and white to yellow, calcareous sandstone; part of a fault block
	Cu	Undivided Cambrian units; Langston, Ute, Blacksmith, Bloomington, Nounan, and St. Charles Formations; limestones, dolostones, sandstones and shales
	Cgc	Geertsen Canyon Quartzite; olive, tan, pink, orange, coarse-grained quartzite with chert and quartz pebble conglomerate
Precambrian	pC-C	Undivided quartzite; slabs and boulders of Geertsen Canyon and Mutual quartzite
	pCm	Mutual Formation; purple, red, white, medium- to coarse-grained quartzite with green to purple argillite; chert and quartz pebble conglomerate interbedded

MAP SYMBOLS

CONTACTS
Dashed where approximate, queried where uncertain

STRIKE AND DIP OF BEDS
Measured Approximated

LOCATION POINTS
Location points used to reference photos, diagrams, or map features explained in the text.

WATER WELLS
35
(depth to Tertiary (?) bedrock indicated in meters)

FAULTS
Dashed where approximate, queried where uncertain, dotted where concealed. Arrow and number indicates direction and amount of dip of a fault.

High-angle normal fault
Bar and ball on downthrown side

Low-angle normal fault
Open boxes on hanging wall

Thrust fault
Teeth on hanging wall

SCALE
1:50,000
0 1 2 miles
0 1 2 kilometers
Contour Interval = 50 meters

UTAH
Map location

Map compiled from original mapping in the Richmond and northern Smithfield quadrangles (Jon Brummer, 1988-1989), and from the mapping of Galloway (1970; Smithfield quad), Mendenhall (1975; Naomi Peak quad), Dover (1987; Mt. Elmer and Smithfield quads), and McCalpin (1989, Smithfield quad and East Cache fault zone).

Mapping base taken from Logan, Utah-Wyoming-Idaho, 1:100,000-scale metric topographic map.

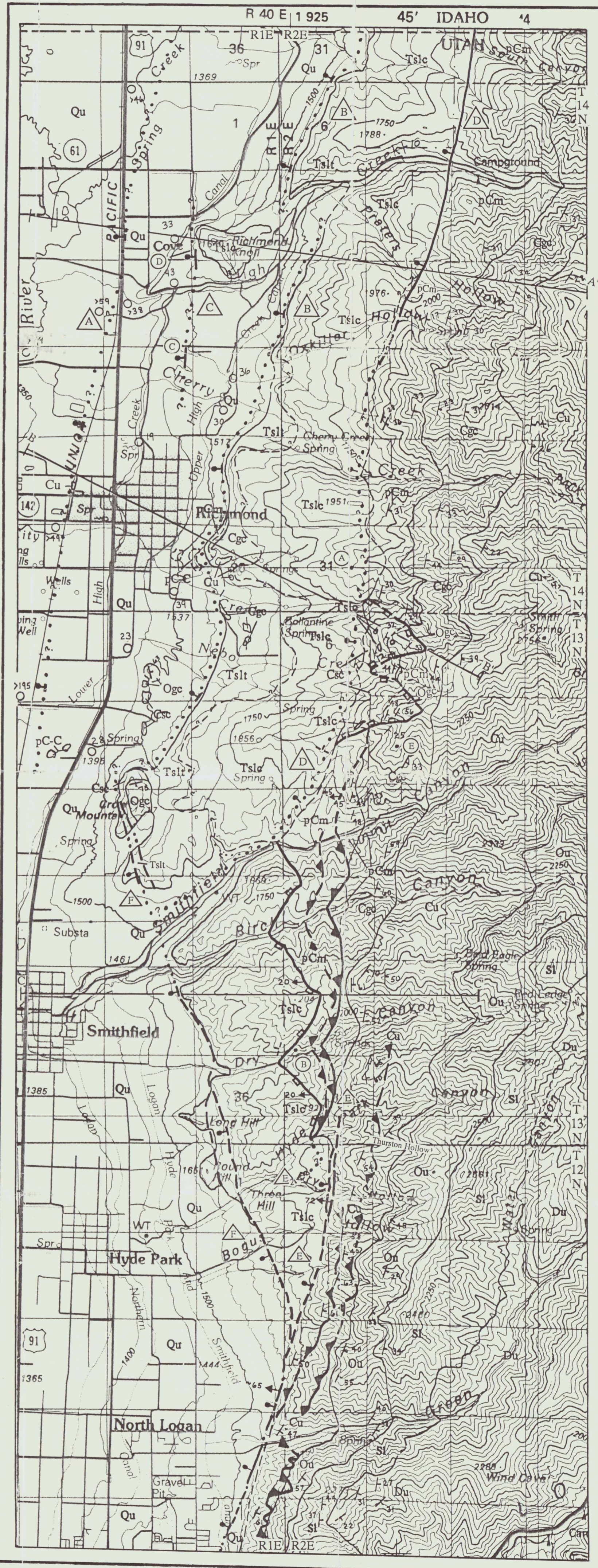


Plate 2. Structure cross sections of faults along the west side of the Bear River Range in northern Utah. Section lines correspond to those on the geologic map.

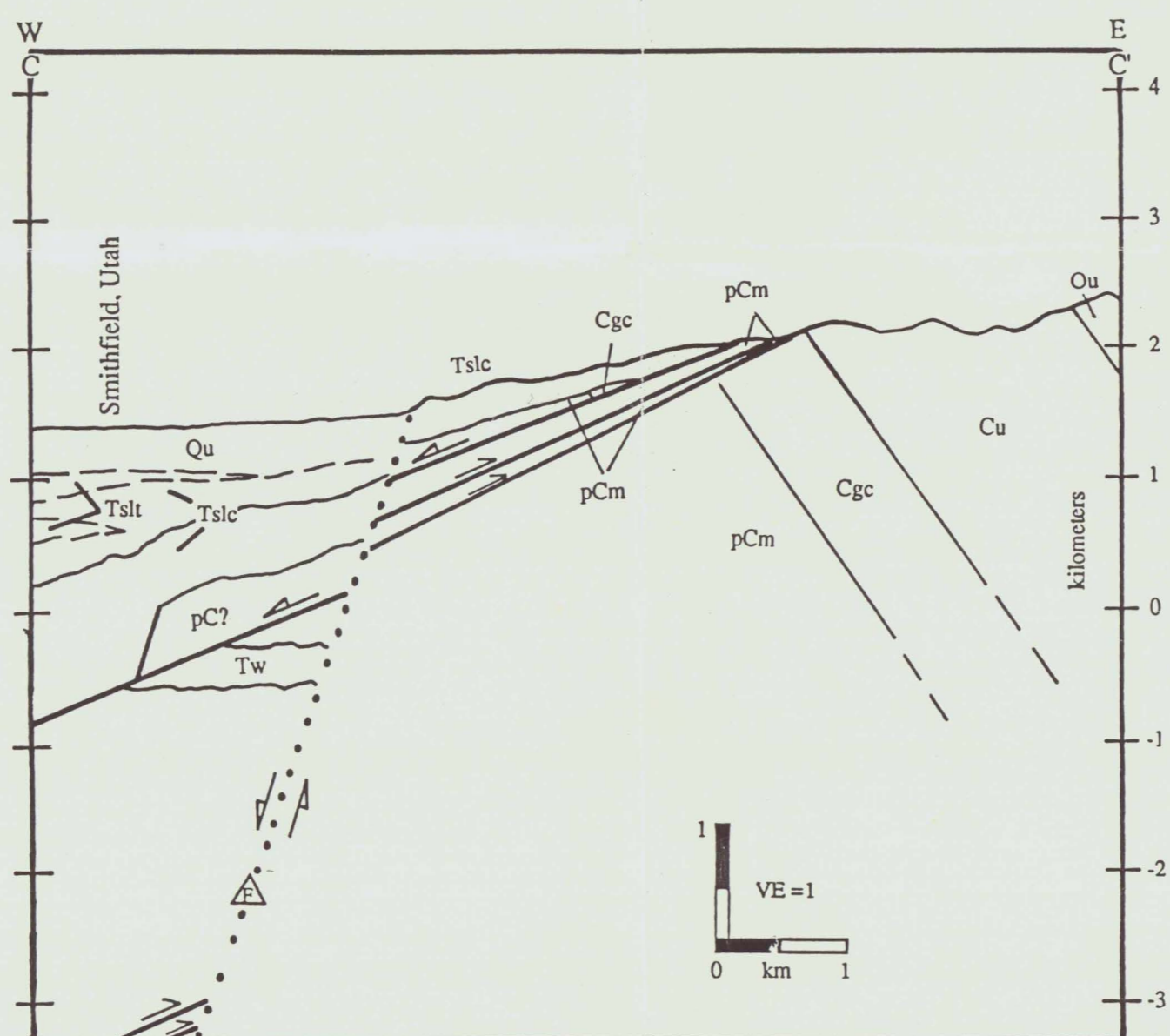
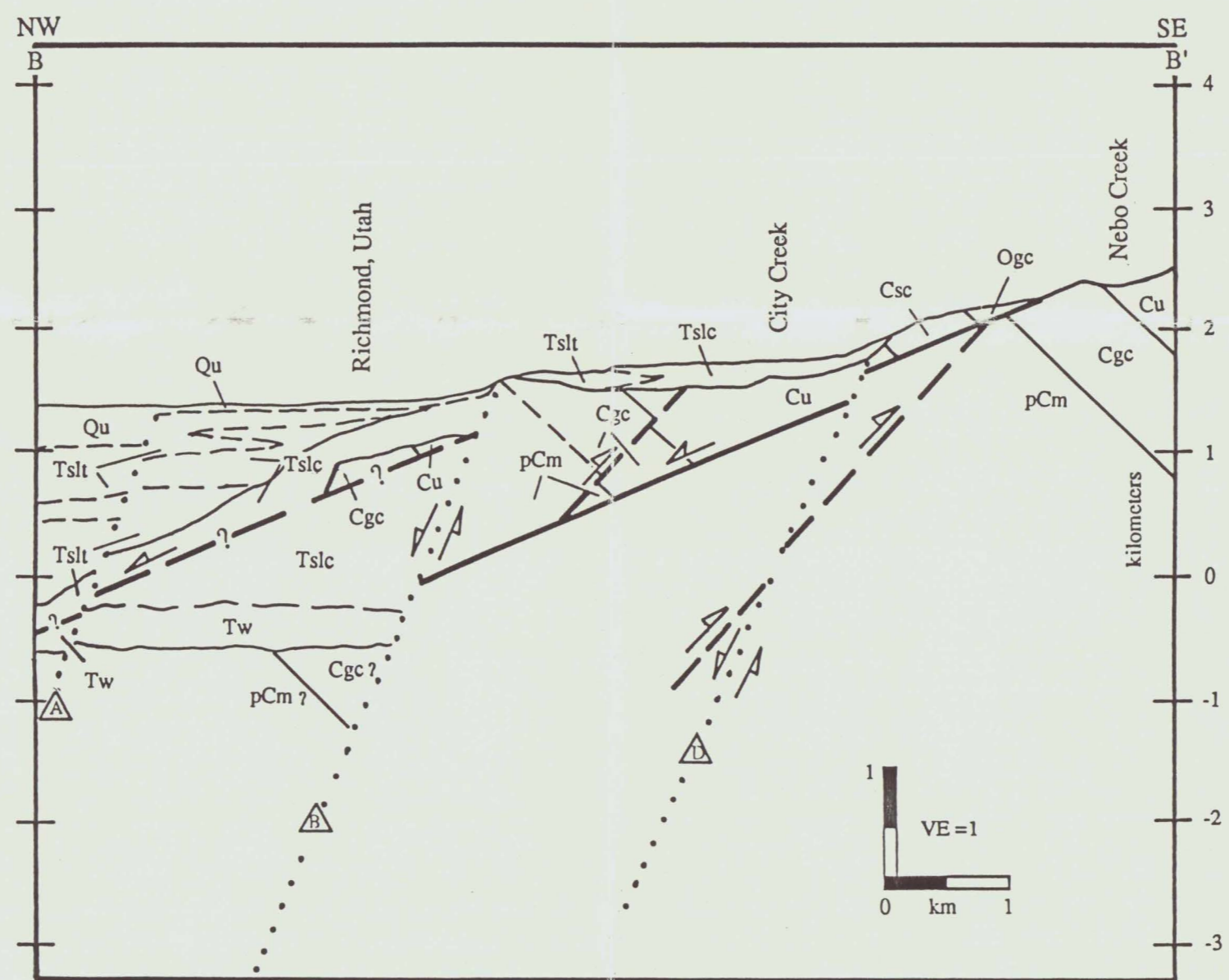
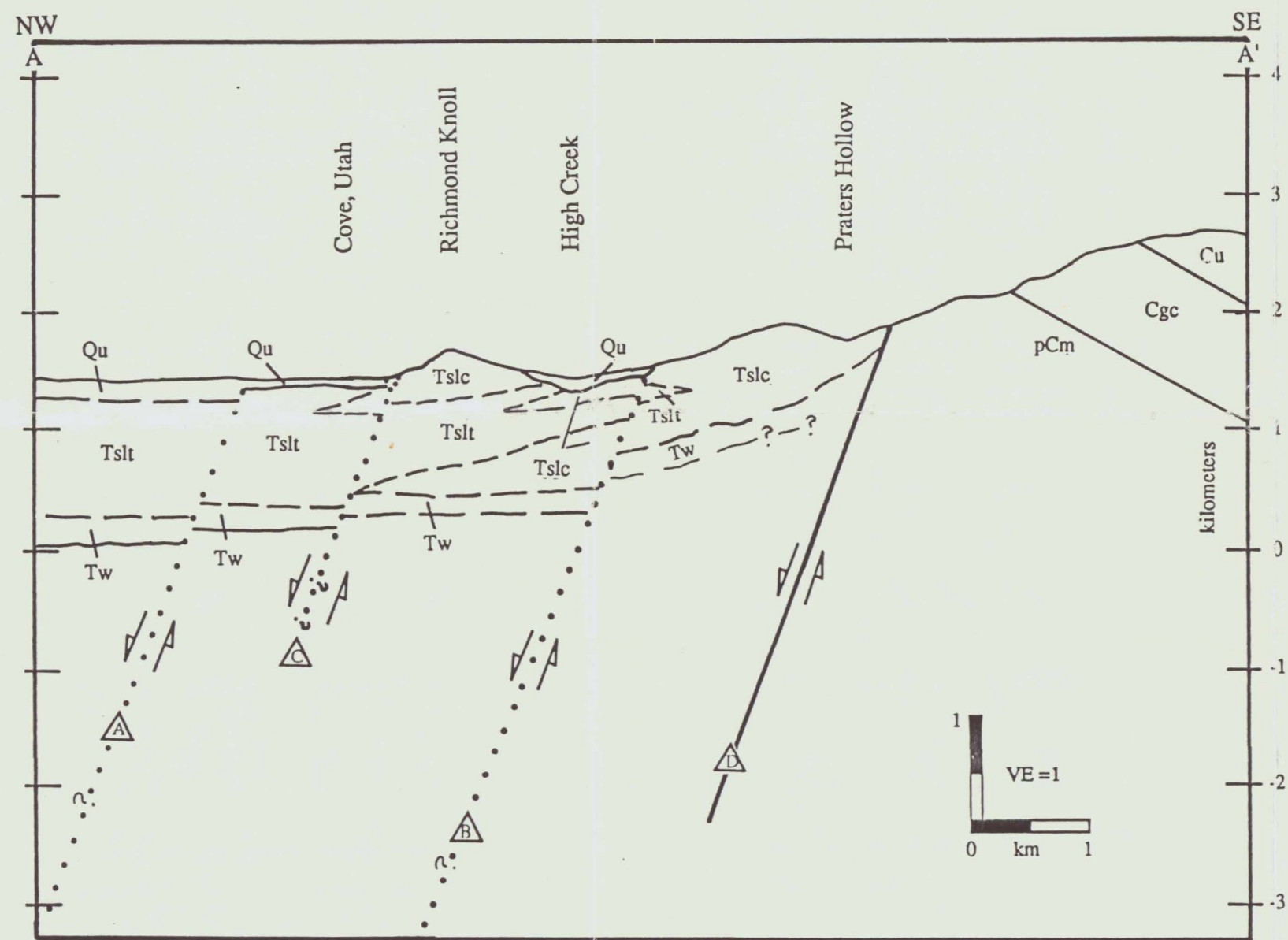


Plate 3. Schematic diagrams of the structural evolution of faults along the west side of the Bear River Range in northern Utah. Ages of degradation and recurrent movement on faults are conjectural. Amount of degradation is approximate.

